

Maneuverability of Wind-Assisted Ships

A Time Domain Simulation Tool

MT54035

Courtland Jensen



Maneuverability of Wind-Assisted Ships

A Time Domain Simulation Tool

by

Courtland Jensen

Thesis for the degree of MSc in Marine Technology in the specialization of Ship Hydromechanics
at Delft University of Technology,
to be defended publicly on Monday August 30, 2022 at 14:00 PM.

Student number: 5242703
Project duration: November 25, 2021 – August 30, 2022
Thesis committee: Dr. ir. I. Akkerman, TU Delft, supervisor
Dr. ir. N. van der Kolk, Blue Wasp Marine
Dr. ir. G. Bordogna, Blue Wasp Marine

This thesis (MT.21/22.046.M) will be made public in August, 2022.

Cover: Ship installed with Ventifoils by Econowind
Style: TU Delft Report Style, with modifications by Daan Zwaneveld

An electronic version of this thesis is available at <http://repository.tudelft.nl/>.

Abstract

Wind-assisted ships are installed with wind propulsors capable of generating thrust for aiding the propulsion of the ship, with the purpose of saving fuel by reducing the required propeller speed and thus engine power. Wind-assisted ships are becoming more common due to high fuel prices and rising environmental concerns. The subject of this thesis is wind-assisted ship maneuverability, which is a relatively new and unexplored topic. There are many factors which this study can involve, and so the goal of this thesis is to study the general behavior of wind-assisted ships during the Turning Circle and Zig-Zag standard maneuvers, and investigate in depth the effect of different control optimization schemes for the wind propulsors. This study requires building a 4 degree-of-freedom (DOF) time domain maneuvering model in which the equations of motions for a wind-assisted ship are solved and the required parameters are input in order to execute the standard maneuvers. The model includes calculation of all the major forces on the ship, including hydrodynamic forces common among maneuvering models, and with the addition of aerodynamic forces due to the wind propulsors. Once the model is built and shows sufficient accuracy, the maneuvers are simulated for a variety of wind conditions, sail configurations, and wind propulsor trim optimization schemes. The behavior of the ship due to these different conditions and the compliance with maneuvering standards are discussed.

The results of the simulations show that the maneuvering behavior of the ship is indeed significantly dependant on the wind, and also how the wind propulsors are controlled. Based on the results, in general, the ship shows the behavior to turn quickly into the wind and slowly while turning against the wind. The effect this has on the maneuvers is that the Turning Circle is generally tighter when the initial turn is turning toward the wind, and larger when the ship is initially turning away from the wind. For the Zig-Zag maneuvers, the ship is alternating in turning toward and away from the wind and so the behavior of turning faster toward the wind is evident in the measured quantities of the Zig-Zag maneuver. The standardized requirements on maneuvering do not yet have considerations for wind-assisted ships and thus it is unknown what will be allowed in the future in terms of wind propulsor control during the standardized tests. Additionally, the abilities of the ships and wind propulsors when it comes to active optimization and wind propulsor trimming are not well known. Thus in this thesis a variety of options for wind propulsor control are studied in order to provide some insight on what is possible, covering some more conservative and more aggressive approaches. The wind propulsor optimization shows to have a big effect on the ship maneuverability, and with thoughtfully constructed optimization schemes there is a general improvement in the measured quantities that result from the maneuvers.

Contents

Abstract	i
Nomenclature	iv
1 Introduction	1
1.1 Fundamental Principles of Wind-Assisted Ship Propulsion	3
1.2 Literature Review	5
1.3 Research Questions	5
1.4 Approach	6
1.5 Document Structure	6
2 Background Theory and Developing the Maneuvering Model	7
2.1 Coordinate System	7
2.2 Equations of Motion	8
2.3 Forces	8
2.3.1 Hydrodynamic Hull Forces	8
2.3.2 Rudder Forces	10
2.3.3 Propeller Forces	11
2.3.4 Aerodynamic Forces	11
2.3.5 Numerical Time Integration	11
2.3.6 Wind Propulsor Trim Optimizaton	12
3 Maneuvering Simulations	13
3.1 Turning Circle	14
3.2 Zig-Zag	14
3.3 Ship Information	15
4 Results	17
4.1 Non-Wind Assisted Ship Maneuvering Validation	17
4.2 Timestep Verification	18
4.3 Holistic Wind-Assist Maneuvering Behavior	19
4.4 Optimization of Wind Propulsor Trim	20
4.4.1 Active and Static Trim Comparison	21
4.5 Dynarig Turning Circle Case	25
4.5.1 Trim Setting S-1	25
4.5.2 Trim Setting A-S1	27
4.5.3 Trim Setting A-F1	29
4.6 Dynarig Zig-Zag 10/10 Case	31
4.6.1 Trim Setting S-1	31
4.6.2 Trim Setting A-F1	33
4.6.3 Trim Setting A-F2	35
4.7 Flettner Rotor Zig-Zag 20/20 Case	37
4.7.1 Trim Setting S-1	37
4.7.2 Trim Setting A-F2	39
4.8 Trim Setting and IMO Compliance	41
4.9 Qualitative Validation of Wind-Assisted Ship Maneuvering	42
5 Conclusion	45
5.1 Recommendations for Further Development	46
References	47

A	Derivations	49
A.1	Equations of Motion	49
A.2	Propeller Speed	50
B	Plots - Main Results	51
B.1	KVLCC2 1/3.7 Dynarig Configuration	52
B.1.1	KVLCC2 1/3.7 Dynarig Turning Circle Tests	52
B.1.2	KVLCC2 1/3.7 Dynarig Zig-Zag 10/10 Tests	55
B.1.3	KVLCC2 1/3.7 Dynarig Zig-Zag 20/20 Tests	60
B.2	KVLCC2 1/3.7 Flettner Rotor Configuration	65
B.2.1	KVLCC2 1/3.7 Flettner Rotor Turning Circle Tests	65
B.2.2	KVLCC2 1/3.7 Flettner Rotor Zig-Zag 10/10 Tests	68
B.2.3	KVLCC2 1/3.7 Flettner Rotor Zig-Zag 20/20 Tests	73
C	Plots - Non-Wind-Assist Validation	78
C.1	KVLCC2 1/45.7 Turning Circle Test	79
C.2	KVLCC2 1/45.7 Zig-Zag 10/10 Test	80
C.3	KVLCC2 1/45.7 Zig-Zag 20/20 Test	81

Nomenclature

Abbreviations

Abbreviation	Definition
WASP	Wind-Assisted Ship Propulsion
WASPS	Wind-Assisted Ship(s)
DOF	Degrees Of Freedom
SHGO	Simplicial Homology Global Optimization
SLSQP	Sequential Least Squares Programming

Symbols

Symbol	Definition	Unit
x_b	Body-Fitted Surge Positive Forward	m
y_b	Body-Fitted Sway Positive Starboard	m
z_b	Body-Fitted Heave Positive Up	m
ϕ_b	Body-Fitted Roll Positive Counter-Clockwise on x_b	$^\circ$
ψ_b	Body-Fitted Yaw Positive Counter-Clockwise on z_b	$^\circ$
x_e	Earth Surge Positive Forward	m
y_e	Earth Sway Positive Starboard	m
z_e	Earth Heave Positive Starboard	m
ϕ_e	Earth Roll Positive Counter-Clockwise on x_e	$^\circ$
ψ_e	Earth Yaw Positive Counter-Clockwise on z_e	$^\circ$
U	Ship Speed	m/s
β	Leeway Angle	$^\circ$
u, \dot{u}	Surge Velocity, Acceleration in Body x_b Direction	$m/s, m/s^2$
v, \dot{v}	Sway Velocity, Acceleration in Body y_b Direction	$m/s, m/s^2$
p, \dot{p}	Roll Rate, Acceleration in Body ϕ_b Direction	$^\circ/s, ^\circ/s^2$
r, \dot{r}	Yaw Rate, Acceleration in Body ψ_b Direction	$^\circ/s, ^\circ/s^2$
u_e	Surge Velocity in Earth x_e Direction	m/s
v_e	Sway Velocity in Earth y_e Direction	m/s
p_e	Roll Rate in Earth ϕ_e Direction	$^\circ/s$
r_e	Yaw Rate in Earth ψ_e Direction	$^\circ/s$
ω	Natural Frequency in Roll	$^\circ/s$
δ	Rudder Angle	$^\circ$
α_R	Rudder Angle of Attack	$^\circ$
β_R	Leeway Angle at the Rudder	$^\circ$
u_R, v_R, U_R	Surge, Sway, and Total Flow Velocity at the Rudder	m/s
L_{pp}	Ship Length between Perpendiculars	m
B	Ship Beam	m
T	Ship Draft	m
∇	Ship Displacement Volume	m^3
GM	Transverse Metacentric Height	m
C_B	Block Coefficient	-
x_{cg}	Location of Center of Gravity in x_b	m
z_{cg}	Location of Center of Gravity in z_b	m
A_R	Movable Rudder Area	m^2

Symbol	Definition	Unit
AR_R	Rudder Aspect Ratio	-
ρ	Density of Water	kg/m^3
g	Acceleration Due to Gravity	m/s^2
X	Force in Body x_b Direction	kN
Y	Force in Body y_b Direction	kN
K	Moment in Body ϕ_b Direction	kNm
N	Moment in Body ψ_b Direction	kNm
$(X, Y, K, N)'_{u,v,r}$	Hydrodynamic Derivatives	-
a_{ij}	Added Mass	$kg, kg\ m^2$
I_{xx}, I_{zz}	Moments of Inertia	$kg\ m^2$
R_T, C_T	Calm Water Resistance, and Coefficient	$kN, -$
t_R	Steering Resistance Deduction Factor	-
a_H	Rudder Force Increase Factor	-
x_H	Position of Additional Lateral Force Component	-
x_R, z_R	Position of the Rudder	m
F_N	Rudder Normal Force	kN
γ_R	Flow Straightening Factor	-
ω_R	Rudder Wake Fraction Coefficient	-
ω_p	Propeller Wake Fraction Coefficient	-
ϵ	Rudder and Propeller Wake Fraction Relation	-
η	Ratio Between Propeller Diameter and Rudder Span	-
κ	Propeller Slip Stream Rudder Coefficient	-
J_A	Propeller Advance Ratio	-
K_T	Propeller Thrust Coefficient	-
k_{t0}, k_{t1}, k_{t2}	Propeller Open Water Coefficients	-

Introduction

Wind-assisted ships, or WASPS, are becoming increasingly more common as an energy saving option for ships as environmental concerns with global emissions are growing. Ships account for 3% of CO₂, 15% of NO_x, and 13% of SO_x emissions globally [29]. The IMO (International Maritime Organization) has put requirements on EEDI (Energy Efficiency Design Index) compliance for new ships, putting the pressure on ship owners to lower the emissions of their ships. The installation of WASP is growing as it is an effective option to increase fuel efficiency, lower emissions, and meet EEDI compliance [1].

There are a variety of WASP systems available on the market, which work to utilize the wind in different ways. Some wind propulsors are direct predecessors to traditional sails, for example Wingsails, Turbosails, and Dynarig sails, which vary in their degree of departure from traditional sail designs. Other wind propulsors like Flettner Rotors, which are large rotating cylinders, and Kites, which are parachute-like kites which pull in the direction of the wind, provide alternative ways of generating ship thrust from the wind. Compared to other fuel saving methods, WASP technology has the advantage of adding propulsion capabilities which are independent of the ship's main propulsion and power generating systems. This allows WASP technology to be applicable to a wide variety of ships, and can be minimally invasive in installation. Blue WASP Marine, the initiators of this thesis, are pioneering specialists in the field of wind-assisted ships. Blue WASP Marine has developed an advanced tool, the Pelican Performance Prediction Program (PPP), for predicting the performance and fuel-savings of wind-assisted ships. The Pelican PPP calculates ship hydrodynamic and aerodynamic forces in static equilibrium.

Wind-assisted ship technology is dependent on the wind, by nature. Wind conditions relative to the ship cannot be chosen without significantly altering the ships heading, which is not always a feasible option for ships on a tight schedule or on a route which does not allow for much alteration. Because of this dependence on the wind, the forces on wind propulsors vary in direction as the wind angle changes. During a ship turn, for example, the angle of the wind to the ship is changing and so the forces from the wind propulsors will also be changing. To achieve the goal of saving fuel, wind propulsors aim to add to the thrust of the ship, which means creating a force which has a component pointing in the forward direction of the ship. This does not mean however, that the total wind propulsor force is pointing directly forward, as there will also be a force component to in the port or starboard direction of the ship, known as the side force. The existence of the side force is an important physical difference between WASP and standard propeller propulsion, the latter of which does not have a side force component. The side force due to wind propulsion is balanced by the hydrodynamic forces on the below the water line which works to counteract the side force. This side force also has an effect on the ship turning, as the wind propulsor side force creates a turning moment on the ship, whereas a ship without wind propulsion uses only the rudder to create a turning moment.

Ship maneuvering is a field which, to put it most generally, studies the ability for a ship to change it's motions. Ship maneuverability has been standardized by the IMO and Maritime Safety Committee (MSC), by way of standardized tests [2]. The most commonly studied maneuvers are the Turning Circle and Zig-Zag tests, in which the results describe the turning tightness and the ability for the ship to change course. Maneuvering simulations are made for predicting the motions of a ship in the time domain, in calm water, during the standardized maneuvers. Maneuvering simulations are designed

to be computationally fast and are useful in the design stages of a ship in order to ensure sufficient maneuverability, and also during the operations of the ship such that the ship operators can predict the behavior of a ship before executing a maneuver. Thus, maneuvering simulations are important for ship safety as collisions and accidents can be avoided when knowledge of the ships maneuverability is known.

With WASPS becoming more common, the maneuverability must be studied and discussed in order to further the development of WASP technology. There have not been many studies which analyze the effects that having WASP installed on a ship has on the ability to execute standard maneuvers. Further, the maneuvering standards are currently set only for ships without WASP, and are not sufficient for ships with WASP systems installed due to the added consideration of wind effects and different wind propulsors, being additional control surfaces. The goal of this thesis is to study the maneuverability of wind-assisted ships and the different control options for the wind propulsors and how those can aid the maneuverability of the ship. This will be achieved by designing a time-domain maneuvering simulation tool, utilizing the capabilities of the Blue WASP Pelican PPP. The desired outcome is for the knowledge gained from the thesis to be expanded which will open the door to further studies.

WASP development is exciting, but to ensure the viability and survivability of the concept, the maneuvering safety needs to be studied. Operators, who at first may not be as comfortable and knowledgeable about WASPS, need to know the expected behavior of the ship they are operating to ensure safety of the crew. This lack of understanding in both the design and operation of such ships would have a negative effect on the impact of wind propulsion and scare away future possible users of WASP systems. Thus, wind-assisted ship maneuverability must be studied and understood in order to avoid these problems.

1.1. Fundamental Principles of Wind-Assisted Ship Propulsion

The wind propulsors on wind-assisted ships provide additional thrust in order to save fuel. The wind propulsors work by translating the wind into a force component which is pointed towards the forward direction of the ship, if the wind conditions allow. There are different wind propulsors available on the market. In this thesis, the Dynarig sails and Flettner Rotors are studied. Figure 1.1 shows the installation of Dynarig sails on the Maltese Falcon, a yacht designed by Dykstra Naval Architects [8]. Figure 1.3 shows the installation of Norsepower Flettner Rotors on the SC Connector, a cargo ship owned by Sea-Cargo [26].



Figure 1.1: Maltese Falcon by Dykstra Naval Architects, with Dynarig Sails [8]

The Dynarig sail generates a force by the wind hitting the sail at an angle of attack, or AOA (figure 1.2). To help understand the physical phenomenon of sail forces, imagine that two particles of air traveling with the wind are initially in line with each other and are about to encounter the front of the sail (the right side of the sail in figure 1.2). One particle decides to go on the top side of the sail, and the other on the bottom of the sail. Before separating, the particles agree that they will reach the other end of the sail at the same time. The particle traveling on the top side of the sail has a further distance to travel and thus has to travel at a higher speed in order to honor the agreement with the other particle. Bernoulli's principle states that a fluid at higher speed results in lower pressure, and so in this case the pressure on the top of the sail will be lower than the pressure on the bottom of the sail. This pressure difference between the bottom and the top of the sail results in a force on the sail which is upwards. Note that this analogy with Bernoulli's principle does not fully and accurately describe the total forces on a sail due to wind, but it provides a base level understanding. Alternatively, a simple experiment can be executed: hold a sheet of paper at a slight angle and blow on it (similar to the configuration of the sail in figure 1.2), then let go, and the paper will fly.

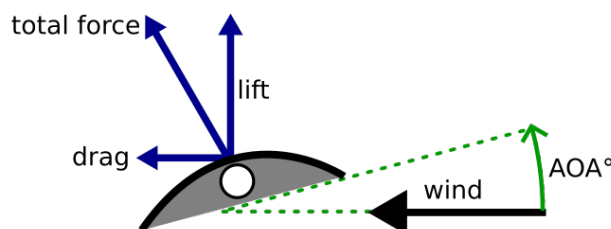


Figure 1.2: Dynarig Sail Forces



Figure 1.3: SC Connector by Sea-Cargo and Norsepower, with Flettner Rotors [26]

The Flettner Rotor wind propulsor is a large rotating cylinder. How lift is generated from a Flettner Rotor is not as intuitive, but the basic principles are the same as for the Dynarig sail. Figure 1.4 shows the forces on a Flettner Rotor which is turning counter-clockwise. The top of the Flettner Rotor has a velocity which is tangentially in the same direction as the wind, whereas the bottom of the Flettner Rotor has a tangential velocity which is directly against the wind. The tangential velocity direction is indicated by the arrows on the surface of the Flettner Rotor in figure 1.4. Since the top of the rotor is going with the wind, it adds to the flow velocity on the top surface of the rotor. Since the bottom of the rotor is opposing the wind, the flow velocity at the bottom surface of the rudder is decreased. Similarly to the Dynarig sails, the force generated can be understood from Bernoulli's principle. Since the flow velocity is higher on the top of the rotor, the pressure is lower, and likewise the pressure is higher at the bottom of the rotor. This pressure difference results in an upward force on the Flettner Rotor.

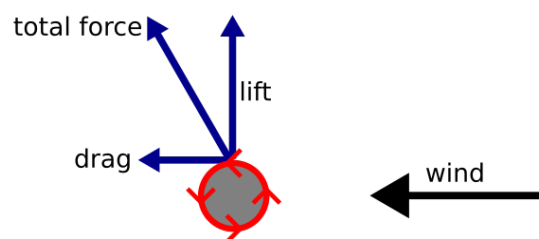


Figure 1.4: Flettner Rotor Forces

1.2. Literature Review

Maneuvering simulations for non-WASP ships are classically done in 3 DOF (degrees of freedom), those being surge, sway, and yaw. The 3 degrees of freedom describe the still-water plane motions of a ship which allow for the simulation of the ship turning. The 3 DOF model ignores heave, pitch, and roll motions which is generally a good assumption for a non-sailing ship in calm water, since there will be no translational or rotational motions in the vertical direction. However for sailing ships, it is necessary to consider a fourth degree of freedom for the roll motion, since ships under sail are typically heeled to some degree, which changes with the wind speed, wind direction, and sail trim. Thus, the maneuvering model developed in this report is in 4 DOF, with surge, sway, yaw, and roll. Maneuvering standards are set for calm water situations, so the simulations assume there are no wave-induced motions [2], and thus the pitch and heave of the ship can be justifiably neglected.

The core of maneuvering models is based on Newton's second law, $F = ma$, where the appropriate hydrodynamic forces, and for WASPS the addition of aerodynamic forces, are implemented. An equilibrium equation is made for each direction, or DOF, to be included in the model. The result is a system of second order ODE's. The coordinate system used is of importance as it dictates how the equations of motions are constructed and interpreted. Typically, there is at least a global coordinate system and a ship-body fitted coordinate system of some kind. The body coordinate system moves with the ship, and thus the equations of motions must account for the moving origin of the coordinate system.

In 1946, Schiff and Davidson produced one of the first known maneuvering models for ships, in which the turning characteristics were studied [7]. The model was built using the method of a moving coordinate system which was initially derived in Lamb's 'Hydrodynamics' in 1916 [21]. Following the work of Schiff and Davidson, Hamamoto introduced the Horizontal Body Axis coordinate system in 1993, along with a maneuvering model, which became the framework for the Maneuvering Modeling Group (MMG) based in Japan [17]. The MMG throughout the years has worked to improve the modelling of maneuvering simulations by works of Yasukawa, Yoshimura, and others ([33], [32], [15]). The work of the MMG and foundations of Hamamoto have been adapted by many other authors working on the same topic and the influences are found in more recent modern maneuvering models, including those which extend to 6 DOF [30].

Wind-assisted propulsion technology is a relatively new field of research, and the effects that wind propulsion has on ship maneuvering has not yet been thoroughly studied. A similar area that has been studied is in the tacking of sailing yachts, where ship maneuvering theory is often used. Masuyama and Keuning ([25], [24], [18], [19]) progressed this area, adapting similar equations of motion by Hamamoto and the MMG ([17], [33]). Nico van der Kolk and Giovanni Bordogna, the founders of Blue WASP Marine, focused their PhD theses on wind-assisted ships ([31], [6]). From this, van der Kolk and Bordogna developed the Blue WASP Pelican Performance Prediction Program tool which is used for this thesis to calculate the aerodynamic forces for the maneuvering model. As for the specific subject of wind-assisted ship maneuverability, Eggers and Kisjes did a study at Marin with model test experiments in 2018 ([9], [10]). From what is known, this is the first study of looking specifically at the standard maneuvering of wind-assisted ships. The Marin study involved executing Zig-Zag maneuvers with a model test ship fitted with Dynarig sails and Flettner Rotors. The tests were done in a tank with simulated wind using fans. The results provide an interesting first look into the maneuvering of sailing ships, in which this thesis aims to expand on.

1.3. Research Questions

1. What is the sufficient level of modelling required to create a maneuvering simulation for wind-assisted ships?
2. How does the addition of WASP systems effect the maneuvering ability of a ship in different wind conditions?
3. To what degree and under what settings can wind propulsor trim optimization improve the outcomes of the standard maneuvers for wind-assisted ships?
4. What are the critical maneuvering characteristics of wind-assisted ships, compared to non-sailing ships, that ship operators and designers should be aware of?

1.4. Approach

By nature, maneuvering models are quite "wide" and multidisciplinary as they estimate all of the major forces on the ship which are necessary to predict the ship motions in the time domain. When depth is added to such a wide model, the complexity increases exponentially. Especially with the additional consideration of more control surfaces, being the wind propulsors, the assumptions in modelling and the inputs to be set in order to execute the maneuver of the ship increase. There are many factors which are expected to influence the maneuverability of a wind-assisted ship, including the design of the sail configuration, the design of the hull and whether or not it is purposefully designed for wind propulsion, the control system of the wind propulsors, the ability of the ship to make frequent optimizations, the speed in which wind propulsors can trim, the balance of propeller speed and wind-assisted thrust, varying wind conditions, etc. Also, with the area of wind-assisted ship maneuverability being not yet thoroughly studied, there are not many guidelines to follow to aid in making these decisions in order to focus on the more important factors and knowing which parameters can be assumed to be constant or simply ignored. So, for this thesis there is a challenge of choosing which influencing factors to wind-assisted maneuverability should be studied. This challenge is approached by focusing on the parts which make wind-assisted ship maneuverability different from that of regular ships, in order to avoid too much overlap with the pre-existing studies on ship maneuvering in general. The wind propulsors are the main focus, specifically with regards to the control systems and the different ways the wind propulsors can be optimized in order to aid the ship in improving the outcomes of the standard maneuvers. What is also clear is the importance of studying a wide range of wind angles and speeds, since the wind propulsors depend completely on the wind, it is expected that the ship maneuverability will depend on the wind as well.

1.5. Document Structure

In this report, the background necessary for the development of the maneuvering model for wind-assisted ships will be covered first. Then, the maneuvers to be run and the chosen measured quantities will be explained, as well as the ships introduced which will be a part of the study. Finally, the results of the maneuvering simulations will be examined. The analysis on the results will begin by looking at the overall, high level, behavior of the wind-assisted ship during each maneuver. Then, an overview of the performance of different wind propulsor optimization schemes will be discussed. With the higher level understanding established, more specific wind cases with time traced results of ship motions will then be examined for each type of maneuver to study both the effects of different wind conditions, and how the wind propulsors are trimmed based on the different optimization schemes.

2

Background Theory and Developing the Maneuvering Model

2.1. Coordinate System

The coordinate system chosen is known as the "horizontal body axis system" developed by Hamamoto in 1993 [17], which has been commonplace in maneuvering models since. The coordinate system, shown in figure 2.1, is fixed at the midship location of the ship, on the still water plane. The coordinate system, being fixed on the ship, follows the motions of the ship, except for the roll motion in which the coordinate system stays on the still water horizontal plane. The origin is placed at midships in order to stay consistent with the maneuvering guidelines in which the measured quantities are defined by the midship location of the ship [2].

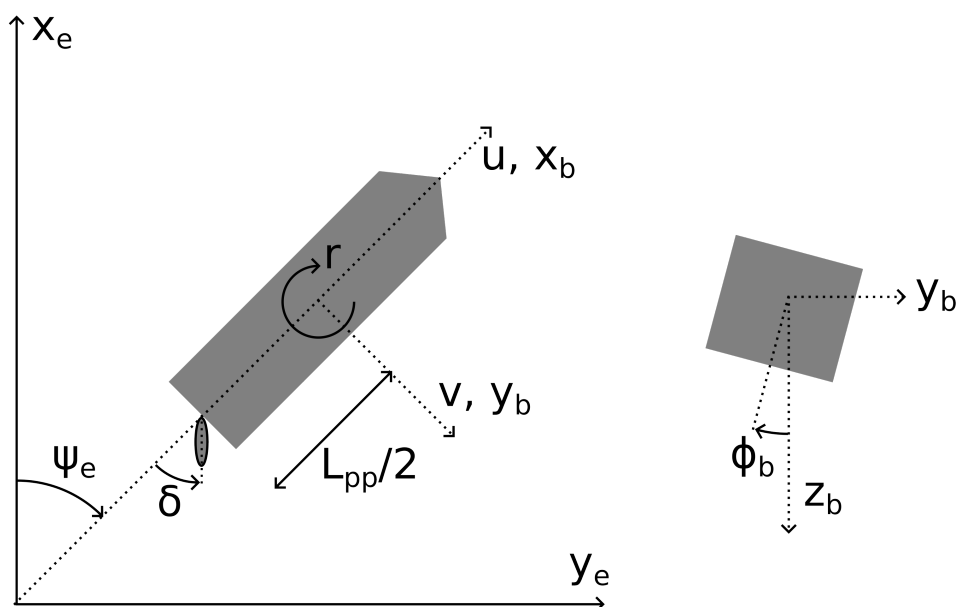


Figure 2.1: 4 DOF Horizontal Body Axis Coordinate System

The transformation matrix shown in equation 2.1 is used to convert the body fixed coordinates to an earth reference frame [13]. This is used in order to follow the location of the ship with reference to its initial position, in order to measure the desired quantities for the maneuvers.

$$\begin{bmatrix} u_e \\ v_e \\ p_e \\ r_e \end{bmatrix} = \begin{bmatrix} \cos\psi_e & -\sin\psi_e & 0 & 0 \\ \sin\psi_e & \cos\psi_e & 0 & 0 \\ 0 & 0 & 1 & 0 \\ 0 & 0 & 0 & 1 \end{bmatrix} \begin{bmatrix} u \\ v \\ p \\ r \end{bmatrix} \quad (2.1)$$

2.2. Equations of Motion

The equations of motion are the core of the maneuvering model which allow the ship motions and behavior to be solved for. The equations of motion are derived in the appendix A.1, and the final result is shown below in equations 2.2 - 2.5. The equations of motion are formed from Newton's second law, $F = ma$, where in the equations below the mass and acceleration terms are on the left hand side, and the sum of forces on the right hand side. Along with the ship's mass m , there are also the added mass terms noted by a , with the subscripts referring to the associated singular and coupled motions, where $(0, 1, 2, 3) = (\text{Surge}, \text{Sway}, \text{Roll}, \text{Yaw})$. There are additional terms on the left hand side which represent the centripetal forces, which are the terms that include vr and ur . The terms with x_{cg} and z_{cg} , which are the x and z positions of the ship's center of gravity, come from the transformation of the equations of motion from the center of gravity to the midship frame of reference.

$$(m + a_{00})\dot{u} - (m + a_{11})vr - mx_{cg}r^2 + mz_{cg}pr = X \quad (2.2)$$

$$(m + a_{11})\dot{v} + (a_{12} - mz_{cg})\dot{p} + (a_{13} + mx_{cg})\dot{r} + (m + a_{00})ur = Y \quad (2.3)$$

$$(I_{xx} + a_{22} + mz_{cg}^2)\dot{p} + (a_{21} - mz_{cg})\dot{v} + (a_{23} - mx_{cg}z_{cg})\dot{r} - mz_{cg}ur = K \quad (2.4)$$

$$(I_{zz} + a_{33} + mx_{cg}^2)\dot{r} + (a_{31} + mx_{cg})\dot{v} - mx_{cg}z_{cg}\dot{p} + mx_{cg}ur = N \quad (2.5)$$

2.3. Forces

The forces on the right hand side of the equations of motion (equations 2.2 - 2.5) are split up into their individual components as shown below in equations 2.6 - 2.9.

$$X = X_H + X_A + X_R + X_p - R_T \quad (2.6)$$

$$Y = Y_H + Y_A + Y_R \quad (2.7)$$

$$K = K_H + K_D + K_A + K_R \quad (2.8)$$

$$N = N_H + N_A + N_R \quad (2.9)$$

Where the subscript H refers to the hull, A refers to the aerodynamic forces from the wind propulsors, R refers to the rudder, and p refers to the propeller. R_T is the calm water resistance of the hull. K_D is force due to roll damping.

In the following sections, some quantities are nondimensionalized, which are notated with an apostrophe. For example, X' is the nondimensionalized version of the force X . Table 2.1 shows the factors to convert the various parameters between their dimensional and nondimensional forms.

2.3.1. Hydrodynamic Hull Forces

Hydrodynamic derivatives in 3 DOF (surge, sway, yaw) as derived by Yasukawa and Yoshimura are shown in equations 2.10, 2.11, 2.13 [33]. The forces are extended to 4 DOF to include roll motion with equation 2.12 which uses the assumption that the roll moment is proportional to the sway force with a moment arm of half the ship's draft [30]. The hydrostatic restoring moment is also included in equation 2.12. The assumption for roll being proportional to the sway force results in some inaccuracy, as ideally you would have a full set of hydrodynamic derivatives for roll, similar to equations equations 2.10, 2.11, and 2.13. The consequence of the assumption for roll is that in the model, the hydrodynamic forces in surge, sway, and yaw, are not directly effected by the ship's roll angle, which results in ship motions which are not strongly effected by the roll motion. At low heel angles, the roll assumption will stand with high accuracy, but at higher heel angles the roll would have a larger effect on the ship motions and

Table 2.1: Nondimensionalization of Quantities Relevant for Force Calculations [33]

Quantity	Factor
Forces	$\frac{1}{2}\rho L_{pp} T U^2$
Moments	$\frac{1}{2}\rho L_{pp}^2 T U^2$
Added mass	$\frac{1}{2}\rho L_{pp} T$
Lengths	L_{pp}
Velocities	U
Rotational Velocities	$\frac{U}{L_{pp}}$

the assumption would lead to some error. Typical maneuvering models do not frequently include the roll motion as non wind-assisted ships do not have a significant heeling nature in calm water. So, the hydrodynamic derivatives in roll are not available for most ships and thus the assumption in equation 2.12 is used.

$$X'_H = X'_{vv}v'^2 + X'_{vr}v'r' + X'_{rr}r'^2 + X'_{vvv}v'^4 \quad (2.10)$$

$$Y'_H = Y'_v v' + Y'_r r' + Y'_{vvv}v'^3 + Y'_{vvr}v'^2 r' + Y'_{vrr}v' r'^2 + Y'_{rrr}r'^3 \quad (2.11)$$

$$K_H = -Y_H(0.5T) - mg GM \phi \quad (2.12)$$

$$N'_H = N'_v v' + N'_r r' + N'_{vvv}v'^3 + N'_{vvr}v'^2 r' + N'_{vrr}v' r'^2 + N'_{rrr}r'^3 \quad (2.13)$$

The calm water resistance is calculated from the resistance curve given by equation 2.14, where C_T is the calm water resistance coefficient.

$$R_T = C_T \frac{1}{2} \rho L_{pp} T U^2 \quad (2.14)$$

The roll damping is calculated from the natural frequency of the ship in roll, ω (equation 2.15), following the results of the roll free decay tests by Zhang, and the method to implement the results by Journée [35] [23]. This method by Journée uses logarithmic decrementation, where the subsequent peaks in the roll decay test are ϕ_n and ϕ_{n+1} (equation 2.16). The damping model is defined based on the results of experimental roll free decay tests, and thus assumes that the ship's roll behavior during the maneuvering simulations will behave similarly to the free decay test.

$$\omega = \sqrt{\frac{mg GM}{I_{xx} + a_{22}}} \quad (2.15)$$

$$K_D = -\frac{mg GM}{\pi \omega} \ln \left(\frac{\phi_n}{\phi_{n+1}} \right) p \quad (2.16)$$

The roll damping model used is linear, whereas roll behavior of ships in reality is nonlinear. More complex and accurate damping models exist in the maritime field of seakeeping, which is the study of ship motions in waves. Studies of ship maneuvering however do not frequently study roll motion, and so a simple linear roll damping model is used as to not expand the scope of this maneuvering model to include seakeeping theory. Bridging the studies of maneuvering and seakeeping into a so-called unified model is an interesting topic and there has been work to take on the challenge, for example by Bailey, and Fossen ([4], [5], [12]). This thesis however is focused on bringing the field of maneuvering to include wind-assisted ships, and expanding the model further to include seakeeping theory is not feasible under the scope of the thesis.

2.3.2. Rudder Forces

Ship maneuverability is very sensitive to the rudder forces, since the rudder is the primary means of turning the ship. Rudder forces are dependent on not only the rudder angle, but also the ship motions because the flow of water at the rudder is changing as the ship turns. Thus, the advanced model following the procedure of Yasukawa and Yoshimura [33] has been used which accurately predicts the inflow velocity to the rudder by taking into account the ship motions, as well as the interaction between the rudder and the propeller. The rudder normal force is modelled following the work of Fujii [14], and the flow straightening factor being estimated by Lee and Shin [22].

The rudder forces and moments are formulated below in equations 2.17 - 2.20 [33]. The roll moment caused by the rudder is assumed to be proportional to the rudder sway force, with a moment arm of the location of the rudder below the still water plane.

$$X_R = -(1 - t_R)F_N \sin(\delta) \quad (2.17)$$

$$Y_R = -(1 + a_H)F_N \cos(\delta) \quad (2.18)$$

$$K_R = Y_R z_R \quad (2.19)$$

$$N_R = -(x_R + a_H x_H)F_N \cos(\delta) \quad (2.20)$$

The normal force F_N is estimated using the empirical formula for C_N [14].

$$F_N = \frac{1}{2} \rho A_R U_R^2 C_N \quad (2.21)$$

$$C_N = 6.13 \sin(\alpha_R) \frac{AR_R}{AR_R + 2.25} \quad (2.22)$$

Flow velocity (U_R) and the angle of attack (α_R) at the rudder are:

$$U_R = \sqrt{u_R^2 + v_R^2} \quad (2.23)$$

$$\alpha_R = \delta - \tan^{-1} \left(\frac{v_R}{u_R} \right) \quad (2.24)$$

The sway velocity at the rudder is effected by the flow straightening factor (γ_R) in equation 2.25, as implemented by Kose et al. [20].

$$v_R = U \gamma_R \beta_R \quad (2.25)$$

With the flow straightening factor being estimated by Lee and Shin, dependent on the sign of the leeway angle at the rudder (β_R) [22].

$$\beta_R \leq 0 : \gamma_R = -\frac{1.20501 C_{BB}}{L} + 0.7391 \quad (2.26)$$

$$\beta_R > 0 : \gamma_R = \frac{2.7236 C_{BB}}{L} + 0.021 \quad (2.27)$$

The leeway angle at the rudder (β_R) is effected by the rudder location (x'_R and z'_R) and the yaw and roll rate (r' and p') [33].

$$\beta_R = \beta - x'_R r' + z'_R p' \quad (2.28)$$

The final inflow velocity to the rudder is obtained by Yasukawa and Yoshimura [33] following the work of Kose et al. [20]. The effects of the propeller slip stream are taken into account.

$$u_R = \epsilon u (1 - w_p) \sqrt{\eta \left(1 + \kappa \left(\sqrt{1 + \frac{8K_T J_A}{\pi J_A^2}} - 1 \right) \right)^2 + (1 - \eta)} \quad (2.29)$$

With ϵ being an experimental constant representing the relation between wake fraction coefficient at the rudder and at the propeller (equation 2.30), and η is the ratio between the diameter of the propeller and span of the rudder.

$$\epsilon = \frac{1 - w_R}{1 - w_p} \quad (2.30)$$

2.3.3. Propeller Forces

Maneuvering guidelines state that the propeller speed is to be kept constant throughout the maneuver [2]. The propeller speed is calculated such that there is equilibrium in the surge direction of the ship so that the ship would maintain a steady speed. For a standard ship without wind propulsion and neglecting the aerodynamic forces on the ship, the propeller only needs to counteract the hydrodynamic resistance of the ship. However for a wind-assisted ship in normal operating conditions, the propeller speed is reduced to save on fuel when there is beneficial thrust generated from the wind-propulsors. The propeller speed is then changed as the ship heading and wind conditions change, to provide as much propeller speed as required to maintain ship speed. However as mentioned, during standard maneuvers, the propeller speed is to be kept constant. For a wind-assisted ship if the propeller speed is calculated based on the initial wind condition, this propeller speed may not be sufficient throughout the maneuver since the ship heading is changing and thus the wind angle and the performance of the wind propulsors change. This can result in a failure to complete maneuvers in some wind conditions, only at the fault of the ship saving fuel. Whereas a non-wind-assisted ship which does not have significant aerodynamic forces will have the benefit of using the same propeller speed regardless of the wind conditions. Thus for the sake of fair comparison, and to have the same propeller speed throughout the different maneuvers, the constant propeller speed used in the maneuvers for the wind-assisted ship will be calculated as if the ship is neglecting aerodynamic effects.

The effective thrust generated by the propeller in the surge direction of the ship is given by:

$$X_p = (1 - t)\rho n_p^2 D_p^4 K_T \quad (2.31)$$

With K_T being the thrust coefficient constructed from open water coefficients k_{t0} , k_{t1} , and k_{t2} :

$$K_T = k_{t0} + k_{t1} J_A + k_{t2} J_A^2 \quad (2.32)$$

With Advance ratio:

$$J_A = U \frac{1 - w_p}{n_p D_p} \quad (2.33)$$

The wake fraction coefficient at the propeller w_p is effected by the leeway angle at the propeller β_p [34].

$$w_p = w(1 - (1 - \cos^2 \beta_p)(1 - |\beta_p|)) \quad (2.34)$$

$$\beta_p = \beta - x'_p r' + z'_p p' \quad (2.35)$$

The propeller speed, n_p , is calculated by combining equations 2.31, 2.32 and 2.33, to get an expression for propeller force in terms of propeller speed. Then, the force balance in surge is solved for the propeller force X_p . The full derivation is in Appendix A.2.

2.3.4. Aerodynamic Forces

The aerodynamic forces on the wind propulsors are calculated using the Pelican software by Blue WASP Marine. The aerodynamic force calculations require inputs about the wind conditions, wind propulsor specifications, and relevant force coefficient data. Sail type propulsors like Dynarig sails use lift and drag data vs. angle of attack. Flettner Rotors use lift and drag data vs. spin ratio, where spin ratio is the ratio between the tangential velocity of the Flettner rotor and the velocity of the air.

2.3.5. Numerical Time Integration

The equations of motion (equation 2.2 - 2.5) are solved using the RK4 (4th Order Runge-Kutta) method. This method is a relatively simple explicit scheme, which works by using a weighted average of multiple slopes to estimate the next point (equations 2.36 - 2.39), rather than for example with the forward Euler scheme which only calculates one slope to estimate the next point. The intermediate slopes are calculated using f which is the function representing the 4 DOF ship accelerations $(\dot{u}, \dot{v}, \dot{p}, \dot{r})$.

$$k_1 = f(t_n, y_n) \quad (2.36)$$

$$k_2 = f\left(t_n + \frac{dt}{2}, y_n + dt \frac{k_1}{2}\right) \quad (2.37)$$

$$k_3 = f\left(t_n + \frac{dt}{2}, y_n + dt \frac{k_2}{2}\right) \quad (2.38)$$

$$k_4 = f(t_n + dt, y_n + dt k_3) \quad (2.39)$$

The 4 DOF ship velocities at each timestep (u, v, p, r) are then solved for by isolating and integrating the acceleration terms with equation 2.40, and the time is then updated with each time-step with equation 2.41.

$$y_{n+1} = y_n + \frac{1}{6}(k_1 + 2k_2 + 3k_3 + k_4) dt \quad (2.40)$$

$$t_{n+1} = t_n + dt \quad (2.41)$$

2.3.6. Wind Propulsor Trim Optimizatopn

For a ship without wind-assistance, the only control surface used during a maneuver is the rudder. For a ship with wind-assistance however, the wind propulsors are additional control surfaces which effect the ship motions and thus the outcome of the maneuver. Since maneuvering guidelines do not yet include special considerations for ships with WASP, the options will be investigated for how the wind propulsors should be treated. Two main control options will be considered: static trim and active trim. With active trim, two different trim rates will be studied. For both these options, the trim must be thoughtfully chosen in order to consider the different logical possibilities. To determine the choice of trim, an optimization is done which determines the best trim conditions for a given objective function.

For the static trim setting, the wind propulsors are trimmed at the start of the maneuver, and then held constant throughout the maneuver. The objective function is to maximize the ships acceleration in the ship-forward direction, being proportional to the total ship thrust, to estimate what might be a typical trim setting for ships with WASP in regular operating conditions. Typically on a ship with WASP installed the goal is to minimize the engine load and thus save fuel. However, in maneuvering guidelines, the propeller speed is kept constant and so significant fuel savings are not possible during the course of a maneuver. So, an objective function which maximizes the ship thrust is an estimation of what could be the wind propulsor trim of a ship in regular operating conditions. The static trim setting is designed with the idea of treating the wind propulsors as an extension of the propulsion capabilities of the ship, which is what they are designed for.

For the active trim setting, the wind propulsors are started (at $t = 0$ seconds) with the same initial condition as the static trim setting, being optimized for forward acceleration. Then for $t > 0$ seconds, the wind propulsors are trimmed continuously during the maneuver with the objective function of maximizing yaw accelerations in the corresponding turning direction, with the idea to increase the turning speed which would then result in a tighter Turning Circle, lower Zig-Zag overshoot angles, and overall more predictable ship turning characteristics. Unlike the static trim setting, the idea behind the active trim setting is to treat the wind propulsors as control surfaces; an aerodynamic extension of the rudder rather than assistants to the propulsion of the ship.

During initial testing, a brute force optimization method is used in order to get a baseline for what should be expected from the trim optimization results. Brute force optimization calculates the outputs from every possible combination of inputs, which is highly inefficient computationally, especially when continuously running optimizations throughout the maneuver. Thus, an optimization scheme is desired which provides similar results to the brute force method but with greater efficiency. The scheme SHGO, or Simplicial Homology Global Optimization, is chosen, which is a highly efficient and robust general purpose scheme to find the global minimum of a function. The SHGO scheme finds subdomains which are convex and finds the local minimums using a local optimization scheme [11]. The global minimum is then found from the local minima. The local optimization scheme SLSQP, or Sequential Least Squares Programming, has been chosen to be used within SHGO for it's efficiency.

3

Maneuvering Simulations

The maneuvering tests to be run are the Turning Circle 35, Zig-Zag 10/10, and Zig-Zag 20/20. These three maneuvers will be run in the simulation tool for a range of wind speeds and angles to test the holistic maneuvering capabilities of the wind-assisted ship/

The range of initial wind speeds are $TWS = [5 \frac{m}{s}, 10 \frac{m}{s}, 15 \frac{m}{s}]$, and initial wind angles are $TWA = [0^\circ, 45^\circ, 90^\circ, 135^\circ, 180^\circ, 225^\circ, 270^\circ, 315^\circ, 360^\circ]$, resulting in 27 simulations for to be run for each maneuver. In maneuvering studies the Turning Circle and Zig-Zag maneuvers are typically run for both initial turning directions (port side turn and starboard turn). For this study however, only the initial port side turn is studied for the Turning Circle and Zig-Zag maneuvers. To study both initial turning directions would double the amount of tests to be run, and it is justifiable to say that the overall wind-assist behavior would be mirrored between both initial turning directions, with possibly some minor differences due to the asymmetrical effects of ship turning. The port side maneuvers are typically denoted with a negative sign, i.e. Zig-Zag -10/-10, but for simplicity since only the port side turns are studied, they will be referenced as Zig-Zag 10/10.

The maneuvering standards are defined in the IMO resolution MSC.137(76), some of which depend on the length and speed of the vessel [2]. The standards for the relevant maneuvers and the KVLCC2 1/3.7 ship in this study are summarized in table 3.1. It should be noted that these maneuvering standards are only applied to vessels of 100 m length and longer, and the ship which is focused on in this study is the KVLCC2 1/3.7 which has a length of 86.8 m (table 3.3). So the specific test case of the KVLCC2 1/3.7 would not be necessarily required to adhere to these standards, but the maneuvering tests will still show the behavior of the ship as it is effected by wind-assistance which is the main interest in this study.

Table 3.1: KVLCC2 1/3.7 IMO Maneuvering Standards [2]

Maneuver	Parameter	Requirement
Turning Circle	Advance	$4.5 L_{pp}$
	Diameter	$5.0 L_{pp}$
Zig-Zag 10/10	Overshoot 1	11.8°
	Overshoot 2	27.6°
Zig-Zag 20/20	Overshoot 1	25.0°

3.1. Turning Circle

The Turning Circle 35 test, or simply the Turning Circle, (Figure 3.1) is done with a constant rudder angle of 35° , and the requirements are based on the location of the midship after a quarter turn, and half turn [2]. The advance is defined as the distance in the global forward direction (forward direction of the ship at the start of the maneuver) in which the ship has achieved a 90° change in heading. The tactical diameter is defined as the distance perpendicular to the global forward direction in which the ship has made a 180° change in heading. The maneuver and measured quantities are shown in figure 3.1.

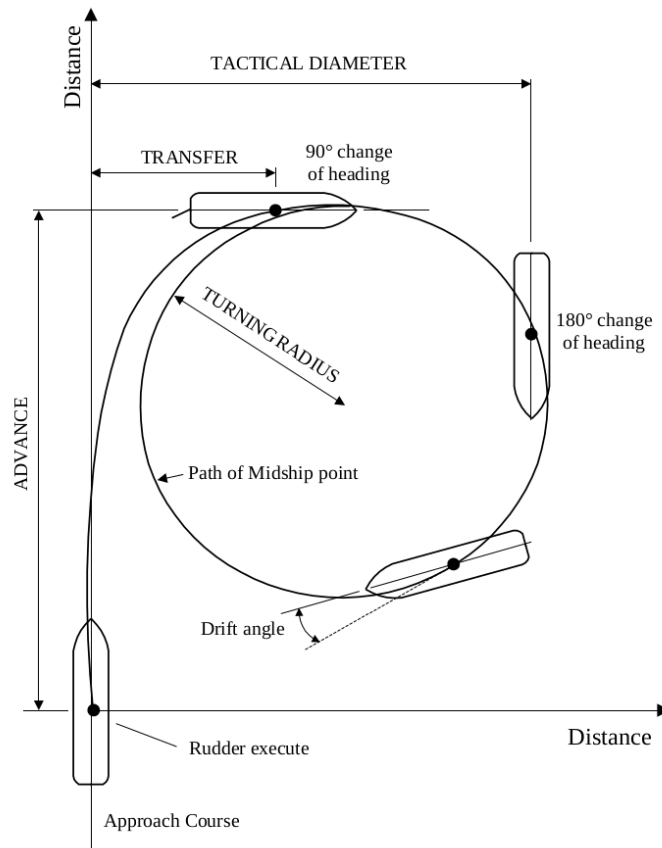


Figure 3.1: Turning Circle Maneuver [28]

3.2. Zig-Zag

The Zig-Zag maneuver (Figure 3.2) has two modes, being 10/10 and 20/20. The angles are referring to the rudder deflection that will be initiated to execute the Zig-Zag motion, and the heading changes that need to be achieved. The rudder angle is initially set at zero, being when the rudder is longitudinally inline with the ship. So for example with the 10/10 test with an initial portside turn, the ship's original heading is straight forward, and then the rudder will be pulled to 10° toward port (which is called the first execute) until the ship heading is 10° to port from its original heading, and then the rudder will be turned 10° toward starboard (the second execute) until the ship heading is 10° starboard from its original heading [2]. The requirements to be met are based on the overshoot angles, in the yaw direction, resulting from the Zig-Zag turns. For example, when the ship heading has reached 10° portside after the first execute, the 10° starboard turn is then initiated, but the ship's inertia will cause the ship to keep heading in the portside direction, and the heading yaw angle will increase to over 10° portside before it starts turning starboard. The overshoot angle is the number of degrees the ship continues to turn over 10° portside.

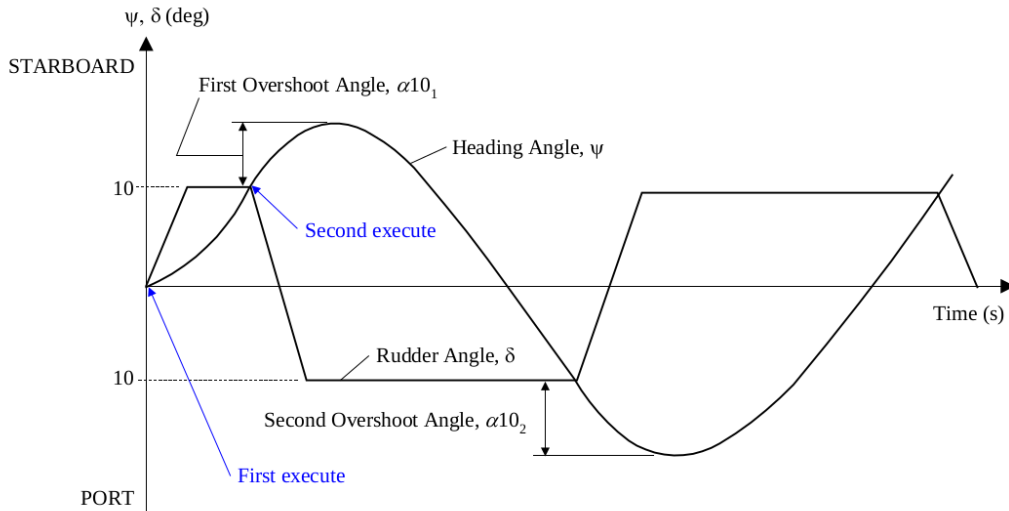


Figure 3.2: Zig-Zag Maneuver [28]

3.3. Ship Information

The ships to be used for the simulations presented in this paper are the KVLCC2 hull forms at two different scales, being 1/45.7 and 1/3.7. As shown in table 3.2 The KVLCC2 1/45.7 is used as a non-wind assisted ship validation for direction comparison to the results of model-scale tests [27]. The KVLCC2 1/3.7 is used to test the maneuverability of a wind-assisted ship, with the scale chosen to match the ship length and sail configuration of the Marin Hybrid Transition Coaster, or MHTC [10]. Qualitative validation and comparison will then be made between the KVLCC2 simulation results and the MHTC experiments. As WASPS become more common, there will be more examples and data to compare to, but as of right now the options are limited. Hence, for simplicity and sake of comparison it has been chosen to use a well studied and reported hull, the KVLCC2, modified to fit with the sail configuration of the MHTC. The main particulars of the ships to be used, as well as the full-scale KVLCC2, and MHTC, are shown in Table 3.3. The hydrodynamic derivatives and added mass values for the KVLCC2 are shown in table 3.4.

Table 3.2: Maneuver Test Schedule

Section	Purpose	Ship
4.1	Non-WASP Ship Validation	KVLCC2 1/45.7
4.2	Timestep Verification	KVLCC2 1/3.7 (without wind-assistance)
4.3 - 4.9	WASP Ship Maneuvering	KVLCC2 1/3.7 (with Dynarig and Flettner Rotors)

The sail configurations from the MHTC, as used on the KVLCC2 1/3.7, are shown in table 3.5. There are two sail configurations studied, being the Dynarig and Flettner Rotor configurations. For both setups, the wind propulsors are placed in the same locations on the ship.

Table 3.3: Main Ship Particulars (KVLCC2: [16], MHTC: [10])

	KVLCC2 fullscale	KVLCC2 1/45.7	KVLCC2 1/3.7	MHTC	Units
L_{pp}	320.0	7.00	86.77	86.77	m
B	58.0	1.27	15.73	14.00	m
T	20.8	0.46	5.64	4.40	m
∇	312,600	3.27	6231.8	4041.0	m^3
C_b	0.81	0.81	0.81	0.756	-
D_p	9.86	0.216	2.67	3.373	m
k_{t0}	0.3243	0.3243	0.3243	-	-
k_{t1}	-0.222	-0.222	-0.222	-	-
k_{t2}	-0.148	-0.148	-0.148	-	-
A_R	112.5	0.0539	8.271	8.378	m^2
AR_R	1.827	1.827	1.827	1.368	-

Table 3.4: KVLCC2 Hydrodynamic Derivatives [33], [24], [30]

Hydrodynamic Derivatives				Added Mass	
X'_{vv}	-0.040	Y'_{vrr}	-0.391	a'_{00}	0.022
X'_{vr}	0.002	Y'_{rrr}	0.008	a'_{11}	0.223
X'_{rr}	0.011	N'_v	-0.137	a_{22}	$mg GM(\frac{T}{2\pi})^2 - I_{xx}$
X'_{vvvv}	0.771	N'_r	-0.049	a'_{33}	0.011
Y'_v	-0.315	N'_{vvv}	-0.030	a_{12}	$-a_{11}(KG - \frac{T}{2})$
Y'_r	0.083	N'_{vvr}	-0.294	a_{21}	a_{12}
Y'_{vvv}	-1.607	N'_{vrr}	0.055		
Y'_{vvr}	0.379	N'_{rrr}	-0.013		

Table 3.5: Marin MHTC and KVLCC2 1/3.7 Sail Configuration Parameters [10]

	Dynarig	Flettner Rotor	Units
Area (per propulsor)	491.50	53.87	m^2
Span	29.926	17.955	m
Location Aft Propulsor (in x_b direction)	-23.68	-23.68	m ($x_b = 0$ at $L_{pp}/2$)
Location Midship Propulsor (in x_b direction)	4.60	4.60	m ($x_b = 0$ at $L_{pp}/2$)
Location Forward Propulsor (in x_b direction)	32.87	32.87	m ($x_b = 0$ at $L_{pp}/2$)

4

Results

4.1. Non-Wind Assisted Ship Maneuvering Validation

To test the validity of the developed wind-assist maneuvering model, there are not many options for studies with results to compare to for wind-assisted ships. So, in this section the simulation results of the model will be compared to a model-scale maneuvering experiment of the non-WASP KVLCC2 1/45.7 ship, a commonly studied ship in the field of maneuvering [27]. Later in section 4.9, the wind-assisted ship maneuverability will be qualitatively compared with for another vessel, the Marin Hybrid Transition Coaster, or MHTC, which is the ship used in the only study on wind-assisted ship maneuvering with data available [10].

Table 4.1 summarizes the results of the model-scale KVLCC2 1/45.7 simulation compared to the experiments. The percent difference between the simulation and experiment results are less than 10% in all cases except for the second overshoot of the Zig-Zag 20/20 test. The plots for the ships course and motions are shown in the appendix, in figures C.1, C.2, and C.3. The plots show a small oscillating behavior in the heel of the ship which is superimposed on the main heel curve. This behavior does not appear in the larger scale tests of the KVLCC2 1/3.7 ship, so it is attributed to be a consequence of the small scale KVLCC2 1/45.7. The small oscillations have the same period as the natural roll period of the ship, being about 4 seconds, so the small oscillations are assumed to be a natural behavior and not an artificial error of the numerical integration.

Table 4.1: KVLCC2 1/45.7 Maneuvering Results Validation with Marin Experimental Results [27]

	Parameter	Simulation	Experiment	Difference
Turning Circle	Advance	3.213	2.98	7.82%
	Diameter	3.240	3.09	4.85%
Zig-Zag 10/10	Overshoot 1	8.603	9.30	-7.49%
	Overshoot 2	14.546	14.70	-1.05%
Zig-Zag 20/20	Overshoot 1	15.912	14.7	8.24%
	Overshoot 2	15.700	12.9	21.71%

4.2. Timestep Verification

Figures 4.1 and 4.2 show the Turning Circle and Zig-Zag 10/10 characteristics, respectively, for the KVLCC2 1/3.7 ship versus a change in time-step to show that the results numerically converge with the timestep decreasing from 0.9 seconds to 0.01 seconds.

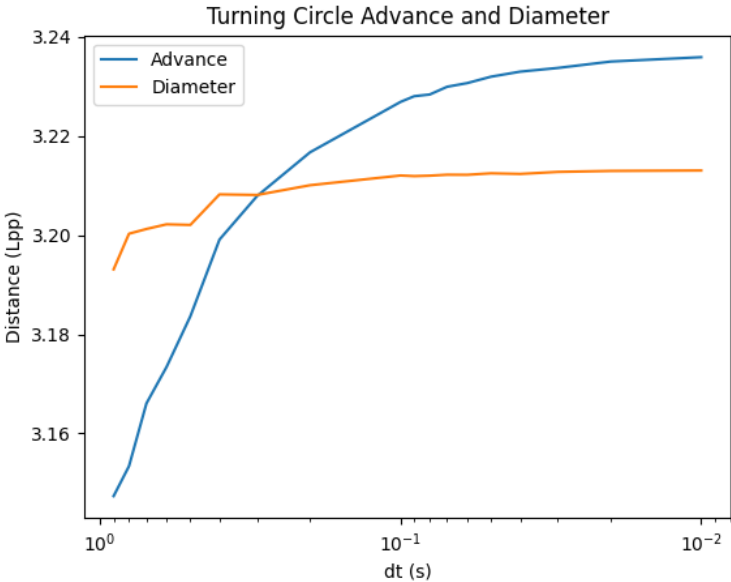


Figure 4.1: Turning Circle Advance and Diameter vs Log-scale Time-step

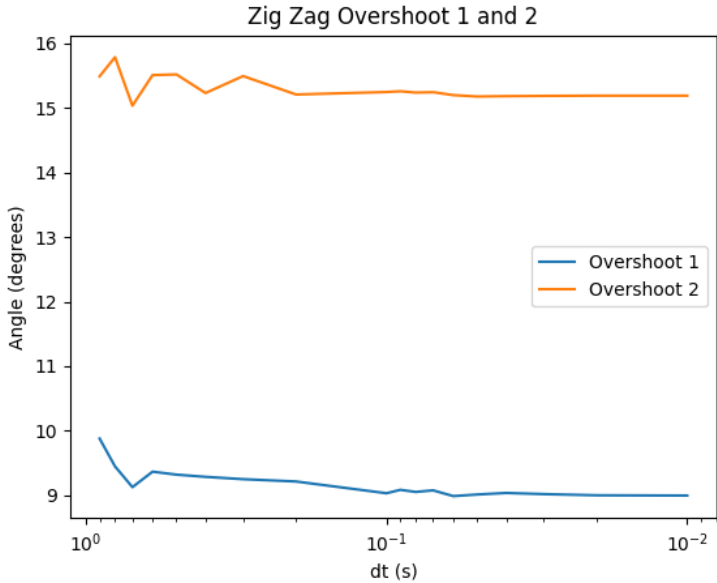


Figure 4.2: Zig-Zag 10/10 Overshoot Angles vs Log-scale Time-step

4.3. Holistic Wind-Assist Maneuvering Behavior

The results showing the maneuvering characteristics across the different wind conditions and trim settings are shown in the appendix in sections B.1 and B.2 for the KVLCC2 1/3.7 ship with Dynarig and Flettner Rotor configurations, respectively. Refer to table 3.3 and 3.5 for the specifications of the KVLCC2 1/3.7 ship and the different sail configurations. The results are shown in the form of polar and line plots which describe the main maneuvering characteristics, being the Turning Circle advance and diameter, and Zig-Zag overshoot angles, in a range of initial true wind angles from $TWA = 0^\circ$ to $TWA = 360^\circ$ and speeds from $TWS = 5 \text{ m/s}$ to $TWS = 15 \text{ m/s}$. The coordinate convention is such that a wind angle of $TWA = 0^\circ$ means the ship is sailing directly into the wind, $TWA = 90^\circ$ is wind coming from the ships starboard side, and $TWA = 270^\circ$ is coming from the ships port side. The maneuvers all start with an initial portside turn, so for example with an initial wind angle of $TWA = 270^\circ$, the ship is turning closer to the wind.

For the Dynarig configuration, the results show that the ship has a tendency to turn faster into the wind. The Turning Circle advance and diameters are smaller with wind coming from the port side than with wind coming from starboard (figure 4.3). Since the initial turn is to port side, this suggests that the ship turns faster when turning into the wind and slower when turning against it. The advance is lower for initial close-hauled winds at from port side at $TWA = 315^\circ$, and the diameter similarly benefits but especially with winds at $TWA = 270^\circ$, since after the advance has been achieved at a heading change of 90° , the ship will then still be turning quickly into the wind to reach the tactical diameter.

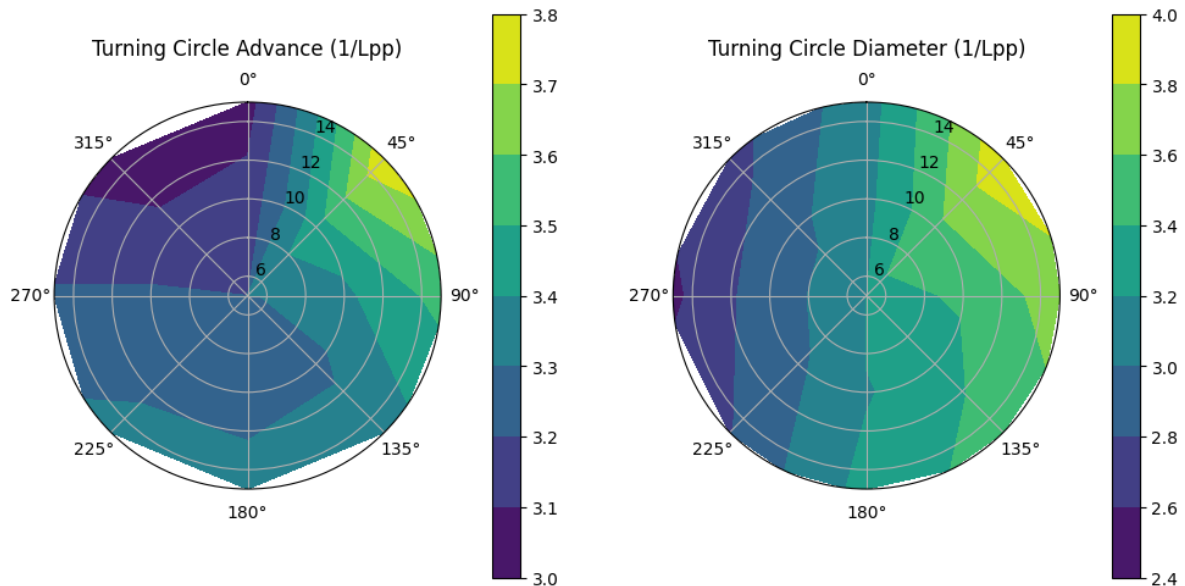


Figure 4.3: Dynarig Turning Circle, Static Trim (radial axis: TWS in m/s , polar axis: TWA in $^\circ$)

The Zig-Zag tests confirm this behavior as well. In general, the overshoot angles are higher when turning toward the wind and lower when turning away from it. For example, with wind coming from the port side, the initial Zig-Zag turn is towards the wind, which results in a high turning rate, quickly turning the ship. Then, when the rudder is at the second execute in order to turn the ship in opposite direction, the first overshoot angle becomes large because the ship is carrying more momentum from its initial fast turn and is slower to turn back away from the wind. Then, after the third execute, the second overshoot is small because the ship is turning back into the wind.

The Flettner Rotor configuration generally shows a similar behavior with faster turns going toward the wind and slower turns going away from the wind. However, the Flettner Rotors also show an ability to turn quickly when sailing directly into the wind during the Zig-Zag maneuvers (at $TWA = 0^\circ$). This is because in the static trim case, the Flettner rotors will be turned off since no thrust can be gained by sailing directly into the wind. Then, the ship will behave similarly to the non wind-assisted ship, with only the relatively small added effect of the windage on the rotors. In the active trim cases, the rotors are able to spin while sailing into the wind in order to create a helpful turning moment on the ship.

4.4. Optimization of Wind Propulsor Trim

The different trim optimization schemes are summarized in table 4.2. As previously mentioned, the static setting, S-1, optimizes for maximum forward acceleration, being proportional to ship thrust. The active settings A-S1 and A-F1 optimize for maximum yaw accelerations in the direction the ship is trying to turn, which is prescribed from the rudder angle, as described by equation 4.1. max is the function which maximizes, sgn is the function which returns the sign of a given value, δ is the rudder angle, and \dot{r} is the yaw acceleration.

$$\text{A-S1 and A-F1 Objective Function} = \max(\dot{r} \operatorname{sgn}(\delta)) \quad (4.1)$$

Two additional active trim settings, A-S2 and A-F2, have been added specifically for the Zig-Zag maneuvers in order to counteract the delay due to the wind propulsor trim rate and decrease the overshoot angles (Table 4.3). The settings A-S2 and A-F2 work by maximizing the yaw accelerations in the desired direction, as with A-S1 and A-F1, however with a constraint on the yaw rate. As shown by equation 4.2, this constraint on yaw rate is set at $\pm 0.5^\circ/s$, meaning that for example if the ship is turning at a negative yaw rate, the sails will try to maximize the yaw moment in that direction, but if the yaw rate exceeds below $-0.5^\circ/s$, the sails will start trimming to turn in the opposite direction.

$$\text{A-S2 and A-F2 Objective Function} = \begin{cases} \max(-\dot{r} \operatorname{sgn}(\delta)) & \text{if } |r| > 0.5^\circ/s \text{ and } \operatorname{sgn}(r) = \operatorname{sgn}(\delta) \\ \max(\dot{r} \operatorname{sgn}(\delta)) & \text{otherwise} \end{cases} \quad (4.2)$$

Table 4.2: Wind Propulsor Trim Optimization Settings

Name	Designation	Objective Function	Frequency
Static	S-1	Maximize \dot{u}	At $t = 0$ seconds
Active Slow	A-S1	Maximize \dot{r} subject to δ	Every 10 seconds
Active Fast	A-F1	Maximize \dot{r} subject to δ	Every 10 seconds
Active Slow Conditional	A-S2	Maximize \dot{r} subject to δ and r	Every 10 seconds
Active Fast Conditional	A-F2	Maximize \dot{r} subject to δ and r	Every 10 seconds

Table 4.3: Wind Propulsor Trim Rates for Active Trim Settings

Trim Setting	Sail Configuration	Trim Rate	Units
A-S1	Dynarig	3.0	$^\circ/s$
	Flettner Rotor	0.6	RPM/s
A-F1	Dynarig	9.0	$^\circ/s$
	Flettner Rotor	6.0	RPM/s
A-S2	Dynarig	3.0	$^\circ/s$
	Flettner Rotor	0.6	RPM/s
A-F2	Dynarig	9.0	$^\circ/s$
	Flettner Rotor	6.0	RPM/s

4.4.1. Active and Static Trim Comparison

In the Turning Circle maneuvers, for both Dynarig and Flettner Rotor configurations, the characteristics overall improve as trimming is increased from the static S-1 to the fastest active trim setting A-F1, with little change in the behavior due to wind conditions. Figure 4.4 shows the Dynarig Turning Circle results averaged across all wind conditions, for each trim setting. The static S-1 case has Turning Circle advances which are mostly above the advance for the non-wind-assisted ship, and tactical diameters which vary around the non-wind-assisted case. The fast active trim case, A-F1, however has advance and diameter values which are almost all lower than the non-wind-assisted case. This suggests that the active trim setting of maximizing the ships yaw acceleration is a success for this maneuver. The Flettner Rotor sees a similar trend of improvement in figure 4.5.

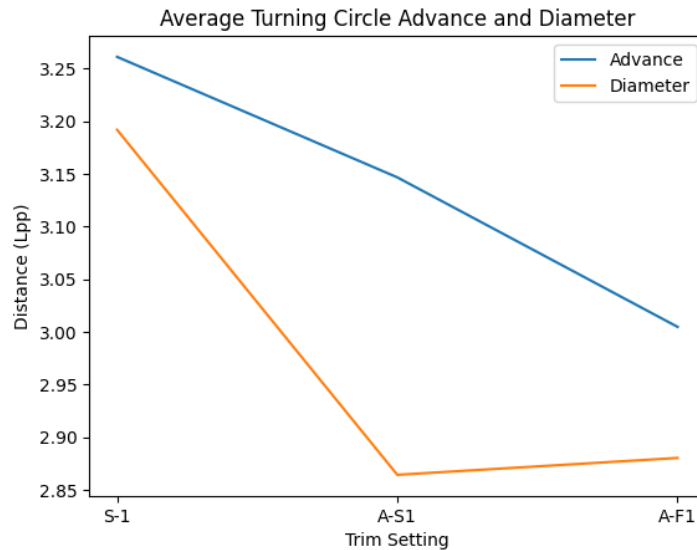


Figure 4.4: Dynarig Average Turning Circle Trim Setting Comparison

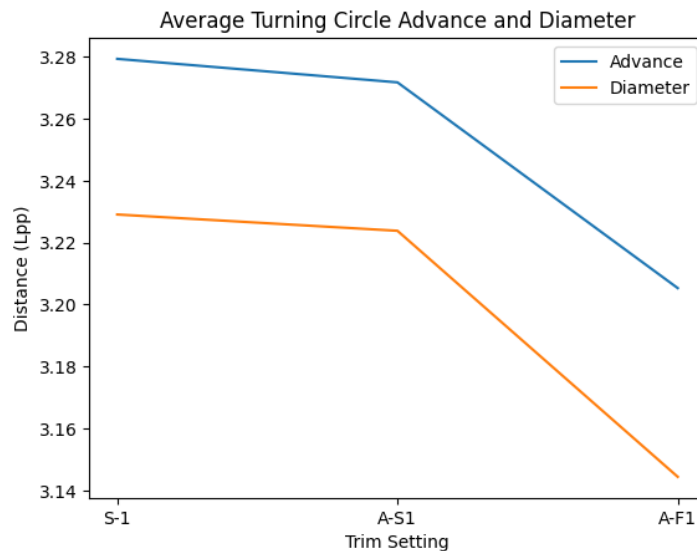


Figure 4.5: Flettner Rotor Average Turning Circle Trim Setting Comparison

For the Zig-Zag 10/10 maneuver, figures 4.6 and 4.7 show that overall, the performance does not improve between the S-1 and A-S1 or A-F1 settings. This is determined to be due to the objective function of maximizing the yaw acceleration in the desired turning direction for the A-S1 and A-F1 settings (equation 4.1), harming the ship performance rather than helping it. This is partly because of the delays in the trimming, for example when the ship is turning to port side initially, the sails start trimming to increase the yaw accelerations to the port side, however when the ship reaches the required 10° heading change and then the rudder is executed to turn to the starboard side, the sails are still trimmed to turn the ship to port and only just start adjusting their trim accordingly. This causes the overshoot angle to increase while waiting for the sails to adjust. Even with faster wind propulsor trim rates with A-F1, maximizing yaw acceleration is not beneficial to reducing the overshoot angles for the majority of cases. The optimized trim for the A-S1 and A-F1 settings increases the turning rate for the approach to the overshoot angle which increases the momentum of the ship which is then harder to counteract when turning the opposite direction. Thus, such a simple optimization scheme is not beneficial to the Zig-Zag maneuver for all wind conditions, and rather a more pre-emptive optimization scheme which does not let the yaw rate become too high for the ship to recover, would be beneficial. Thus, the A-S2 and A-F2 settings were introduced with the purpose to improve the maneuvering behavior for the Zig-Zag maneuver by utilizing an objective function which changes based on not only the rudder angle but also the yaw rate. 4.2.

The performance of the ship with the Dynarig configuration during the Zig-Zag 10/10 maneuver shows a general improvement using the A-S2 and A-F2 settings (figure 4.6 and 4.8). The Flettner Rotor configuration also show a general improvement, but mainly for the A-F2 setting due to the trim rate for the A-S2 setting being too slow (table 4.3). The trends are similar for the Zig-Zag 20/20 maneuver compared to the Zig-Zag 10/10 maneuver, and there are significant drops in overshoot angles at the A-F2 setting (figures 4.8 and 4.9).

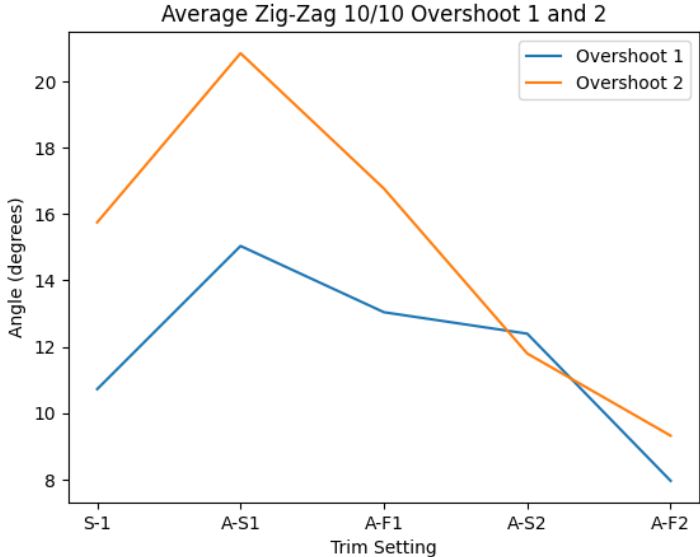


Figure 4.6: Dynarig Average Zig-Zag 10/10 Trim Setting Comparison

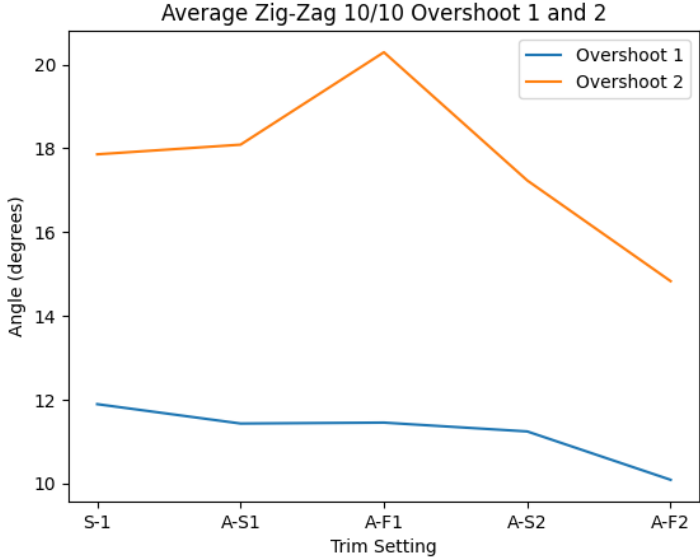


Figure 4.7: Flettner Rotor Average Zig-Zag 10/10 Trim Setting Comparison

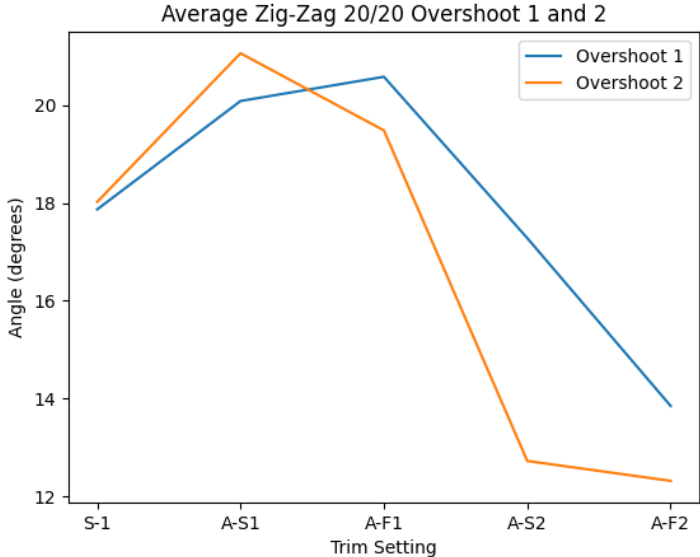


Figure 4.8: Dynarig Average Zig-Zag 20/20 Trim Setting Comparison

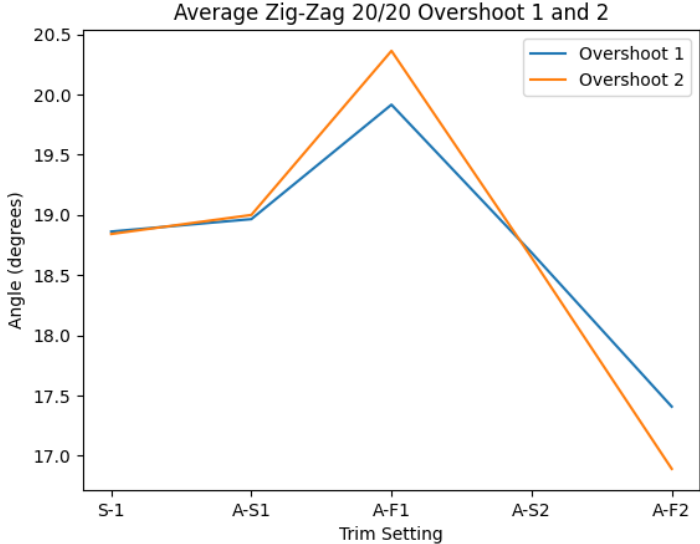


Figure 4.9: Flettner Rotor Average Zig-Zag 20/20 Trim Setting Comparison

4.5. Dynarig Turning Circle Case

To better understand how the trim optimization works and effects the maneuverability, a specific wind case will be looked at for the Dynarig sail configuration carrying out the Turning Circle maneuver at a specific wind case of $TWS = 15 \text{ m/s}$ and $TWA = 270^\circ$. This wind case is chosen because it is an example of the Turning Circle being significantly impacted by the wind-assistance, with very low values for tactical diameter (figures B.1, B.2, B.3).

4.5.1. Trim Setting S-1

Figure 4.10 shows the results of the maneuver with the static S-1 trim setting. The sails initially start as optimized for thrust and remain constant for the remainder of the maneuver. The measured Turning Circle characteristics for this case is an advance of $3.21L_{pp}$, being the distance in the global y_e direction of the ship from it's original location after a 90° change in heading, and tactical diameter of $2.56L_{pp}$, being the distance in the global x_e direction of the ship from it's original location after a 180° change in heading. As discussed, the ship has a tendency to turn quickly into the wind. With the initial TWA of 270° , the wind is coming directly at the ships port side at the start of the maneuver. With the turn to port, the ship is constantly turning toward the wind until the completion of the maneuver at a heading change of 180° , when the tactical diameter is measured. So, with the ship constantly turning close to the wind, the turn is fast and it results in a tighter circle, producing a relatively low advance and tactical diameter. For comparison, the advance and diameter are $0.02L_{pp}$ and $0.65L_{pp}$, respectively, smaller than those of the same ship without wind-assistance.

After the tactical diameter is achieved at 180° change in heading, the ship continues to turn, completing the "circle" which is now more of a teardrop shape, and begins another circle which is above and to the right of the original circle as seen in the plotted course in figure 4.10. For a ship without wind-assistance, the second circle would carry on with a similar course and overlap the original circle. But this is not the case for the wind-assisted ship. After the ship completes the first tactical diameter, it is turning away from the wind and eventually running with the wind. At this point, with the sails at a trim of around 126° , the ship velocity increases, as can be seen in the plot of U at around $t = 150$ seconds (figure 4.10).

The coordinate system is such that at 0° trim, the sails are longitudinally parallel with the ship with the concave side of the sail pointing starboard. Also it is important to note that the sails are bound on -180° to $+180^\circ$, so any vertical lines on the Dynarig trim plots, for the active cases which follow, are when the sails are wrapping around the bounds between -180° and $+180^\circ$. So, with the sails fixed at 126° , and the ship travelling down wind at $t = 150$ seconds, the sails are close to being perpendicular with the wind generating ship thrust due to drag on the sails, and a component which is to the ships starboard side. This results in a sailing condition which does not help the ship turn to port and so the ship makes a large arching turn into it's second Turning Circle. This behavior then results in the second Turning Circle being shifted downwind, and above (in global coordinates) of the first Turning Circle. At the very end of the plotted course, the ship is turns quickly as it is turning back into the wind, mimicking the behavior in the first Turning Circle.

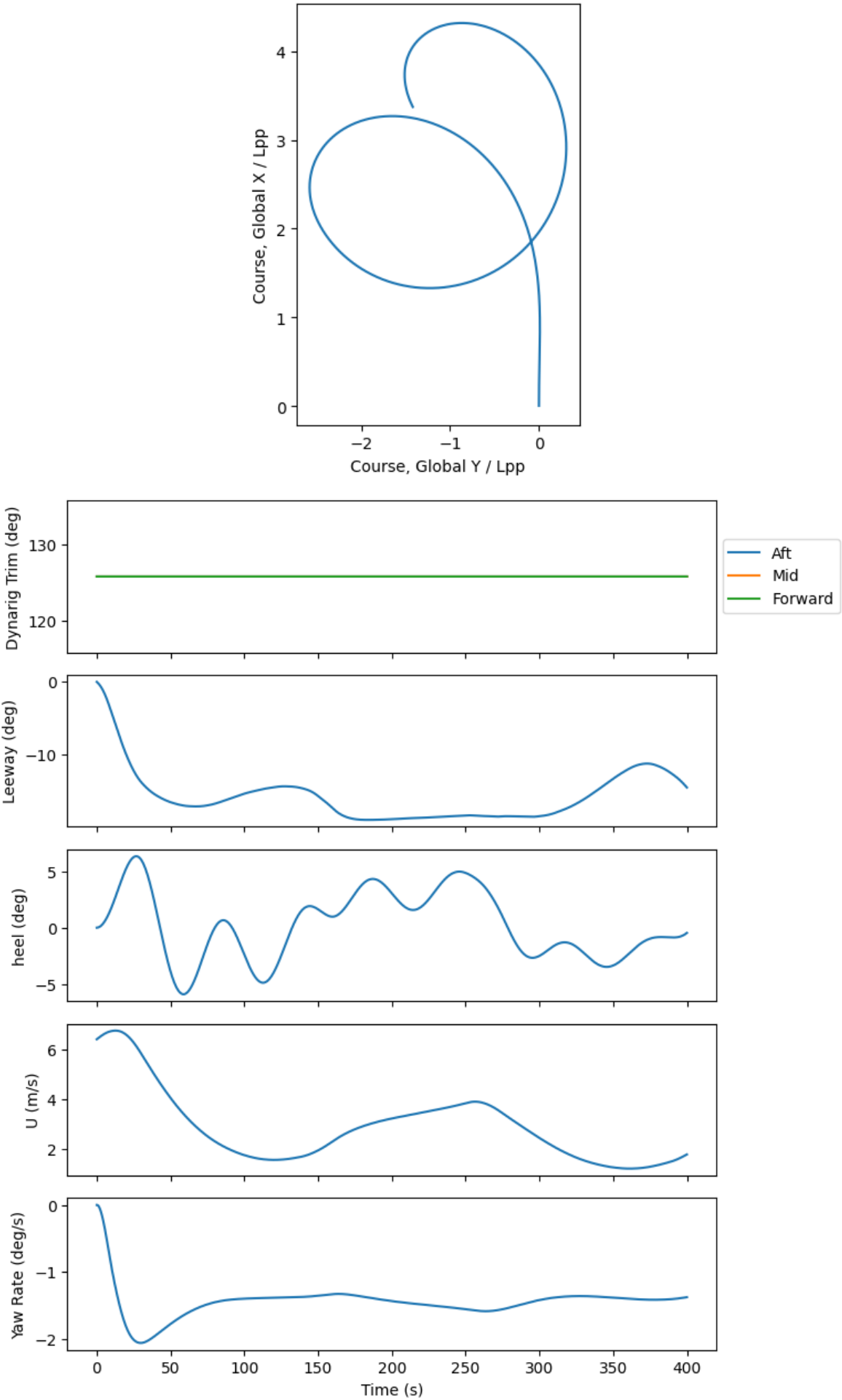


Figure 4.10: KVLCC2 1/3.7 Dynarig S-1 Turning Circle Maneuver TWS = 15 m/s , TWA = 270°

4.5.2. Trim Setting A-S1

Figure 4.11 shows the Turning Circle maneuver for the same wind conditions as above, but for the A-S1 setting, being the slower of the active trim settings which work to maximize the ship's yaw accelerations based on which direction the rudder is turning the ship. The effect of this objective function can be seen clearly in the plot of yaw rate in 4.11, where the yaw rate mostly stays around $-1.7^\circ/s$ with some variance, where as for the static S-1 case in figure 4.10, the raw rates settles around $-1.4^\circ/s$.

The Dynarig sails trim slowly due to the slower trim rate of the A-S1 setting (table 4.3), and so the sails might not always be reaching their desired set point before a different set point is calculated from the optimization scheme. For example, when the simulation begins the sails move from their initial condition of being optimized for thrust and start aiming for their new set points. This takes the sails to being trimmed at -180° by around $t = 20$ seconds. From this point, the aft sails stay at this position for another $t = 50$ seconds but the front and middle sail start trimming to another set point, but it is not clear what the goal was because the ship heading is changing which changes the TWA, which then results in a new set point being calculated. Eventually at $t = 75$ seconds the trim of the front and middle sail is at 0° and the aft sail is trimming to a new set point but is at about -150° . At this point the ship is sailing close to the wind, and the sails are creating a yaw moment which helps the ship turn as the front and middle sails have a resulting force which is to the port side of the ship, and the aft sail has a resulting force which is starboard and aft. This yaw moment turns the ship toward port, as desired by the trim optimization. However, it takes some time to reach a helpful set point.

The resulting Turning Circle advance is $3.17L_{pp}$ and tactical diameter is $2.04L_{pp}$. The results for the A-S1 show a decrease from the S-1 case by $0.04L_{pp}$ and $0.52L_{pp}$ for the advance and tactical diameter, respectively. This supports the observation that the slower trim setting A-S1 does not trim fast enough to significantly improve the Turning Circle advance, being the earliest measured quantity, but after about 75 seconds from the start of the maneuver a trim is reached which helps the ship turn more effectively, causing a significantly lower turning diameter. Similarly to the S-1 case, the second Turning Circle is also shifted downwind of the original Turning Circle, but with tighter turns due to the active trim setting A-S1 which allows the ship to turn faster and complete a full second circle. Additionally, the second Turning Circle for the A-S1 is more inline downwind of the first Turning Circle, whereas the for the S-1 the second circle was further above the first, in the global x_e direction.

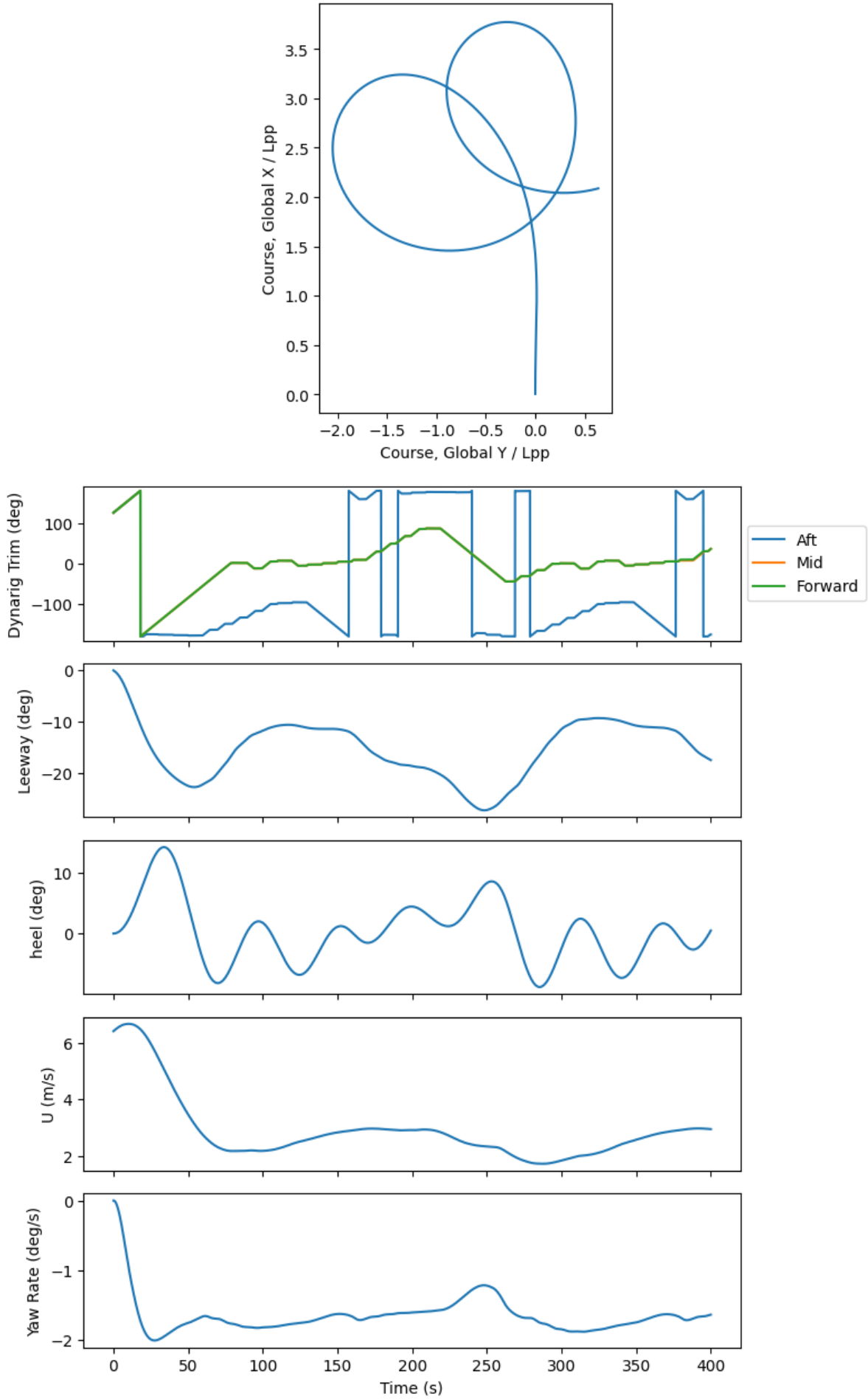


Figure 4.11: KVLCC2 1/3.7 Dynarig A-S1 Turning Circle Maneuver TWS = 15 m/s , TWA = 270°

4.5.3. Trim Setting A-F1

The Turning Circle maneuver for the A-F1 trim setting is shown in figure 4.12, with the same wind conditions as the above discussed. The result is a Turning Circle advance of $2.72L_{pp}$ and tactical diameter of $1.94L_{pp}$. Unlike the A-S1, the advance is decreased significantly by $0.45L_{pp}$, supporting the claim that the A-S1 is too slow for these conditions to reduce the advance due to the slower trim rates, whereas the A-F1 setting was able to decrease the advance significantly, benefiting from the faster trim rate. The Turning Circle diameter is also reduced from the A-S1 to the A-F1 setting with a reduction of $0.10L_{pp}$, however being not as large of a reduction since the diameter was already significantly reduced from the S-1 to the A-S1 setting. The sail trim in the A-F1 acts similarly to the A-S1 setting, but is able to reach it's set points faster. Most significantly in the range of $t = 0$ seconds to $t = 50$ seconds where the Turning Circle advance is being approached, the A-S1 setting was not able to reach it's optimized trim but the A-F1 succeeds which results in a reduction in Turning Circle advance. The second Turning Circle is similar between the A-S1 and A-F1 settings, where the second circle is downwind of the first circle, being slightly lower and tighter in the A-F1 setting.

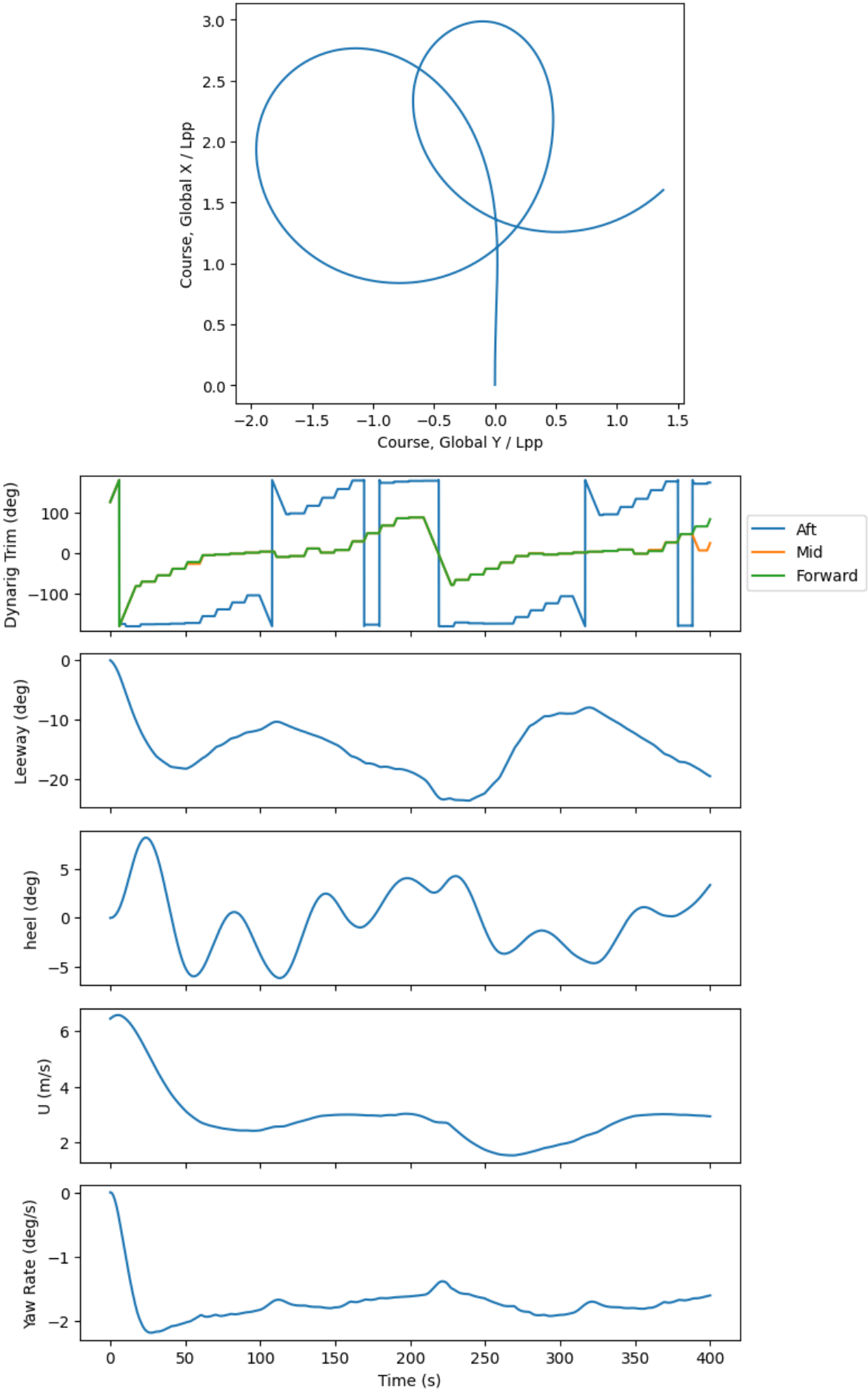


Figure 4.12: KVLCC2 1/3.7 Dynarig A-F1 Turning Circle Maneuver TWS = 15 m/s , TWA = 270°

4.6. Dynarig Zig-Zag 10/10 Case

Now, a specific wind case will be studied for the Dynarig sail configuration and the Zig-Zag 10/10 maneuver. Figure B.4 shows that for the S-1 setting the wind conditions of $TWS = 15 \text{ m/s}$ and $TWA = 315^\circ$ are the most severe conditions with the highest first overshoot angle and lowest second overshoot angle of the Dynarig Zig-Zag 10/10 tests. Figure B.8 shows that for the A-F2 setting, being the most successful for the Zig-Zag maneuvers, the first overshoot is greatly reduced. Hence this specific wind case for the Zig-Zag 10/10 has been chosen because the actively trimmed sails are able to improve the results in the harsh wind conditions.

The following figures 4.13, 4.15, and 4.16, show the results for the Dynarig configuration and Zig-Zag 10/10 maneuver for $TWS = 15 \text{ m/s}$ and $TWA = 315^\circ$, for the S-1, A-F1, and A-F2 trim settings, respectively. The progression of these trim settings shows that the overshoot angles get more and more consistent and within an acceptable range. The trim settings A-S1 and A-S2 will not be investigated further since they are the slower counterpart of A-F1 and A-F2 and will not add significantly to the discussion.

4.6.1. Trim Setting S-1

For the static trim setting S-1 in figure 4.13, the wind on the Dynarig sails causes the ship to sway far into the port side turns, but then switches directions quickly on the starboard turns. This behavior leads to a large first overshoot and small second overshoot. Since the wind is at $TWA = 315^\circ$, the ship is sailing close hauled with the wind coming from the port side. As discussed in previous sections, the ship has a tendency to turn quickly toward the wind and slowly when turning away from the wind, which is strongly on display in these wind conditions. Since the sail trim is static, it is optimized for thrust in the initial state of the ship and then kept constant throughout the maneuver. With the Dynarig sails in this position, the resulting force has components in the forward direction, contributing to the thrust, and also toward starboard. The resulting overshoots are a high first overshoot at 29.5° and a low second overshoot of 4.8° .

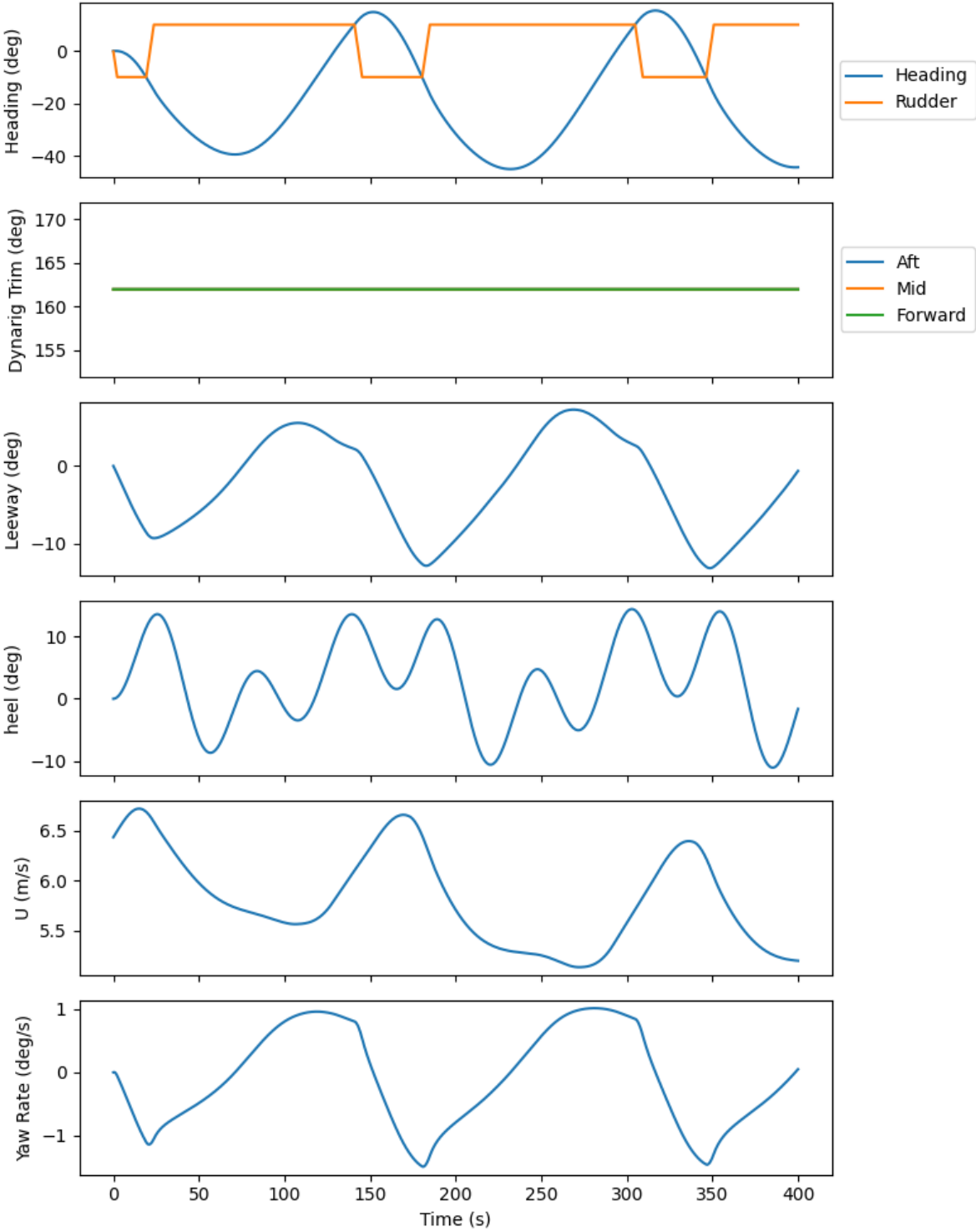


Figure 4.13: KVLCC2 1/3.7 Dynarig S-1 Zig-Zag 10/10 Maneuver TWS = 15 m/s , TWA = 315°

4.6.2. Trim Setting A-F1

The next trim setting to be investigated is the A-F1 setting, being the faster active trim setting for the objective function of maximizing the yaw accelerations in the turning direction as prescribed by the rudder (table 4.2). The results of the overshoot angles are more consistent compared to the S-1 setting, with lowering the first overshoot of 18.2° but increasing the second overshoot with 14.1° . As discussed in section 4.4.1, the A-S1 and A-F1 settings are not very successful overall for the Zig-Zag maneuvers. This conclusion can be clearly seen in figure 4.15, where the yaw rates quickly accelerate, as achieved through the objective function, which makes it hard for the ship to recover and change directions once required by the maneuver. For the static S-1 setting, the yaw rates reach around $-1.1^\circ/s$ and $0.9^\circ/s$ for the first two overshoots, respectively (figure 4.13). In comparison, for the A-F1 setting the yaw rates reach $-1.3^\circ/s$ and $1.2^\circ/s$ and at a higher acceleration (figure 4.15).

These higher yaw rates are reached by the sails trimming mainly between around -180° and -45° , as shown in figure 4.14. The mid and forward sails follow the trim mostly identically, while the aft sails oppose them. So, with the sails trimmed at -180° , the sails are inline with the ship with the concave side pointing port side, which in this case with $TWA = 315^\circ$, results in a starboard side resultant force from the sails. When the sails are trimmed at about -45° , the sails are pointing toward the wind with the resultant force pointing aft and port. So when the front and mid sails are at -180° and the aft sail is at -45° , the resulting force of the front of the ship is toward starboard and the aft of the ship is toward port. These opposing forces creates a counter-clockwise yaw moment on the ship which helps the ship turn to starboard (right side of figure 4.14).

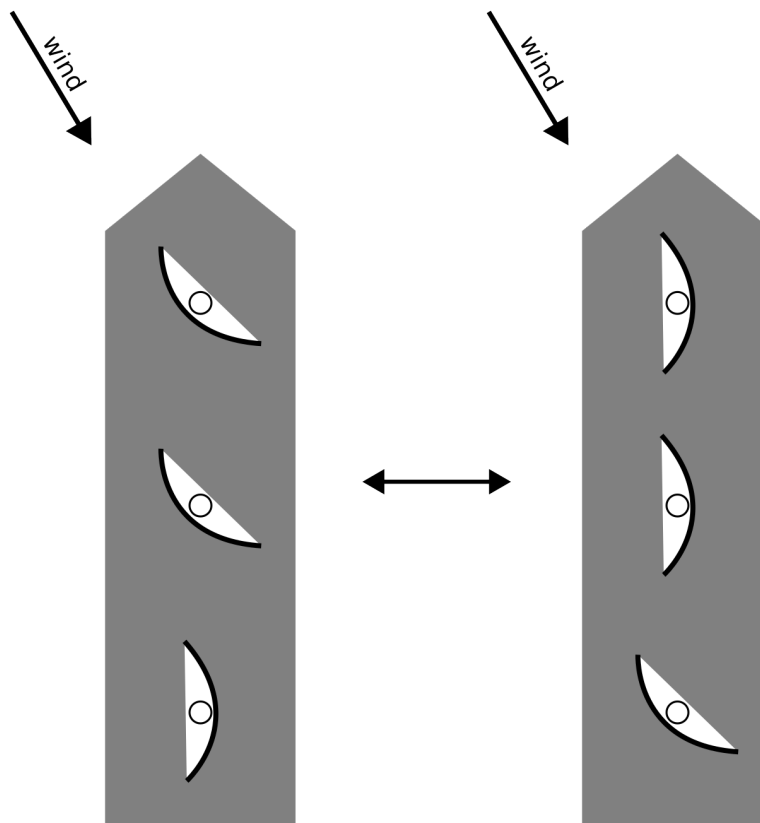


Figure 4.14: KVLCC2 1/3.7 Dynarig A-F1 Zig-Zag 10/10 Trim TWS = 15 m/s , TWA = 315°

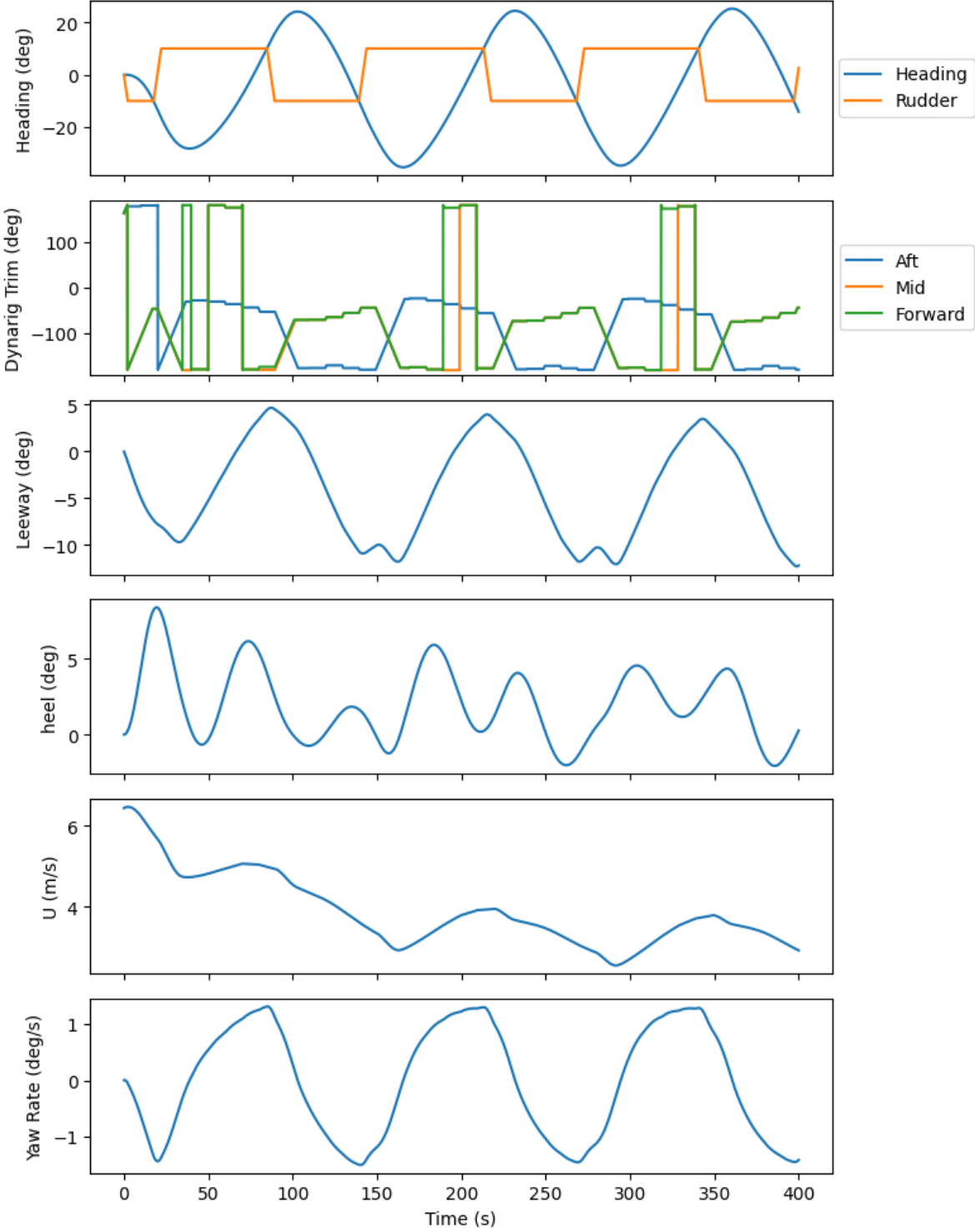


Figure 4.15: KVLCC2 1/3.7 Dynarig A-F1 Zig-Zag 10/10 Maneuver TWS = 15 m/s , TWA = 315°

4.6.3. Trim Setting A-F2

The final trim setting which is most successful in improving the Zig-Zag maneuver is the A-F2 setting. The objective function differs from the A-F1 setting, where the objective is for maximizing the yaw accelerations and the direction is subject to the ship reaching a yaw rate of $\pm 0.5^\circ/s$, as well as the rudder angle (table 4.2). The purpose of this objective function is to keep the yaw rates in a more beneficial range, not allowing them to become too high where the ship cannot compensate. Similarly to the the A-F1 setting, the sails trim between around -180° and -50° (figure 4.14), but the difference is that the sails change their set point more frequently in A-F2 as the ship's yaw rate exceeds $\pm 0.5^\circ/s$ (figure 4.16). With this objective function for A-F2 being more pre-emptive to help the the ability of the ship to change course, the yaw rates reach $-0.9^\circ/s$ and $1.0^\circ/s$ for the first two overshoots, respectively. These are less than the yaw rates for the A-F1 setting which allows the ship to achieve the turns more easily and produce lower overshoot angles, with the first and second overshoot angles being 6.8° and 5.0° , respectively. The drop in overshoot angles is significant between the trim settings, where the first overshoot angle for the A-F2 case is 22.7° lower than in the S-1 case. The increase of the second overshoot angle in the A-F1 case is also recovered in the A-F2 case with a decrease of 9.1° .

An interesting behavior can be seen in the yaw rate plot of figure 4.16 where due to the A-F2 setting the change in yaw rate does not directly go back and forth from negative to positive as it did for the S-1 and A-F1 settings but instead has regions when approaching the overshoot angles in which the yaw rate decreases in magnitude. These dips occur because, for example when the ship is turning toward starboard from $t = 20$ seconds to $t = 90$ seconds in figure 4.16, the sails are initially trimmed to turn the ship toward starboard but once the ship reaches a $\pm 0.5^\circ/s$ yaw rate at $t = 50$ seconds, due to the A-F2 setting, the sails trim to turn the ship toward port meanwhile the rudder is still turning the ship in the starboard direction. This reduces the yaw rate, as desired by the objective function, but at this stage from $t = 50$ seconds to $t = 90$ seconds the sails and rudder are in essence fighting each other to try to turn the ship in opposite directions. The rudder regains control of the ships turn at $t = 75$ seconds which allows the ship to complete the second turn and then the rudder changes to turn the ship to port. The overshoot angle is then small for two main reasons: (1) because the yaw rate is not as high going into the overshoot, reducing the ships inertia, making it easier to change directions, and (2) because the negative effects of the sail trim delay are reduced because the sails begin trimming to change the ship directions pre-emptively rather than waiting for the rudder to change

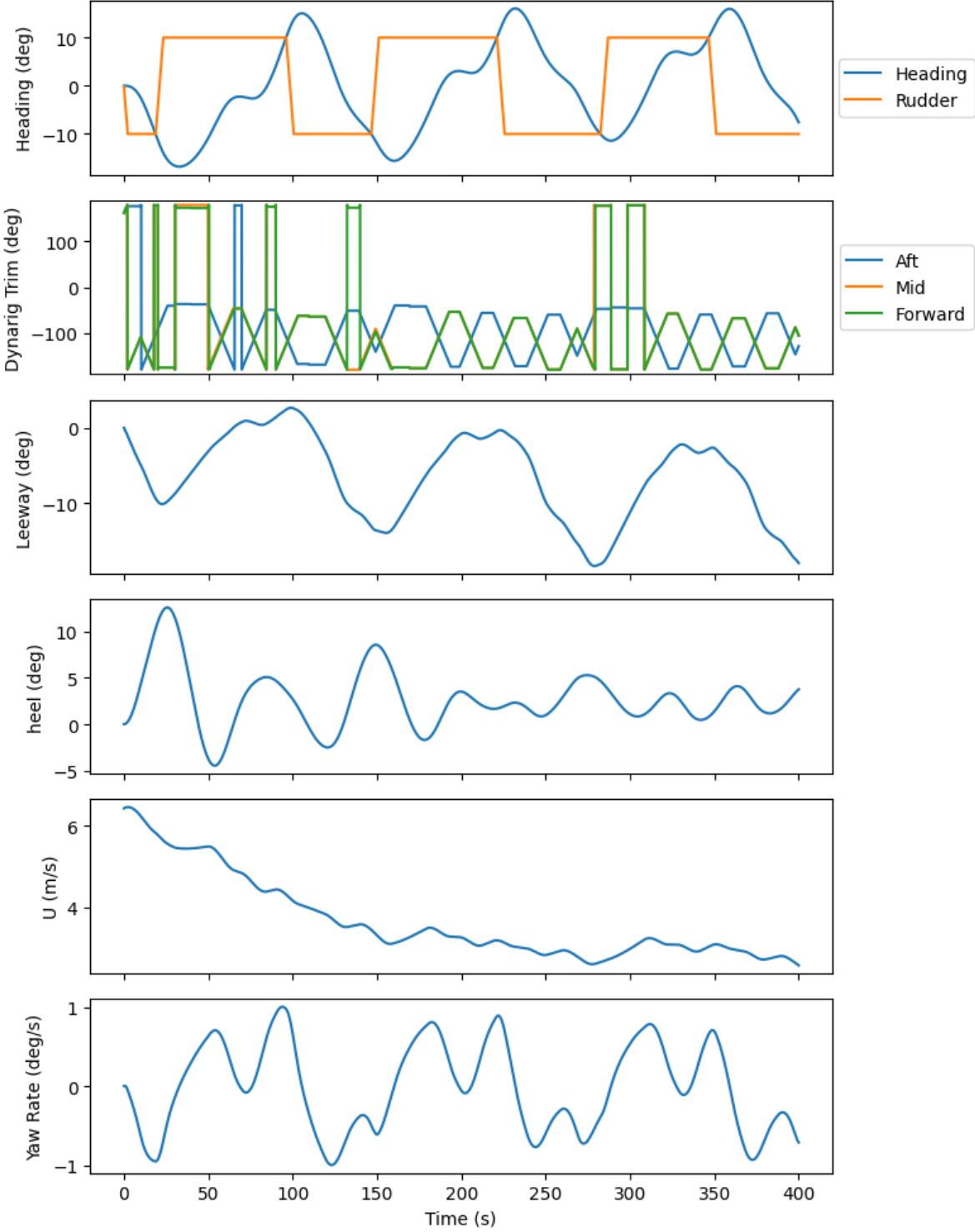


Figure 4.16: KVLCC2 1/3.7 Dynarig A-F2 Zig-Zag 10/10 Maneuver TWS = 15 m/s , TWA = 315°

4.7. Flettner Rotor Zig-Zag 20/20 Case

A specific wind case for the Flettner Rotor will be looked at now for the Zig-Zag 20/20 maneuver, with wind conditions of $TWS = 15 \text{ m/s}$, and $TWA = 45^\circ$. The trim settings S-1 and A-F2 will be looked at as they are the two ends of the spectrum with regards to their maneuvering performance. The A-F1 setting will not be discussed here, as the differences between the objective functions between A-F1 and A-F2 are discussed in section 4.6 for the Dynarig configuration, and the comparisons remain true for the Flettner Rotor configuration. The A-S2 setting will not be discussed here either since it is the same objective function as A-F2 but with slower trim rates in which the results do not vary significantly from the S-1 case (figures B.22 and B.26).

4.7.1. Trim Setting S-1

Figure 4.17 shows the results of the Zig-Zag 20/20 maneuver for the static trim setting S-1 with wind conditions $TWS = 15 \text{ m/s}$, and $TWA = 45^\circ$. The trim is optimized for thrust in the initial conditions, which results in the three Flettner Rotors turning at 250 RPM . The sign convention for the Flettner Rotors is such that a positive RPM translates to a counter-clockwise rotation. The results of the maneuver are a first overshoot angle of 13.7° and a second overshoot angle of 24.2° . The second overshoot is higher than the first overshoot due to the tendency of the ship to turn quickly towards the wind and slowly turning away from the wind, and since the wind is at $TWA = 45^\circ$ from the starboard side, the first turn is turning away from the wind and the second turn is turning toward the wind. Hence the behavior is oppositely mirroring the results in section 4.6 where the Dynarig configuration was executing the Zig-Zag 10/10 but with wind coming from the port side and the first overshoot was higher than the second overshoot.

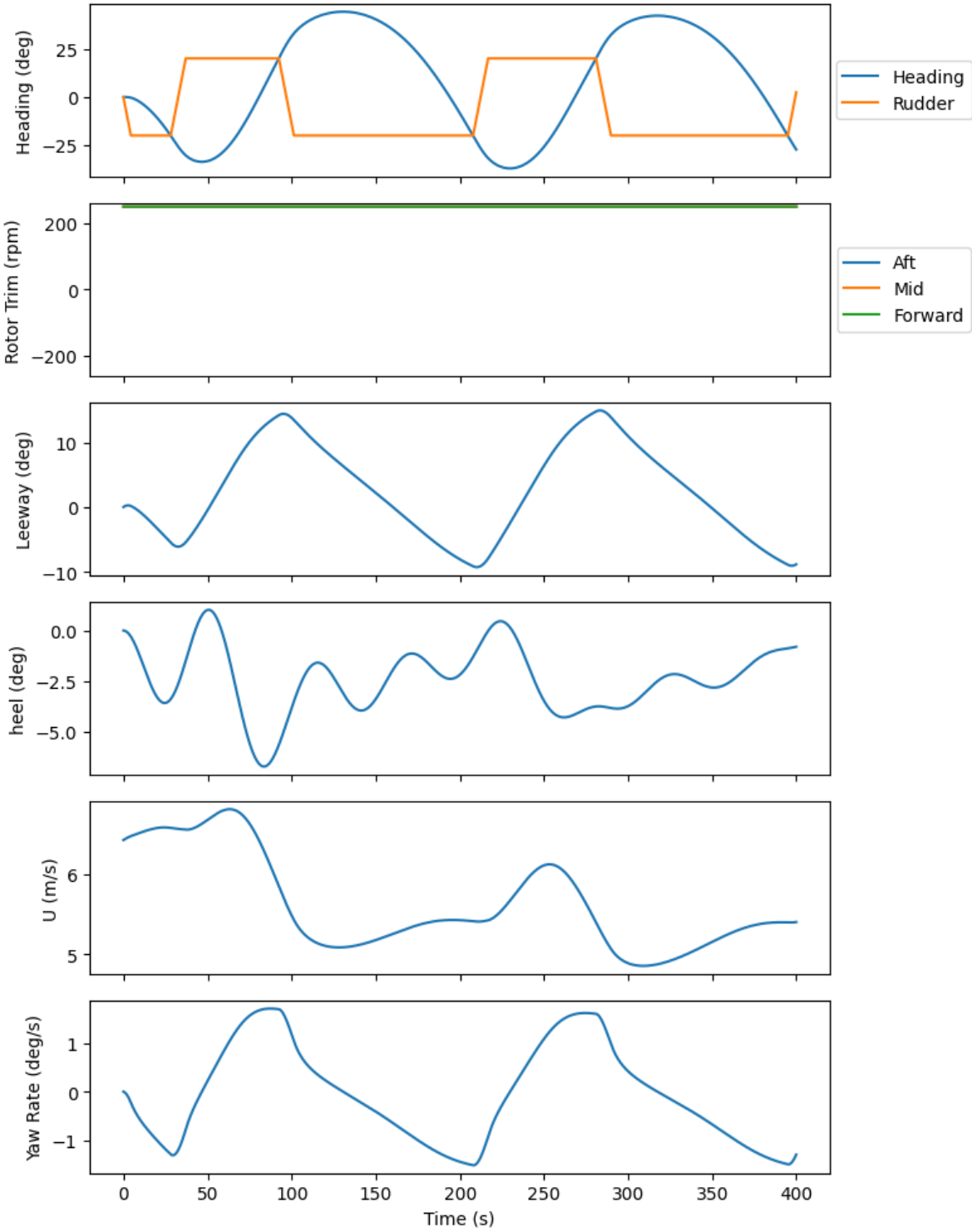


Figure 4.17: KVLCC2 1/3.7 Rotor S-1 Zig-Zag 20/20 Maneuver TWS = 15 m/s , TWA = 45°

4.7.2. Trim Setting A-F2

The Flettner Rotor Zig-Zag 20/20 results for the A-F2 trim setting are shown in figure 4.19. The objective function of A-F2 improves the results of the maneuver by changing trim in order to help the ship turn more effectively. The overshoot angles are 13.2° for the first overshoot and 17.0° for the second overshoot. This is a decrease of 0.6° and 7.2° for the first and second overshoots, respectively, going from the S-1 to the A-F2 trim setting. The active trimming on the Flettner Rotors is similar to the Dynarig configuration as discussed in section 4.6 in that the forward and middle propulsors oppose the aft propulsor to create the turning yaw moment on the ship. As seen in the Rotor Trim plot of figure 4.19, and displayed in the diagram of figure 4.18, the rotors come to a pattern of switching between positive and negative *RPM* to create this aforementioned opposing behavior. With $TWA = 45^\circ$ and when the front and middle rotors are at a positive *RPM* and the aft rotor is at a negative *RPM* (left side of figure 4.18), the resulting force vector of the front and middle rotors will be port-side and forward, while the resulting force vector of the aft rotor will be starboard-side and aft. The resulting yaw moment on the ship is then acting to turn the ship to port.

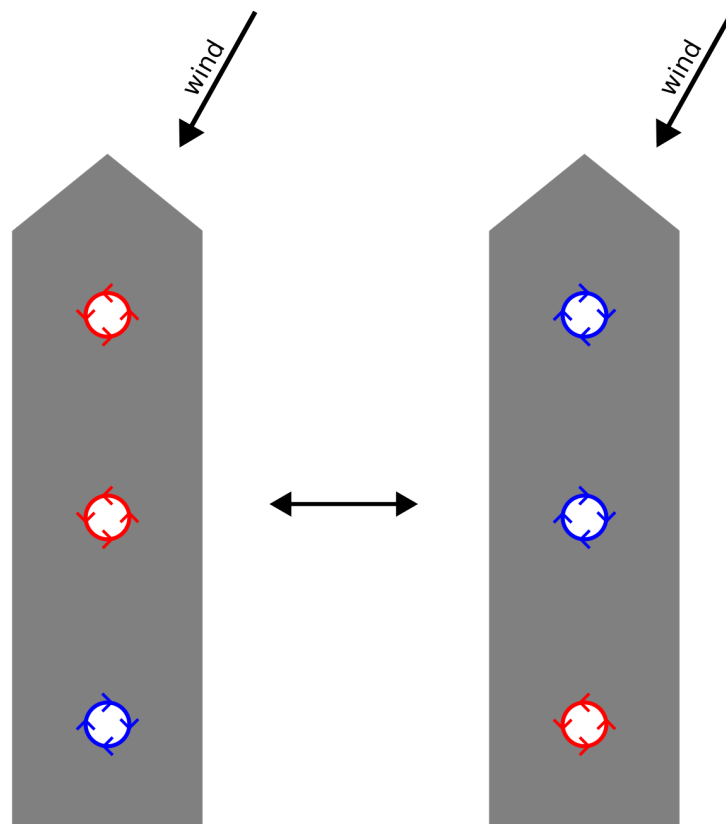


Figure 4.18: KVLCC2 1/3.7 Flettner Rotor A-F2 Zig-Zag 20/20 Trim TWS = 15 m/s , TWA = 45°

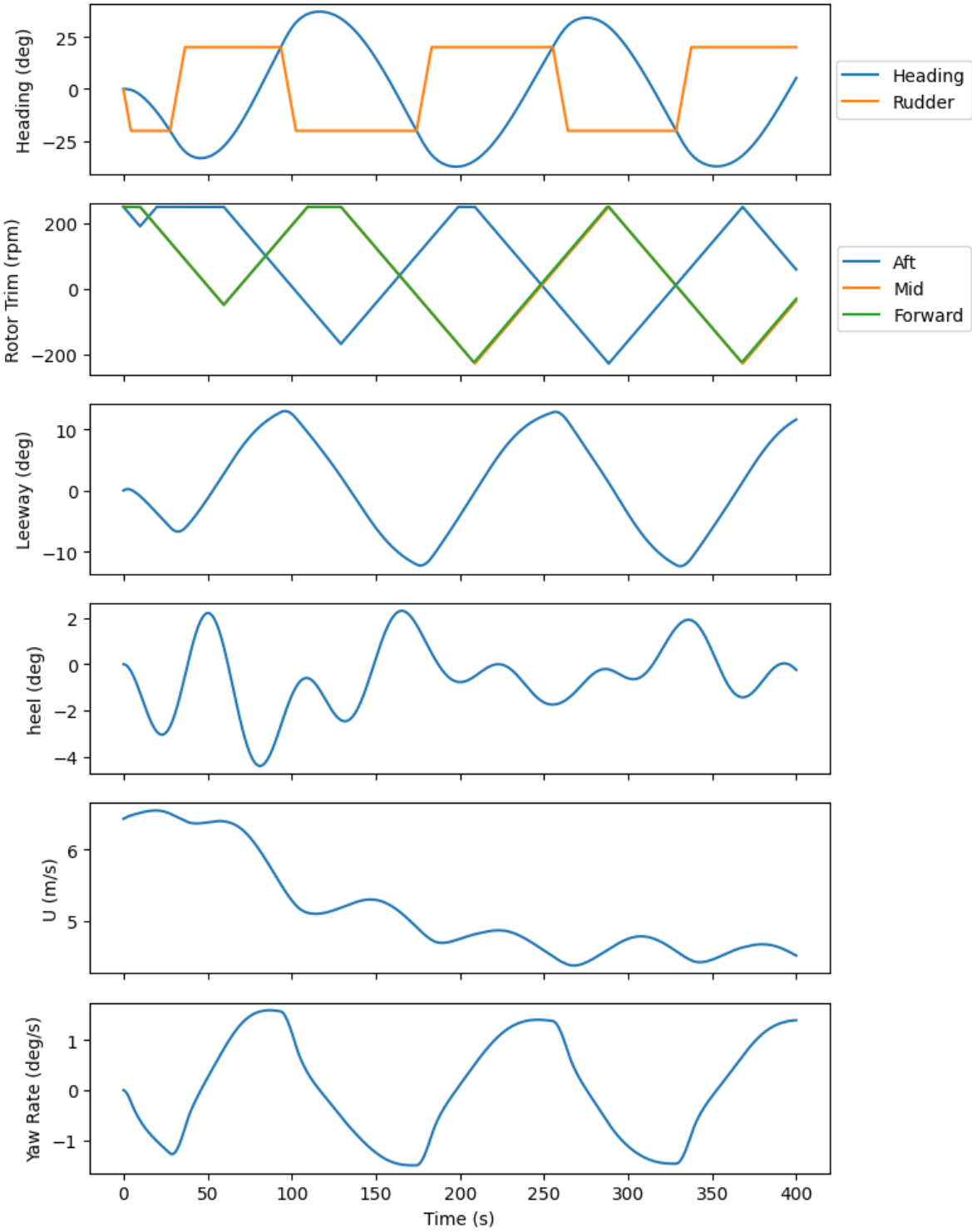


Figure 4.19: KVLCC2 1/3.7 Rotor S-1 Zig-Zag 20/20 Maneuver TWS = 15 m/s , TWA = 45°

4.8. Trim Setting and IMO Compliance

Table 4.4: Maneuvering Results for Active and Static Trim Settings

			% Passed IMO Standards				
			S-1	A-S1	A-F1	A-S2	A-F2
Turning Circle	Dynarig	Advance	100	100	100	-	-
		Diameter	100	100	100	-	-
	Rotor	Advance	100	100	100	-	-
		Diameter	100	100	100	-	-
Zig-Zag 10/10	Dynarig	Overshoot 1	75	50	50	58	96
		Overshoot 2	96	83	100	100	100
	Rotor	Overshoot 1	71	71	58	71	71
		Overshoot 2	88	88	100	88	100
Zig-Zag 20/20	Dynarig	Overshoot 1	100	88	92	100	100
	Rotor	Overshoot 1	96	96	100	100	100

Table 4.4 summarizes the main results of the maneuvering tests for different control schemes and their compliance with IMO standards [2]. For the Turning Circle maneuver with both sail configurations and all trim settings, the maneuvers were successfully completed for every wind condition and control scheme.

For the Zig-Zag 10/10 maneuver the Dynarig configuration sees moderate success with the static sail trim case with a 75% pass rate for overshoot 1 and 96% for overshoot 2. The active trim cases show worse IMO compliance on average for the first overshoot angle, for the reasons discussed in the previous section. The second overshoot angle however has the most success in the fastest active trim setting with 100% compliance. This is likely due to the general trend that a higher first overshoot angle results in a lower second overshoot angle, since the turns are in opposing directions. If the ship is able to adjust course from starboard to port quickly, then adjusting from port to starboard will be more difficult.

Similarly with the Flettner rotor configuration, the Zig-Zag 10/10 maneuvers show an overall less successful first overshoot and a more successful second overshoot when the trim setting is increased from static to fast active trimming. The static (S-1) and slow active trim (A-S1 and A-S2) settings are almost identical due to the slow trimming rate of $0.6 \text{ RPM}/s$. The Zig-Zag 20/20 maneuver shows more success than for the Zig-Zag 10/10 maneuver, due to its more forgiving first overshoot angle requirements.

4.9. Qualitative Validation of Wind-Assisted Ship Maneuvering

In 2018, Marin completed a series of experimental tests of the maneuvering of wind-assisted ships [9]. The study included Zig-Zag maneuver tests for a model ship, the Marin Hybrid Transition Coaster, or MHTC, with a Dynarig and Flettner rotor configuration. The Dynarig configuration completed the Zig-Zag 10/10 maneuver under close-hauled starboard side wind conditions, and the Flettner Rotor configuration under broad-reached starboard side wind conditions. The relative scale and sail configurations are the same for the simulated KVLCC2 1/3.7 ship and the Marin MHTC ship, but the hull forms and rudders are different, as well as the experimental setup and wind modelling, so a direct quantitative comparison is not done at this stage. Instead, the results are compared for the two different ships under similar wind conditions and the overall maneuvering behavior and comparison between the two sail configurations are studied. The results are shown in table 4.5.

Table 4.5: Qualitative Maneuvering Validation

			Simulation KVLCC2 1/3.7	Experiment MHTC [9]	Units
Zig-Zag 10/10	Dynarig Close-Hauled	Overshoot 1	2.66	7.7	°
		Overshoot 2	31.82	21.5	°
	Rotor Broad-Reached	Overshoot 1	9.77	21.4	°
		Overshoot 2	19.72	-	°

For the Dynarig configuration, the behavior is similar between the KVLCC2 simulation results and the Marin MHTC experiments but the effects are more extreme in the simulation results. Figure 4.20 shows the motions of the simulated ship throughout the maneuver, and what is surprising is that the ship takes quite some time to achieve the first overshoot, and actually diverts its heading in the starboard direction before it can turn to port side to complete the first execute. The sails are thus overpowering the rudder and throwing the ship off course before it can react and settle on the correct turning behavior. This behavior did not occur in the Marin experiment, and the ship was able to execute the first port side turn quickly. The difference here is likely due to the difference in sail control and initial rudder state. Both the simulation and Marin experiment use statically trimmed sails, but the trim is achieved differently. In the Marin experiment, before the maneuver is carried out, the trim is manually chosen which results in the highest forward speed while keeping a stable course. Additionally, in the Marin experiment, the initial rudder angle is chosen which allows for the ship to stay at a stable course before the maneuver, and this initial rudder angle is then considered the 0° rudder angle and the subsequent changes (i.e. $+10^\circ$ and -10°) are made relative to the starting point. However in this simulation, the sail trim is chosen which only maximizes the ship-forward acceleration and does not pay attention to the course stability. The initial rudder angle in the simulation is set to true 0° , being in line with the ship longitudinally. Thus, in the simulation the ship is thrown off course by the forces on the sails and lack of rudder to compensate initially which drives the ship to turn to starboard.

The Zig-Zag tests for the Flettner Rotor configuration have less similarities between the KVLCC2 simulation and the Marin MHTC experiment results (figure 4.21). In the Marin MHTC tests, while sailing in broad-reached wind with the initial turn going toward the wind, the first overshoot is large, and the recovery time was long such that the second overshoot was not able to be achieved due to the limitations of the test basin. The large first overshoot for the MHTC is attributed to the increase in Flettner Rotor side forces as the ship turns closer to the wind, and since the MHTC center of lateral resistance is expected to be near the bow, these side forces create a yaw moment on the ship which is opposite to the direction the ship is trying to turn [9]. The KVLCC2 on the other hand, seems to have a center of lateral resistance which is more toward midships, and this means that the side forces on the Flettner Rotors due to these wind conditions do not create as overwhelmingly large of a yaw moment that cannot be counteracted by the rudder.

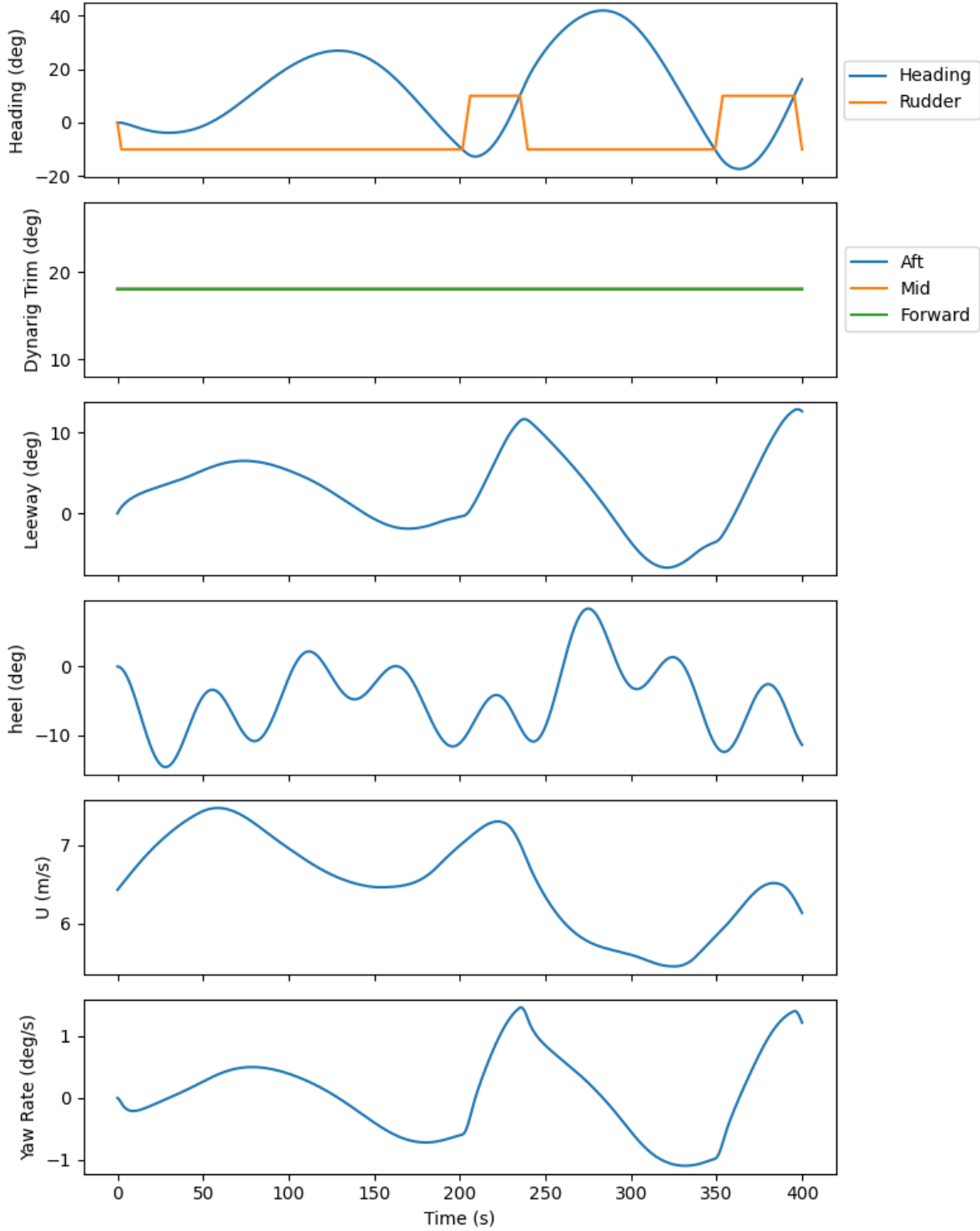


Figure 4.20: KVLCC2 1/3.7 Dynarig Static Trim Zig-Zag 10/10 Maneuver TWS = 15 m/s , TWA = 45°

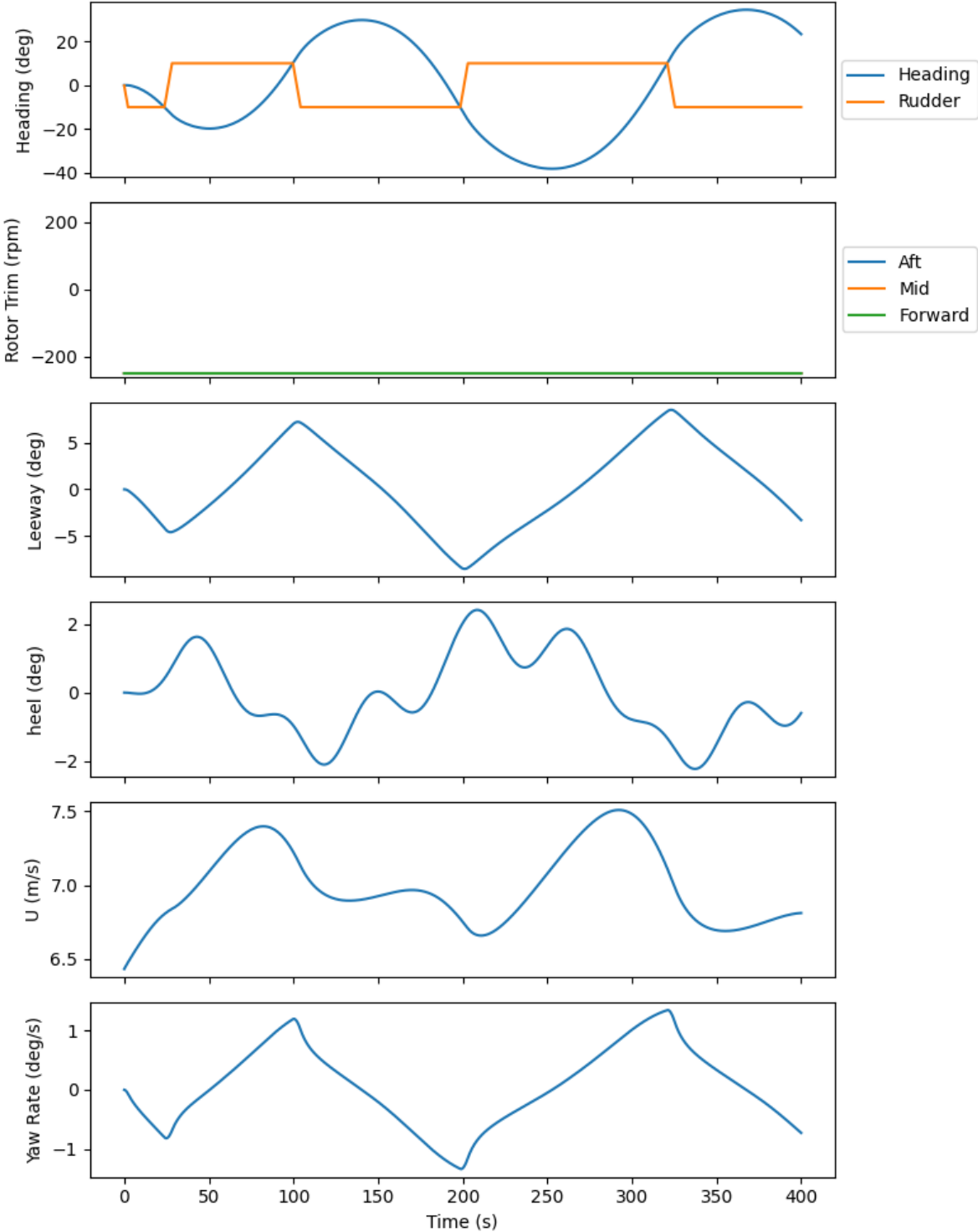


Figure 4.21: KVLCC2 1/3.7 Flettner Rotor Static Trim Zig-Zag 10/10 Maneuver TWS = 15 m/s , TWA = 225°

5

Conclusion

This thesis sets out to study the maneuverability of wind-assisted ships and to explore different options regarding wind propulsor optimization settings. Wind-assisted ships are an up-and-coming field in the maritime industry in which there is a lot of potential for fuel savings. The studies on the topic of WASP are at early stages and there is still a lot to explore, with one of those areas being maneuvering. Maneuvering itself is a broad study as all of the major forces on the ship need to be accounted for within a single model. The addition of WASP on the ship only adds to this complexity. Due to this breadth of complexity that comes with the topic of wind-assisted ship maneuverability, there is an amount of narrowing down that needs to be done in order to fit the study into a single masters thesis. Thus, it was chosen to focus mainly on the wind propulsor trim objective function and trimming rates, and keep other factors constant. But there are other important factors on maneuverability that should be studied, for example different hull forms and/or appendages which are designed for wind-assistance, optimum propeller speed to be used, different sail configuration designs with varying locations of wind propulsors, and others.

For the holistic maneuvering behavior of the wind-assisted ship, the characteristic in which the ship turns quickly into the wind and slowly turning away from the wind is apparent in all of the simulations, and is the main behavioral factor which effects the maneuverability of the ship. For the Turning Circle maneuvers, this means that turning toward the wind results in lower values for advance and tactical diameter. For the Zig-Zag maneuvers, the first overshoot is generally large when initially turning into the wind, since the yaw rate becomes high and it is more difficult for the ship to the turn away from the wind once the heading change requirement has been achieved of 10° or 20° , depending on the maneuver. The high first overshoot then usually results in a lower second overshoot, since the ship is turning slower away from the wind while approaching the second overshoot able to turn quickly when turning back into the wind to achieve the second overshoot.

When considering the effectiveness of different wind propulsor optimization schemes, the Turning Circle simulations were overall successful for the wind-assisted ship. The results of different trim settings showed that the Turning Circle becomes much tighter with fast trim settings, with the goal of maximizing turning rate being successful. The IMO standards were reached with a comfortable margin for all of the Turning Circle simulations. The Zig-Zag tests were more difficult to complete to stay within IMO standards, due to the demanding nature of changing course so rapidly. The trim rates of the wind propulsors, in their current state in technology, are quite slow. Hence, faster theoretical trim rates were introduced. After the initial tests with the Zig-Zag maneuvers, it was clear that the objective function of maximizing yaw accelerations in the turning direction prescribed by the rudder (A-S1 and A-F1) was not helpful in reducing overshoot angles. Thus, a new objective function was introduced (A-S2 and A-F2) which changes the sail trim if a certain yaw rate has been reached, or if the rudder has changed directions. The A-F2 trim setting shows overall higher success over the static trim case for the Zig-Zag maneuvers.

There is a clear potential for wind-assisted ships to be sufficiently maneuverable in order to comply with IMO standards. The ship maneuverability however depends highly on the control and optimization of the wind propulsors, and the trim rate the wind propulsors are able to achieve. It is not yet known what will be required of wind-assisted ships due to IMO standards since there are no such standards

as of yet. In this thesis, the approach was to adhere to the existing requirements and definitions of the maneuvers as they apply to ships without wind propulsion, and then take full freedom with regards to the wind propulsor control and optimization in order to help the ship maneuver. But since it is not yet known what will be required, it could be the case in the future that the standards require the wind propulsors to be static, remaining at a single setting throughout the maneuver, or even disabled altogether. The opinion of this thesis, is that the maneuvering standards should allow the wind propulsors to act in any way within the ships abilities, but that is of course with heavy bias since a big part of the thesis was testing different trim optimization settings. But regardless of the maneuvering standards, the knowledge gained on the effects of the wind propulsors on the ship's turning behavior and ability to change course can be still quite useful during the regular operations of wind-assisted ships.

5.1. Recommendations for Further Development

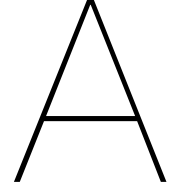
One area for improvement which is touched on in this thesis is to have further understanding of what is feasible for the wind propulsors when it comes to active trim optimization. This thesis studies a variety of options, from a static trim setting in which the wind propulsors do not change trim during the maneuver, to settings with continuously optimized sail trimming with slower and faster trim rates considered. The results show that the optimization settings have a significant effect on the maneuverability of the ship, so it is important to know the details of a wind-assisted ship's capabilities when it comes to trimming the wind propulsors. Working directly with the manufacturers of the different wind propulsors would be helpful with knowing what is currently realistic, and what is feasible in terms of improving the ability of the wind propulsors.

The design of the ship is also of great interest, and the holistic behavior of a wind-assisted ship has the potential to change significantly with different combinations of hull and wind propulsor designs. It would be interesting to compare more options regarding the design of the vessel and the relevant effects on maneuverability. For instance, based on the results in this thesis it seems useful to have wind propulsors both longitudinally in front of and behind the center of lateral resistance of the hull, such that a beneficial turning moment can be created by the sails when turning both into and away from the wind. It is important for designers of wind-assisted ships to understand the different consequences and behaviors that come with wind-assisted propulsion. And further, the designers should ensure that the ship operators and owners are aware of these behaviors. Wind-assisted ship propulsion is an aggressive means of saving fuel which could be of great importance in the coming time of environmental concern. There will be little impact or success however, if the effects of the technology are not well understood and the prospective ship owners are not confident in the technology.

References

- [1] International Maritime Organization (IMO). “Resolution MEPC.203(62) Amendments To The Annex Of The Protocol Of 1997 To Amend The International Convention For The Prevention Of Pollution From Ships, 1973, As Modified By The Protocol Of 1978 Relating Thereto”. In: (July 2011).
- [2] International Maritime Organization (IMO). “Resolution MSC.137(76) Standards for Ship Manoeuvrability”. In: (Dec. 2002).
- [3] Martin A Abkowitz. In: *Lectures on Ship Hydrodynamics - Steering and Manoeuvrability* (May 1965).
- [4] P.A. Bailey, W.G. Price, and P. Temarel. “A Unified mathematical model describing the manoeuvring of a ship travelling in a seaway”. In: *Trans. RINA* 140 (Jan. 1997), pp. 131–149.
- [5] P.A. Bailey et al. “Time simulation of manoeuvring and seakeeping assessments using a unified mathematical model”. In: *Royal Institution of Naval Architects Transactions 2002 Part B* 144 (Jan. 2002), pp. 57–78.
- [6] G. Bordogna. “Aerodynamics of wind-assisted ships: Interaction effects on the aerodynamic performance of multiple wind-propulsion systems”. English. PhD thesis. Delft University of Technology, 2020. ISBN: 978-94-6323-977-6. DOI: 10.4233/uuid:96eda9cd-3163-4c6b-9b9f-e9fa329df071.
- [7] K. Davidson and L. Schiff. “TURNING AND COURSE KEEPING QUALITIES OF SHIPS”. In: *Transactions of The Society of Naval Architects and Marine Engineers* (1946).
- [8] *Dykstra Naval Architects Maltese Falcon*. URL: <https://www.dykstra-na.nl/designs/maltese-falcon/>.
- [9] R. Eggers and A.S. Kisjes. “Seakeeping and manoeuvring for wind assisted ships”. In: *Wind Propulsion 2019* (Nov. 2019). DOI: 10.3940/rina.win.2019.09.
- [10] R. Eggers and A.S. Kisjes. “WindLab: Seakeeping and manoeuvring model tests with for wind assisted ship propulsion”. In: (Feb. 2022).
- [11] Stefan C. Endres, Carl Sandrock, and Walter W. Focke. “A simplicial homology algorithm for Lipschitz optimisation”. In: *Journal of Global Optimization* 72.2 (2018), pp. 181–217. DOI: 10.1007/s10898-018-0645-y.
- [12] T.I. Fossen. “A Nonlinear Unified State-Space Model for Ship Maneuvering and Control in a Seaway.” In: *I. J. Bifurcation and Chaos* 15 (Sept. 2005), pp. 2717–2746. DOI: 10.1142/S0218127405013691.
- [13] Thor I. Fossen. *Marine control systems: Guidance navigation and control of ships, rigs and underwater vehicles*. Marine Cybernetics, 2002.
- [14] Hitoshi Fujii and Tatsuo Tsuda. “Experimental researches on rudder performance (3)”. In: *Journal of Zosen Kiokai* 1962.111 (1962), pp. 51–58. DOI: 10.2534/jjasnaoe1952.1962.51.
- [15] Y. Fukui et al. “4-DOF Mathematical Model for Manoeuvring Simulation including Roll Motion”. In: *Journal of the Japan Society of Naval Architects and Ocean Engineers* 24 (Jan. 2016), pp. 167–179. DOI: 10.2534/jjasnaoe.24.167.
- [16] *Geometry and conditions*. July 2015. URL: <https://simman2014.dk/ship-data/moeri-kvlcc2-tanker/geometry-and-conditions-moeri-kvlcc2-tanker/>.
- [17] M. Hamamoto and Y. Kim. “A new coordinate system and the equations describing manoeuvring motion of a ship in waves (Japanese)”. In: *Journal of the Society of Naval Architects of Japan* 1993.173 (1993), pp. 209–220. DOI: 10.2534/jjasnaoe1968.1993.209.

- [18] J.A. Keuning and U.B. Sonnenberg. "Approximation of the Hydrodynamic Forces on a Sailing Yacht based on the 'Delft Systematic Yacht Hull Series'". In: *National Association of Watersport Indistrius Yacht Design and Yacht Construction* 15 (Nov. 1998). DOI: <http://resolver.tudelft.nl/uuid:f691828f-1fc2-49ca-b221-71acecc95ee2>.
- [19] J.A. Keuning, K.J. Vermeulen, and E.J. de Ridder. "A generic mathematical model for the maneuvering and tacking of a sailing yacht". In: *Society of Naval Architects and Marine Engineers Chesapeake Sailing Yacht Symposium* 17 (Mar. 2005). DOI: 10.5957/csyz-2005-012.
- [20] K Kose, A Yumuro, and Y Yoshimura. "Concrete of Mathematical Model for Ship Maneuvering". In: *Proceedings of the 3rd symposium on ship maneuverability. Society of Naval Architects of Japan* (1981), pp. 27–80.
- [21] H. Lamb. *Hydrodynamics fourth edition*. Cambridge, 1916.
- [22] Ho-Young Lee and Sang-Sung Shin. "The prediction of ship's manoeuvring performance in initial design stage". In: *Developments in Marine Technology* (1998), pp. 633–639. DOI: 10.1016/s0928-2009(98)80205-9.
- [23] J. Journée J M and W. W. Massie. "Single Linear Mass-Spring System". In: *Offshore hydromechanics*. Delft University of Technology, 2008, pp. 213–214.
- [24] Y. Masuyama and T. Fukasawa. "Tacking Simulation of Sailing Yachts With New Model of Aerodynamic Force Variation During Tacking Maneuver". In: *Journal of Sailboat Technology* 2.10 (Apr. 2010), pp. 1–34. ISSN: 1548-6559. eprint: <https://onepetro.org/JST/article-pdf/2/10/1/642612/sname-jsbt-2011-01.pdf>.
- [25] Yutaka Masuyama et al. "Dynamic performance of sailing cruiser by full-scale sea tests". In: *Day 3 Sat, January 30, 1993* (1993). DOI: 10.5957/csyz-1993-018.
- [26] *Norsepower, Sea-Cargo, SC Connector*. URL: <https://sea-cargo.no/resources/fleet/>.
- [27] Frans Quadvlieg and Joris Brouwer. "KVLCC2 Benchmark Data Including Uncertainty Analysis To Support Manoeuvring Predictions". In: *International Conference on Computational Methods in Marine Engineering* (2011), pp. 325–338.
- [28] American Bureau of Shipping (ABS). "Guide For Vessel Maneuverability". In: (Mar. 2006).
- [29] T. Smith et al. *Third IMO GHG Study 2014: Executive Summary and Final Report*. July 2014.
- [30] G. Taimuri et al. "A 6-DOF maneuvering model for the rapid estimation of hydrodynamic actions in deep and shallow waters". In: *Ocean Engineering* 218 (2020). DOI: 10.1016/j.oceaneng.2020.108103.
- [31] N. van der Kolk. "Sailing Efficiency and Course Keeping Ability of Wind Assisted Ships". English. PhD thesis. Delft University of Technology, 2020. ISBN: 978-94-6384-147-4. DOI: 10.4233/uuid:8707309f-b9a3-4e09-916d-8fb64328a138.
- [32] H. Yasukawa, R. Sakuno, and Y. Yoshimura. "Practical maneuvering simulation method of ships considering the roll-coupling effect". In: *Journal of Marine Science and Technology* 24.4 (2019), pp. 1280–1296. DOI: 10.1007/s00773-019-00625-4.
- [33] H. Yasukawa and Y. Yoshimura. "Introduction of MMG standard method for ship maneuvering predictions". In: *Journal of Marine Science and Technology* 20.1 (2014), pp. 37–52. DOI: 10.1007/s00773-014-0293-y.
- [34] Yasuo Yoshimura. "Mathematical model for the manoeuvring ship motion in shallow water". In: *Journal of the Japan Society of Naval Architects and Ocean Engineers KASNAJ* (Jan. 1986), pp. 41–51.
- [35] Xiaohui Zhang et al. "Experimental investigation into the effect of roll amplitude on roll damping". In: *Journal of Shanghai Jiaotong University (Science)* 24.6 (2019), pp. 732–738. DOI: 10.1007/s12204-019-2120-4.



Derivations

A.1. Equations of Motion

Newton's second law equations of motion for a 4 DOF rigid body in a body fixed coordinate frame, following the model developed by Abkowitz which has been the foundation of many modern maneuvering models [3].

$$m(\dot{u}_{cg} - v_{cg}r_{cg}) = F_x \quad (\text{A.1})$$

$$m(\dot{v}_{cg} + u_{cg}r_{cg}) = F_y \quad (\text{A.2})$$

$$I_{xx}\dot{p}_{cg} = M_x \quad (\text{A.3})$$

$$I_{zz}\dot{r}_{cg} = M_z \quad (\text{A.4})$$

Maneuvering standards are defined by the midship position, so maneuvering models typically solve for velocities at midships instead of at center of gravity. The surge, roll, and yaw velocities are equal at midships and at the center of gravity of the ship, so only the sway velocity is effected. So, the transformation to achieve the midship sway velocity is [33]:

$$v = v_{cg} - x_{cg}r \quad (\text{A.5})$$

And including that in the equations of motion:

$$m(\dot{u} - vr + x_{cg}r^2) = F_x \quad (\text{A.6})$$

$$m(\dot{v} + x_{cg}\dot{r} + ur) = F_y \quad (\text{A.7})$$

$$I_{xx}\dot{p} = M_x \quad (\text{A.8})$$

$$I_{zz}\dot{r} = M_z \quad (\text{A.9})$$

The RHS forces are expanded into the components of added mass terms, and the total midship forces (X, Y, K, N).

$$F_x = -a_{00}\dot{u} + a_{11}vr + X \quad (\text{A.10})$$

$$F_y = -a_{11}\dot{v} - a_{00}ur - a_{12}\dot{p} - a_{13}\dot{r} + Y \quad (\text{A.11})$$

$$M_x = -a_{22}\dot{p} - a_{21}\dot{v} - a_{23}\dot{r} + K + z_{cg}F_y \quad (\text{A.12})$$

$$M_z = -a_{33}\dot{r} - a_{31}\dot{v} + N - x_{cg}F_y \quad (\text{A.13})$$

Equation A.7 is substituted into equations A.12 and A.13, resulting in the terms:

$$M_x = K - a_{22}\dot{p} - a_{21}\dot{v} - a_{23}\dot{r} + mz_{cg}\dot{v} + mx_{cg}z_{cg}\dot{r} - mz_{cg}^2\dot{p} + mz_{cg}ur \quad (\text{A.14})$$

$$M_z = N - a_{33}\dot{r} - a_{31}\dot{v} - mx_{cg}\dot{v} - mx_{cg}^2\dot{r} + mx_{cg}z_{cg}\dot{p} - mx_{cg}ur \quad (\text{A.15})$$

And the equations of motion are finally:

$$(m + a_{00})\dot{u} - (m + a_{11})vr - mx_{cg}r^2 + mz_{cg}pr = X \quad (\text{A.16})$$

$$(m + a_{11})\dot{v} + (a_{12} - mz_{cg})\dot{p} + (a_{13} + mx_{cg})\dot{r} + (m + a_{00})ur = Y \quad (\text{A.17})$$

$$(I_{xx} + a_{22} + mz_{cg}^2)\dot{p} + (a_{21} - mz_{cg})\dot{v} + (a_{23} - mx_{cg}z_{cg})\dot{r} - mz_{cg}ur = K \quad (\text{A.18})$$

$$(I_{zz} + a_{33} + mx_{cg}^2)\dot{r} + (a_{31} + mx_{cg})\dot{v} - mx_{cg}z_{cg}\dot{p} + mx_{cg}ur = N \quad (\text{A.19})$$

A.2. Propeller Speed

$$X_p = (1 - t)\rho D_p^4 \left(n_p^2 k_{t0} + n_p k_{t1} \left(U \frac{1-w}{D_p} \right) + k_{t2} \left(U \frac{1-w}{D_p} \right)^2 \right) \quad (\text{A.20})$$

$$\frac{X_p}{(1-t)\rho D_p^4} = n_p^2 k_{t0} + n_p k_{t1} \left(U \frac{1-w}{D_p} \right) + k_{t2} \left(U \frac{1-w}{D_p} \right)^2 \quad (\text{A.21})$$

$$X_p = -X_H - X_R - X_A \quad (\text{A.22})$$

$$n_p^2 k_{t0} + n_p k_{t1} \left(U \frac{1-w}{D_p} \right) + k_{t2} \left(U \frac{1-w}{D_p} \right)^2 + \frac{X_H + X_R + X_A}{(1-t)\rho D_p^4} = 0 \quad (\text{A.23})$$

Where the positive result of the quadratic formula is then used to solve for n_p , with:

$$a = k_{t0} \quad (\text{A.24})$$

$$b = k_{t1} \left(U \frac{1-w}{D_p} \right) \quad (\text{A.25})$$

$$c = k_{t2} \left(U \frac{1-w}{D_p} \right)^2 + \frac{X_H + X_R + X_A}{(1-t)\rho D_p^4} \quad (\text{A.26})$$

$$n_p = \frac{-b + \sqrt{b^2 - 4ac}}{2a} \quad (\text{A.27})$$

B

Plots - Main Results

B.1. KVLCC2 1/3.7 Dynarig Configuration

B.1.1. KVLCC2 1/3.7 Dynarig Turning Circle Tests

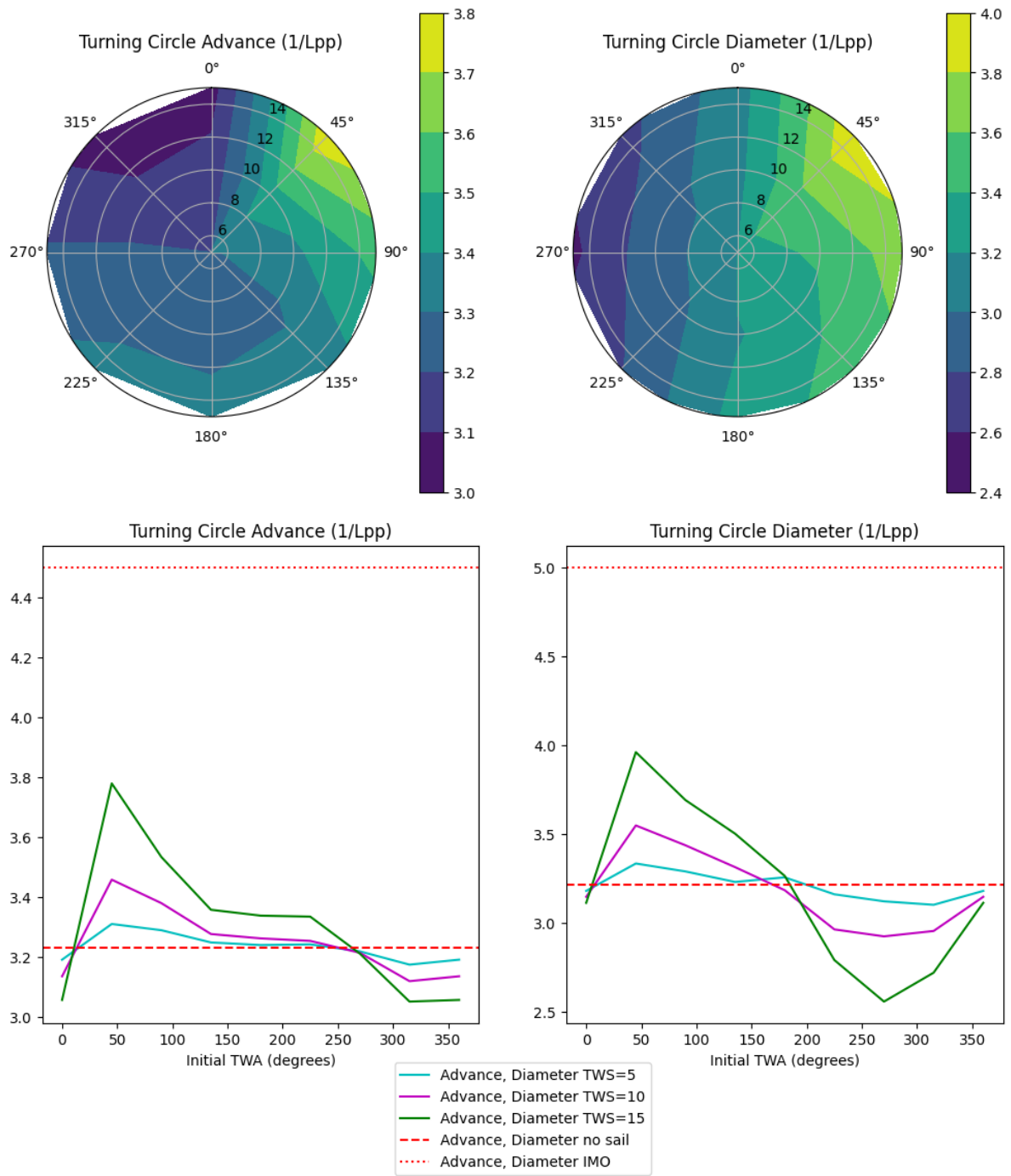


Figure B.1: Dynarig Turning Circle, Trim Setting: S-1 (radial axis: TWS in m/s , polar axis: TWA in $^\circ$)

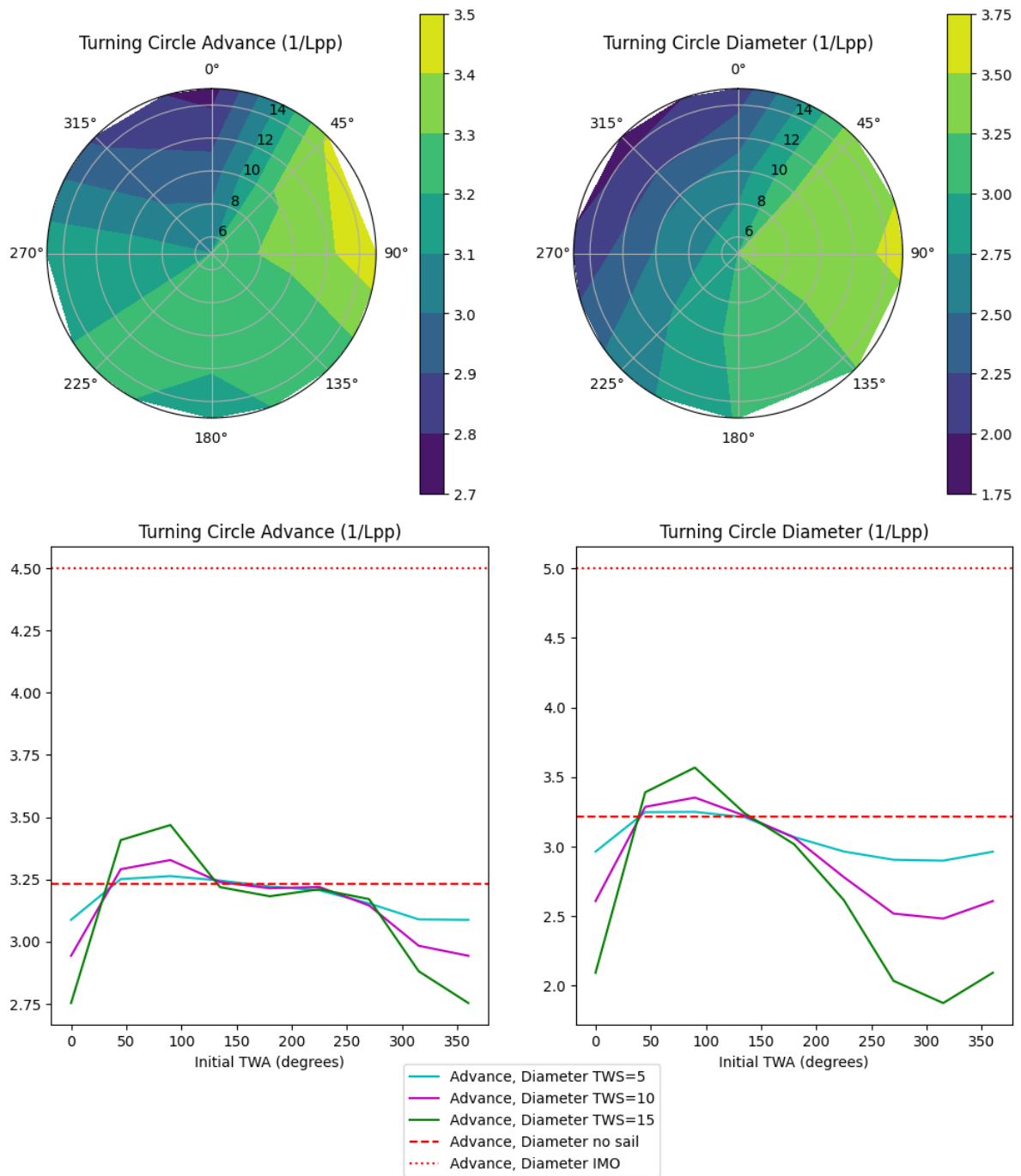


Figure B.2: Dynarig Turning Circle, Trim Setting: A-S1 (radial axis: TWS in m/s , polar axis: TWA in $^\circ$)

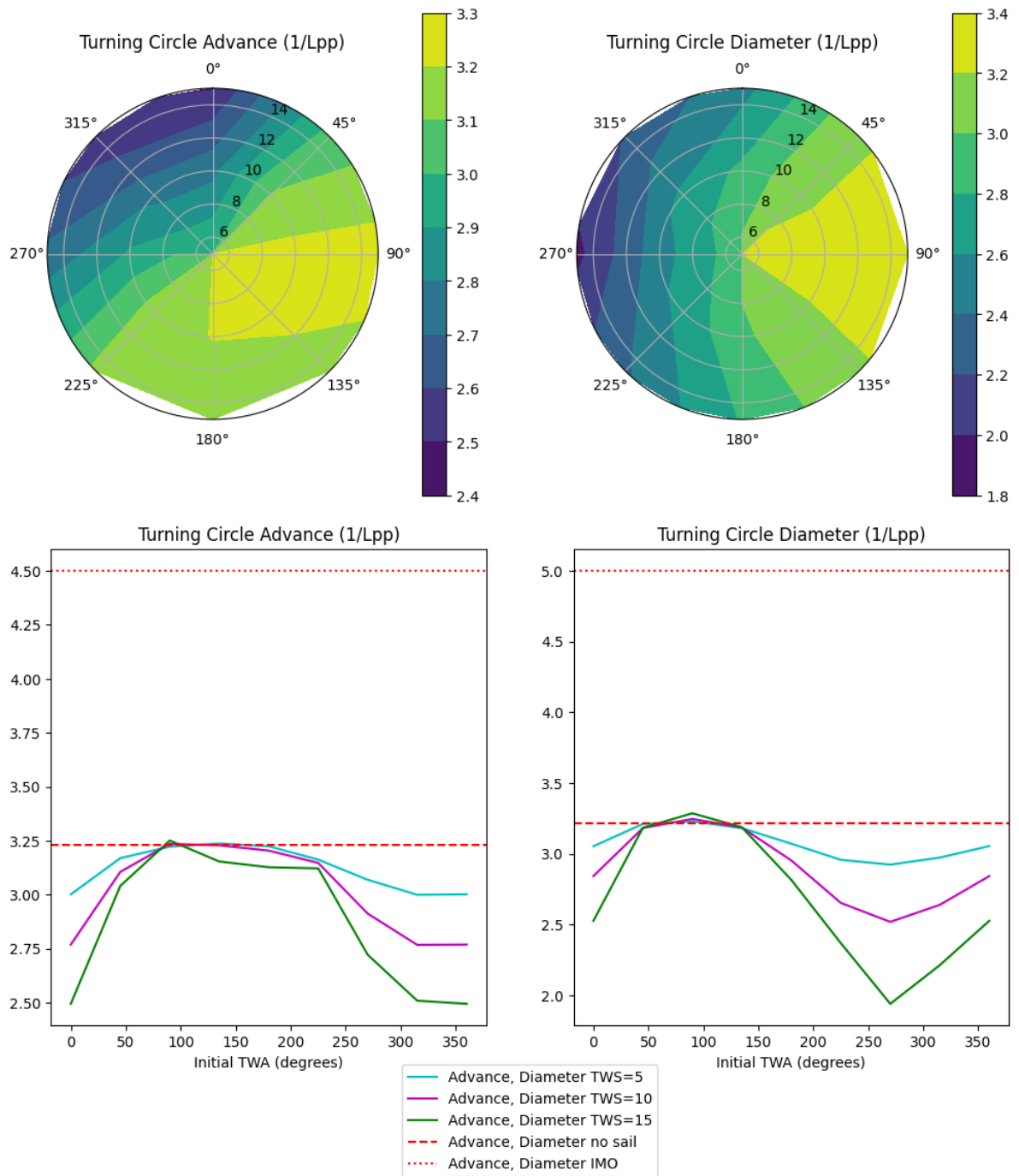


Figure B.3: Dynarig Turning Circle, Trim Setting: A-F1 (radial axis: TWS in m/s , polar axis: TWA in $^\circ$)

B.1.2. KVLCC2 1/3.7 Dynarig Zig-Zag 10/10 Tests

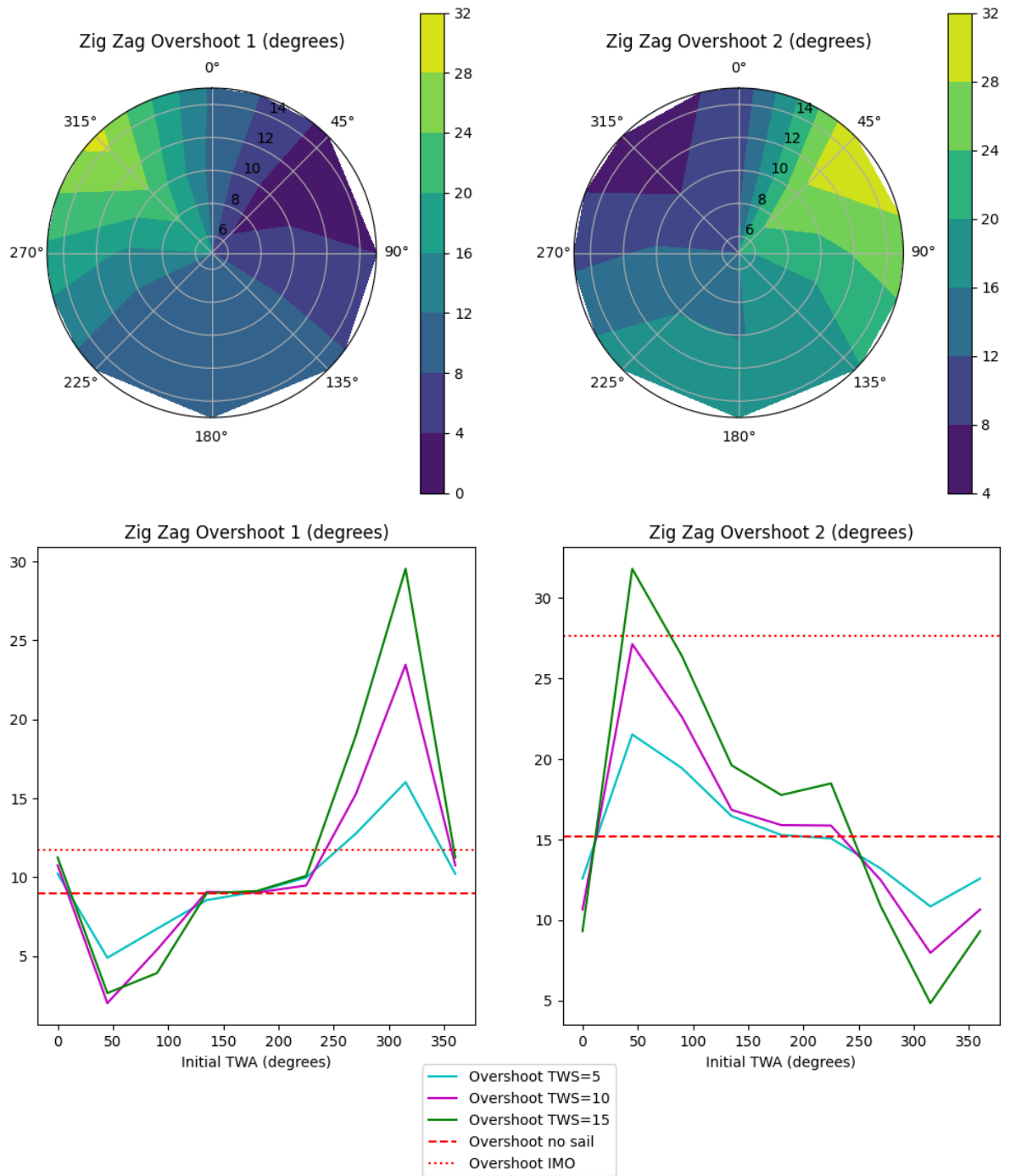


Figure B.4: Dynarig Zig-Zag 10/10, Trim Setting: S-1 (radial axis: TWS in m/s , polar axis: TWA in $^\circ$)

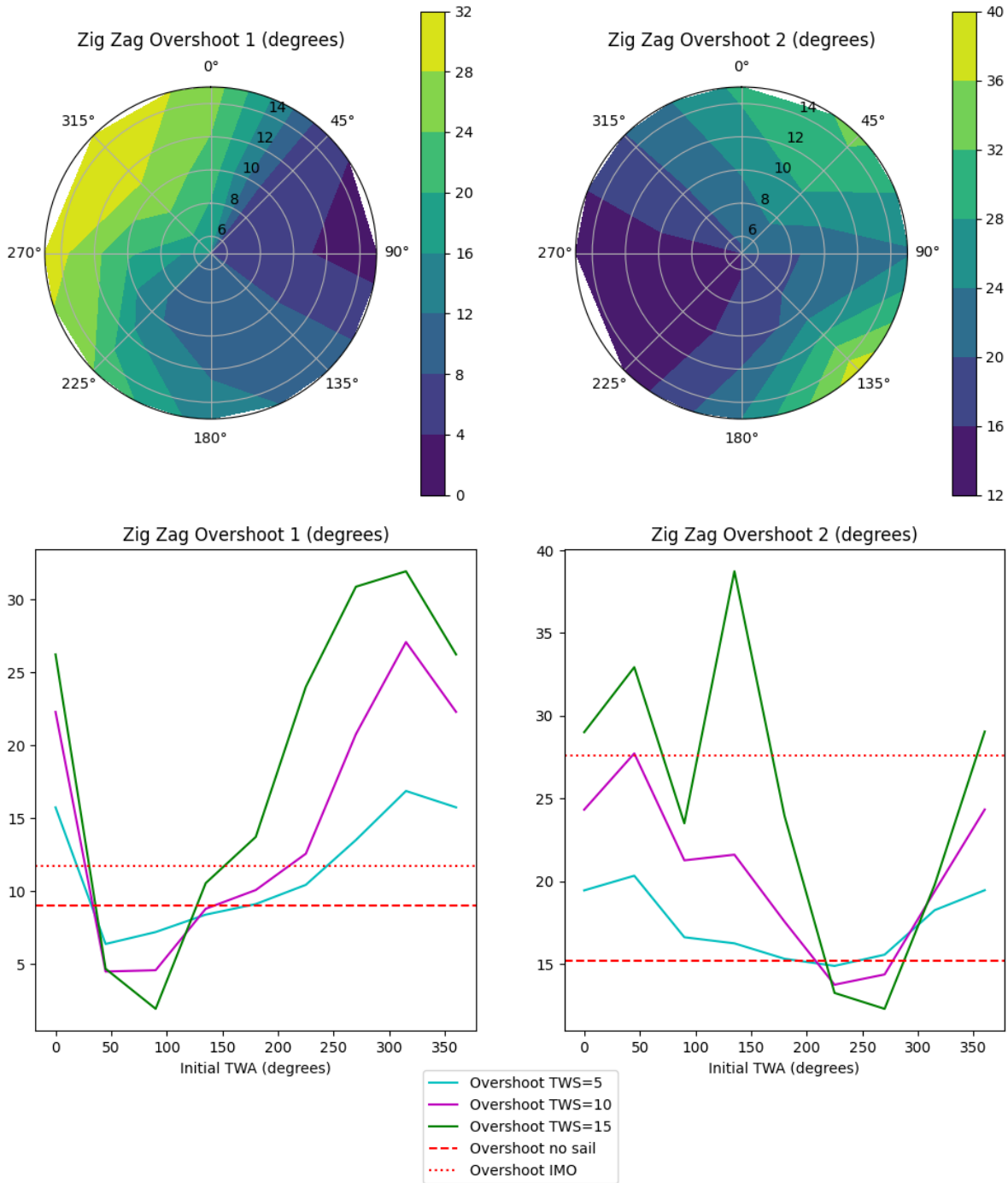


Figure B.5: Dynarig Zig-Zag 10/10, Trim Setting: A-S1 (radial axis: TWS in m/s , polar axis: TWA in $^\circ$)

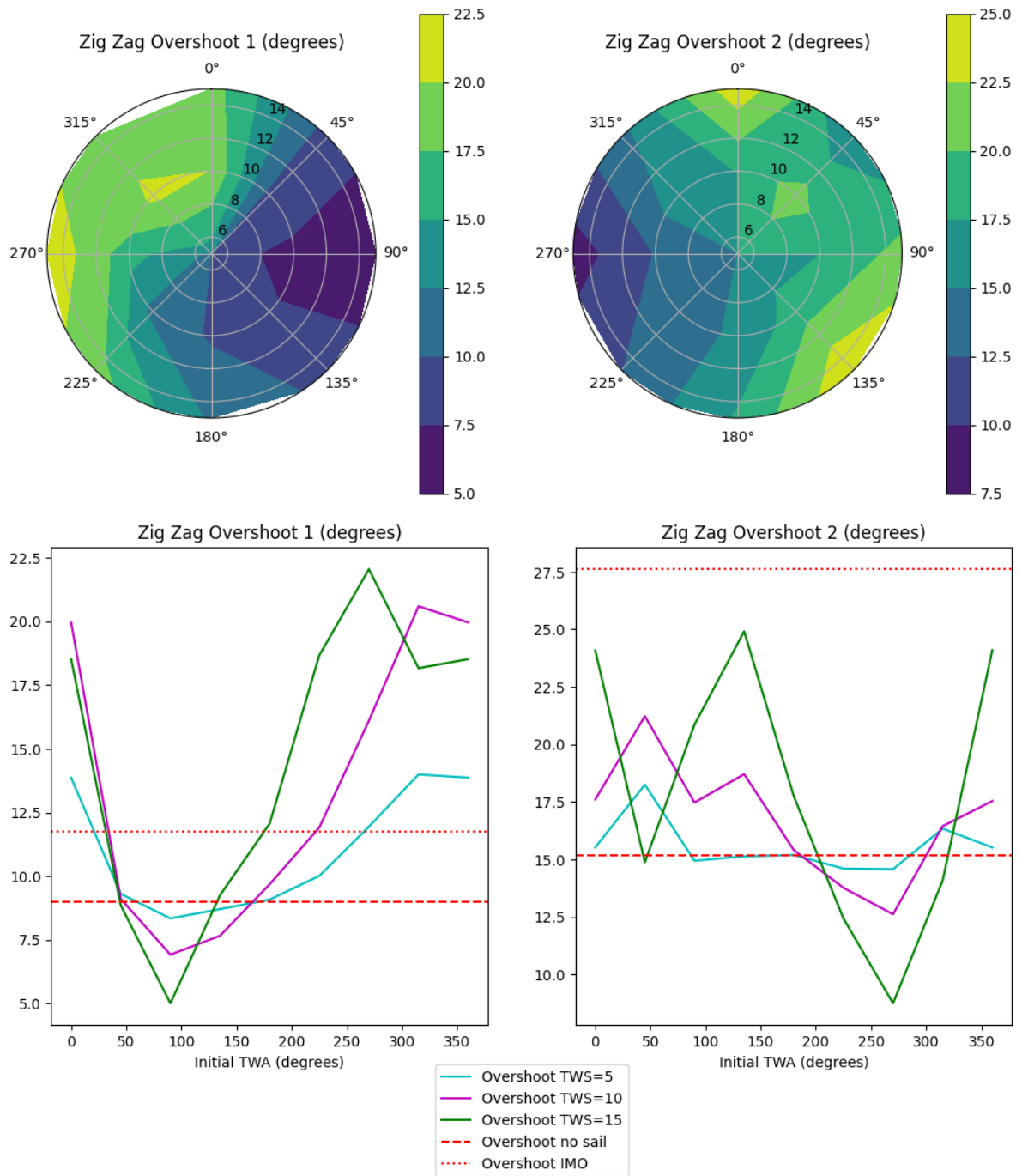


Figure B.6: Dynarig Zig-Zag 10/10, Trim Setting: A-F1 (radial axis: TWS in m/s , polar axis: TWA in $^\circ$)

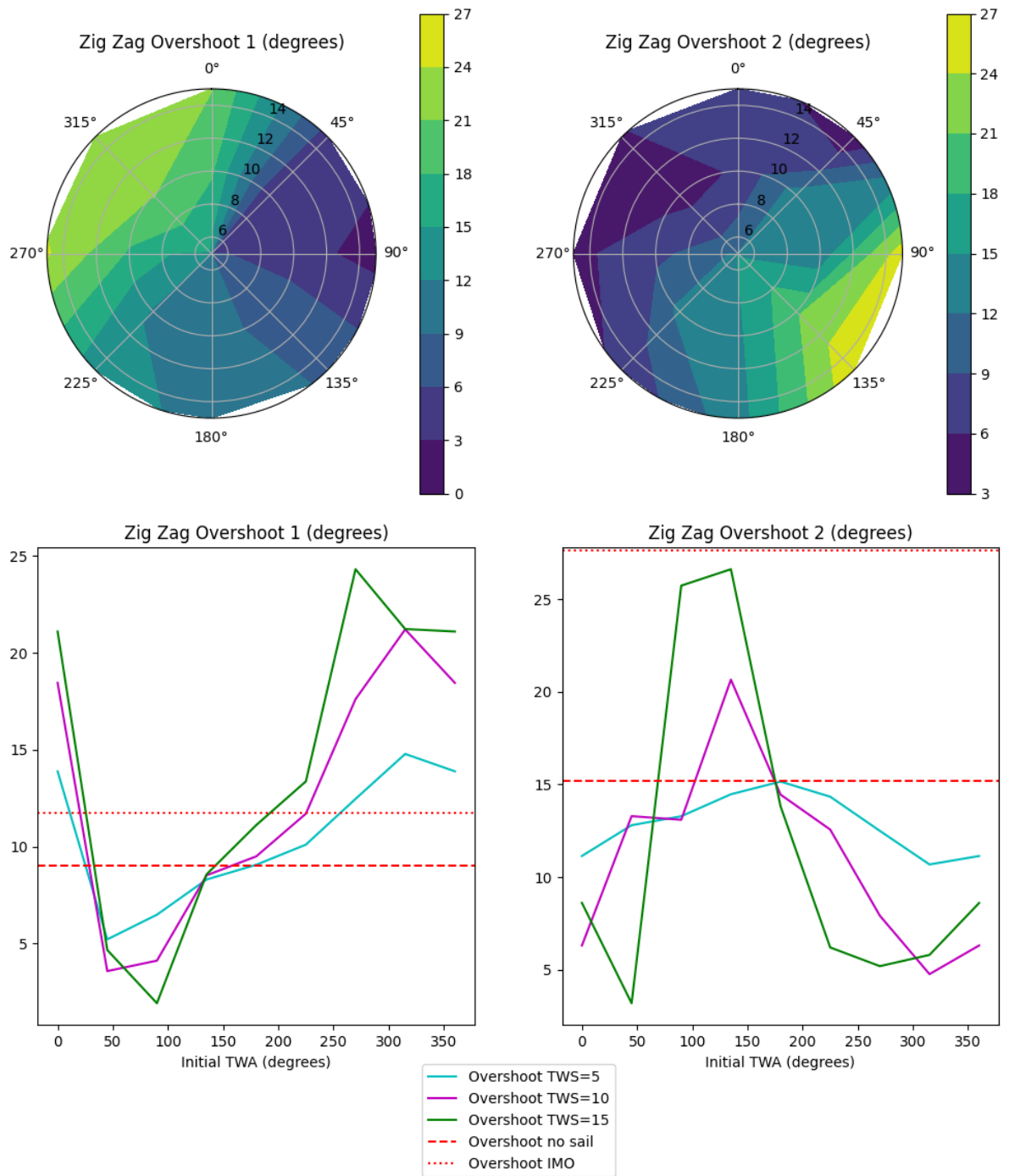


Figure B.7: Dynarig Zig-Zag 10/10, Trim Setting: A-S2 (radial axis: TWS in m/s , polar axis: TWA in $^\circ$)

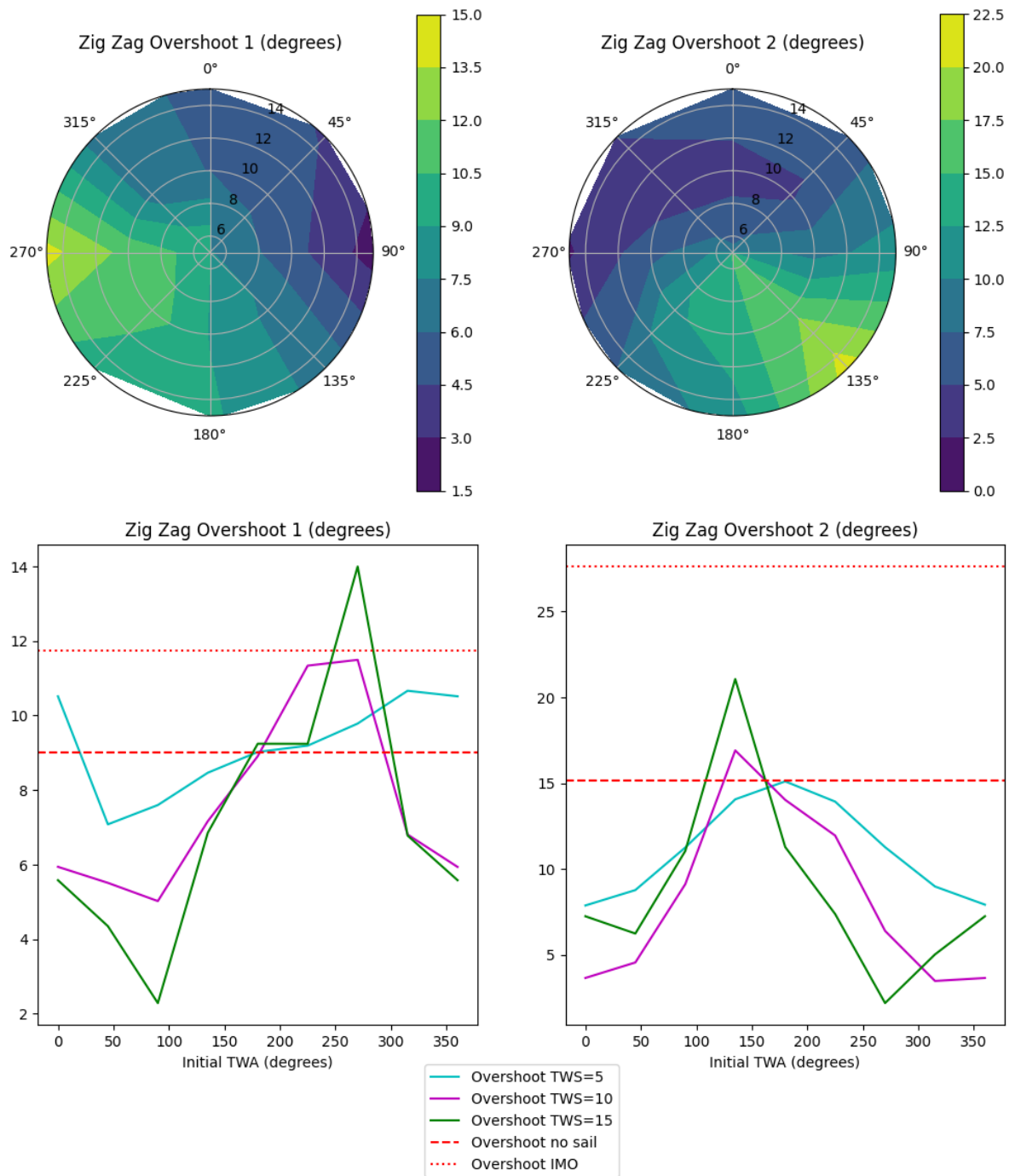


Figure B.8: Dynarig Zig-Zag 10/10, Trim Setting: A-F2 (radial axis: TWS in m/s , polar axis: TWA in $^\circ$)

B.1.3. KVLCC2 1/3.7 Dynarig Zig-Zag 20/20 Tests

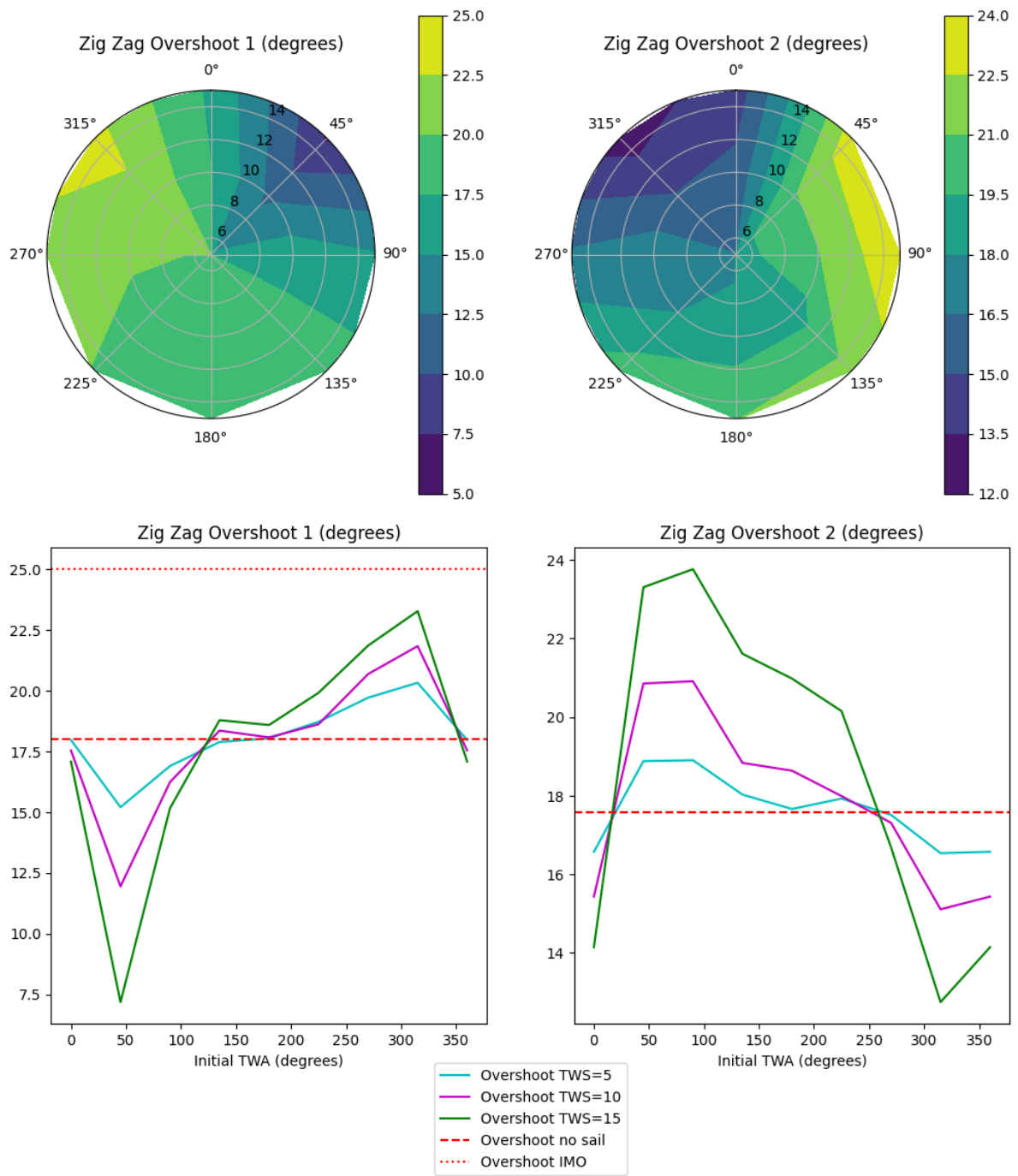


Figure B.9: Dynarig Zig-Zag 20/20, Trim Setting: S-1 (radial axis: TWS in m/s , polar axis: TWA in $^\circ$)

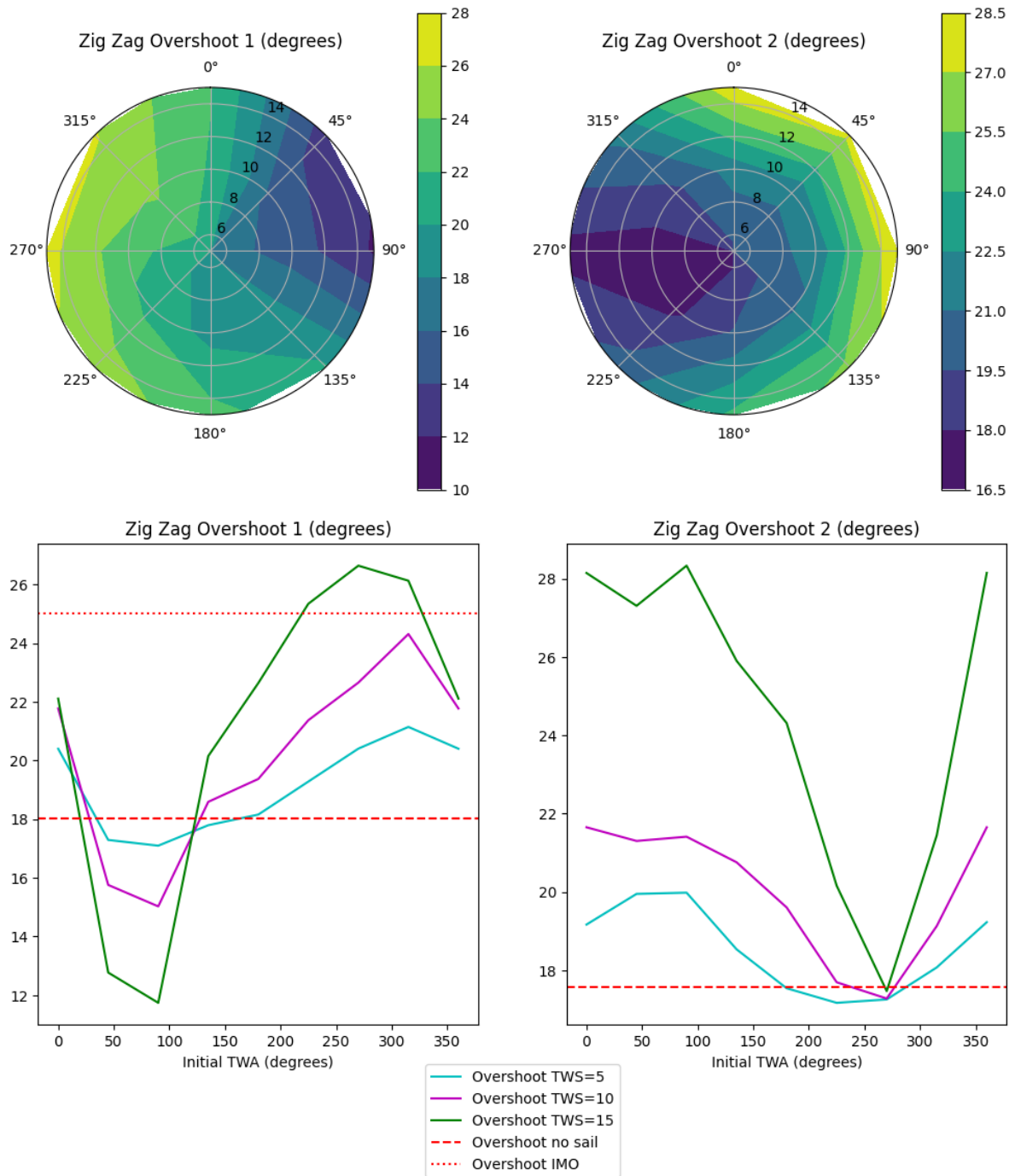


Figure B.10: Dynarig Zig-Zag 20/20, Trim Setting: A-S1 (radial axis: TWS in m/s , polar axis: TWA in $^\circ$)

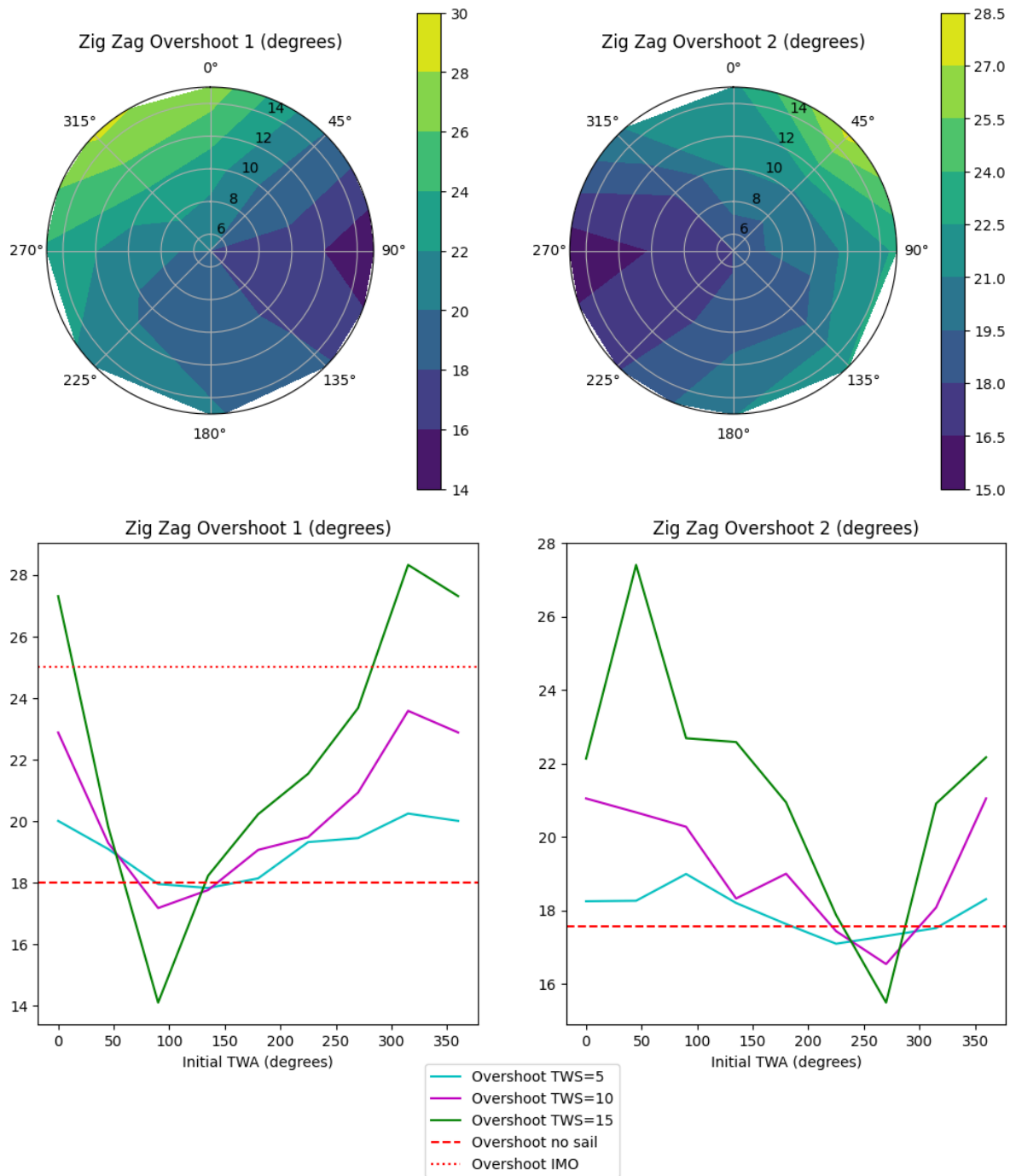


Figure B.11: Dynarig Zig-Zag 20/20, Trim Setting: A-F1 (radial axis: TWS in m/s , polar axis: TWA in $^\circ$)

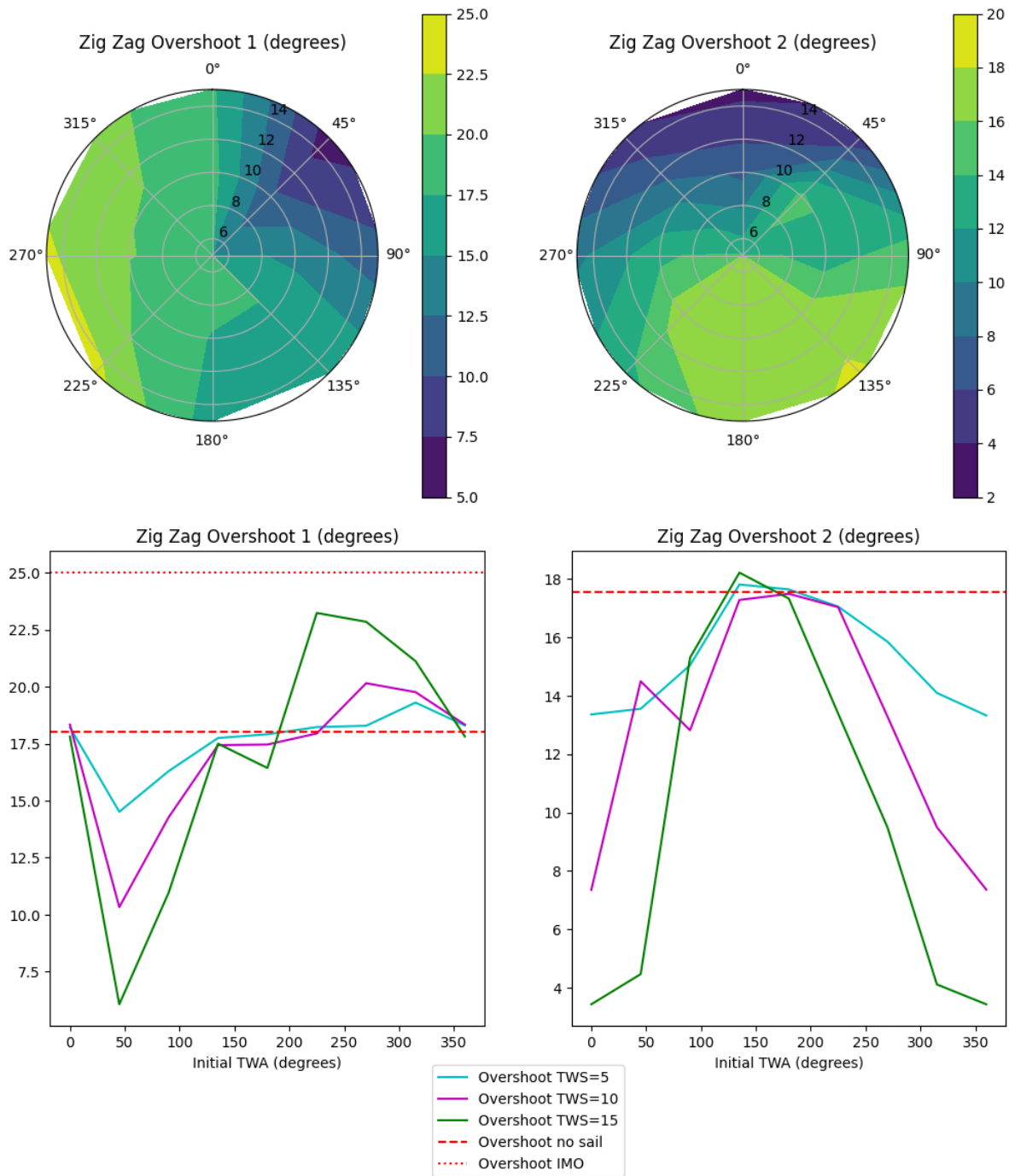


Figure B.12: Dynarig Zig-Zag 20/20, Trim Setting: A-S2 (radial axis: TWS in m/s , polar axis: TWA in $^{\circ}$)

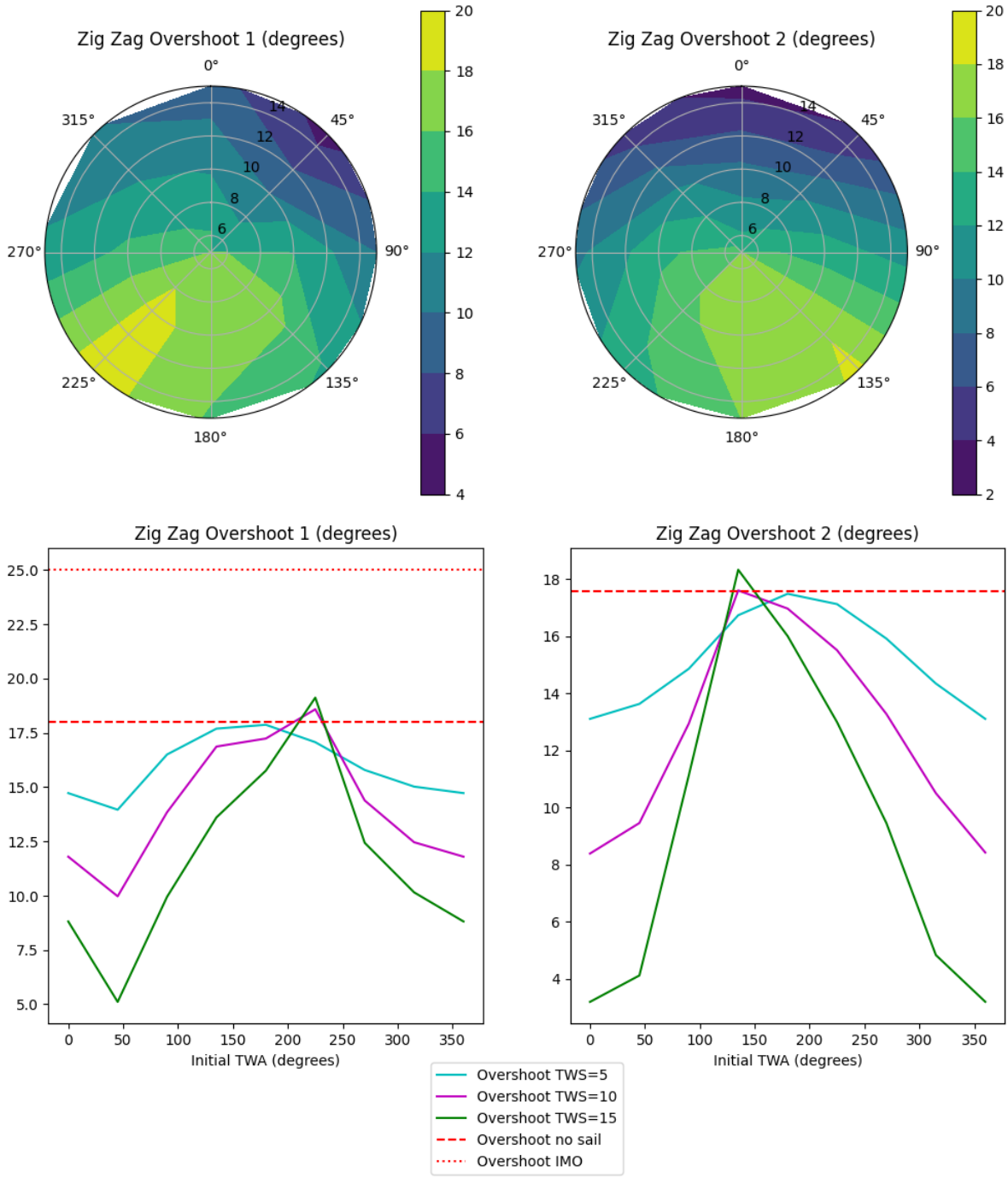


Figure B.13: Dynarig Zig-Zag 20/20, Trim Setting: A-F2 (radial axis: TWS in m/s , polar axis: TWA in $^{\circ}$)

B.2. KVLCC2 1/3.7 Flettner Rotor Configuration

B.2.1. KVLCC2 1/3.7 Flettner Rotor Turning Circle Tests

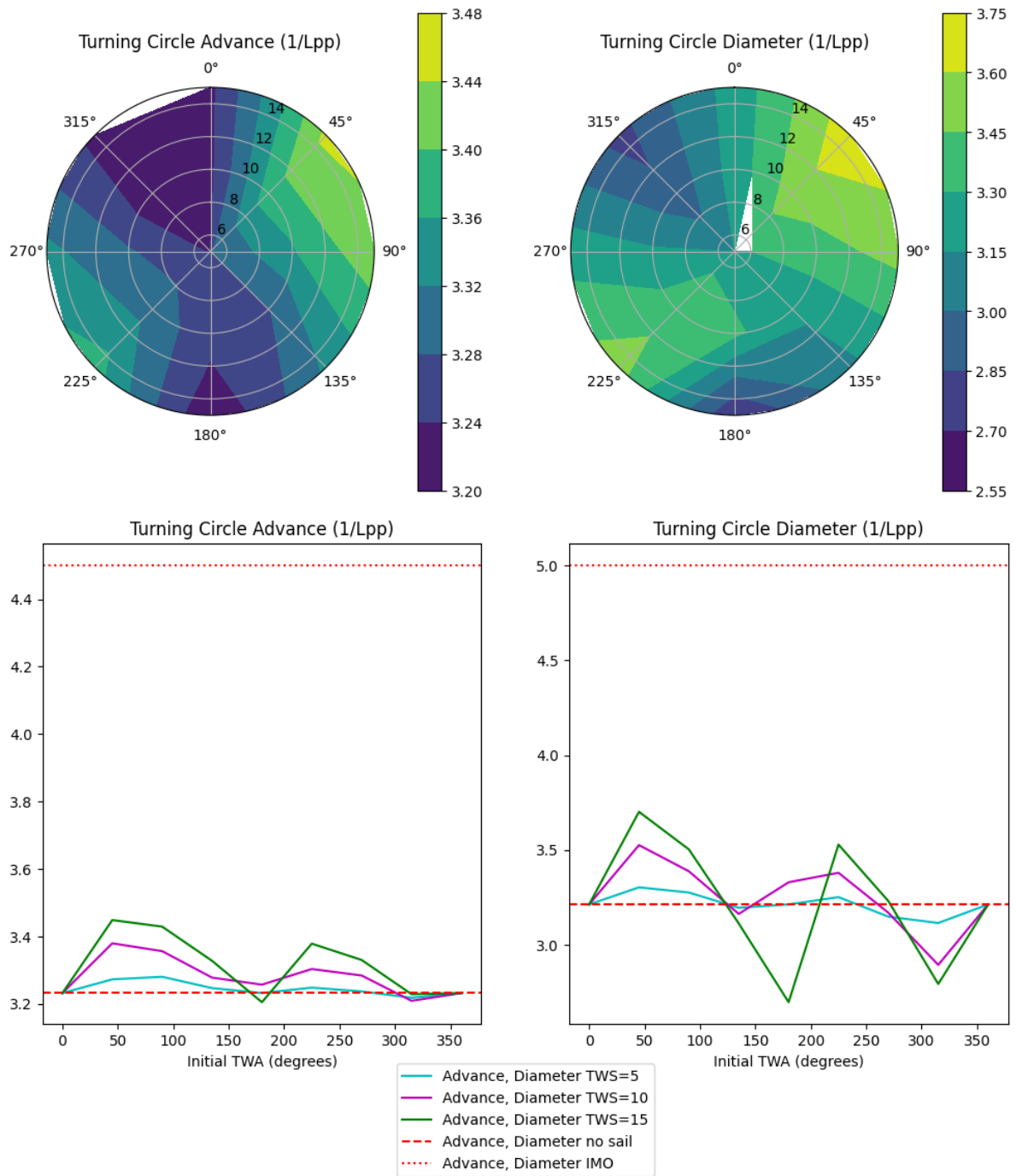


Figure B.14: Rotor Turning Circle, Trim Setting: S-1 (radial axis: TWS in m/s , polar axis: TWA in $^\circ$)

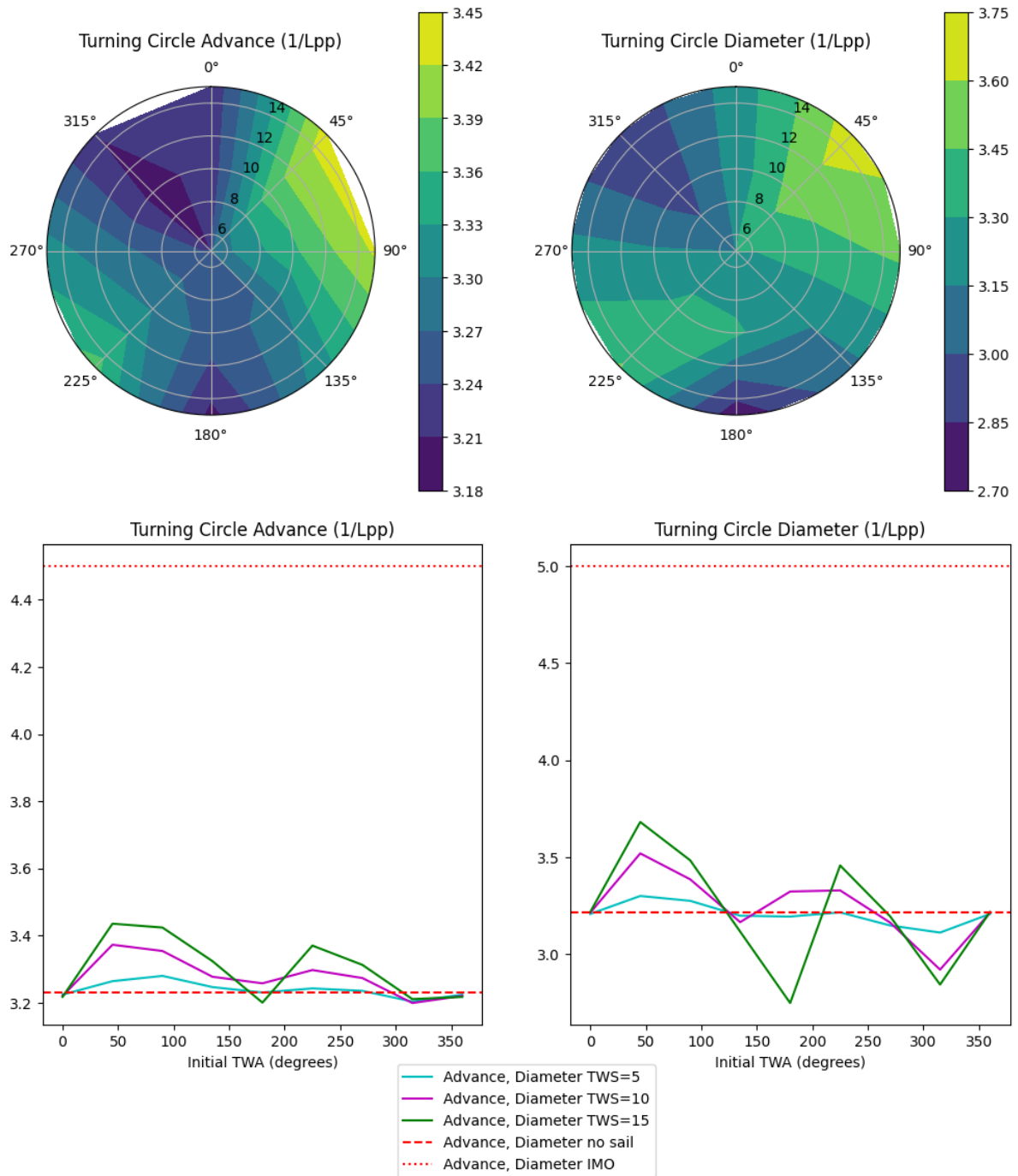


Figure B.15: Rotor Turning Circle, Trim Setting: A-S1 (radial axis: TWS in m/s , polar axis: TWA in $^\circ$)

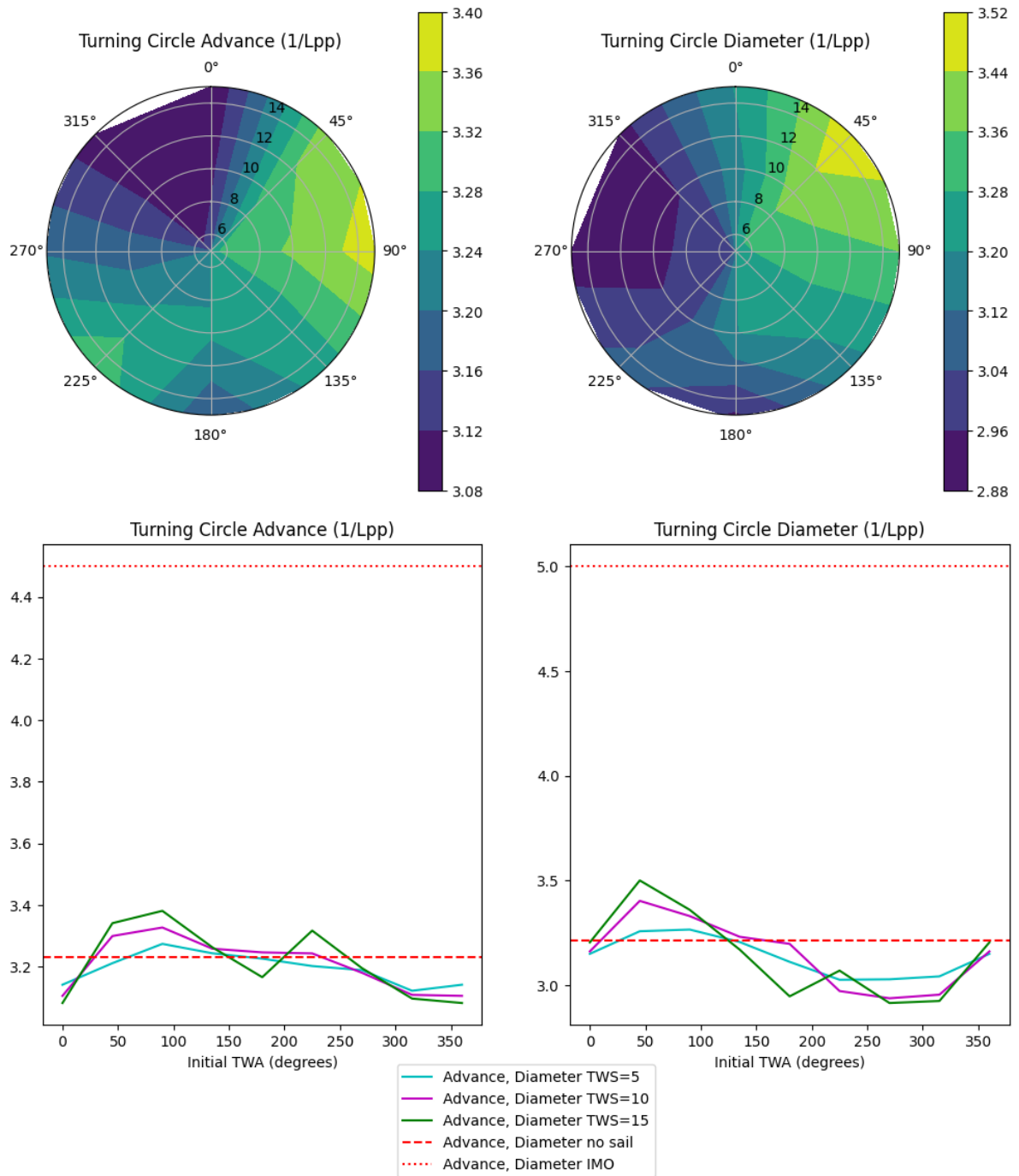


Figure B.16: Rotor Turning Circle, Trim Setting: A-F1 (radial axis: TWS in m/s , polar axis: TWA in $^\circ$)

B.2.2. KVLCC2 1/3.7 Flettner Rotor Zig-Zag 10/10 Tests

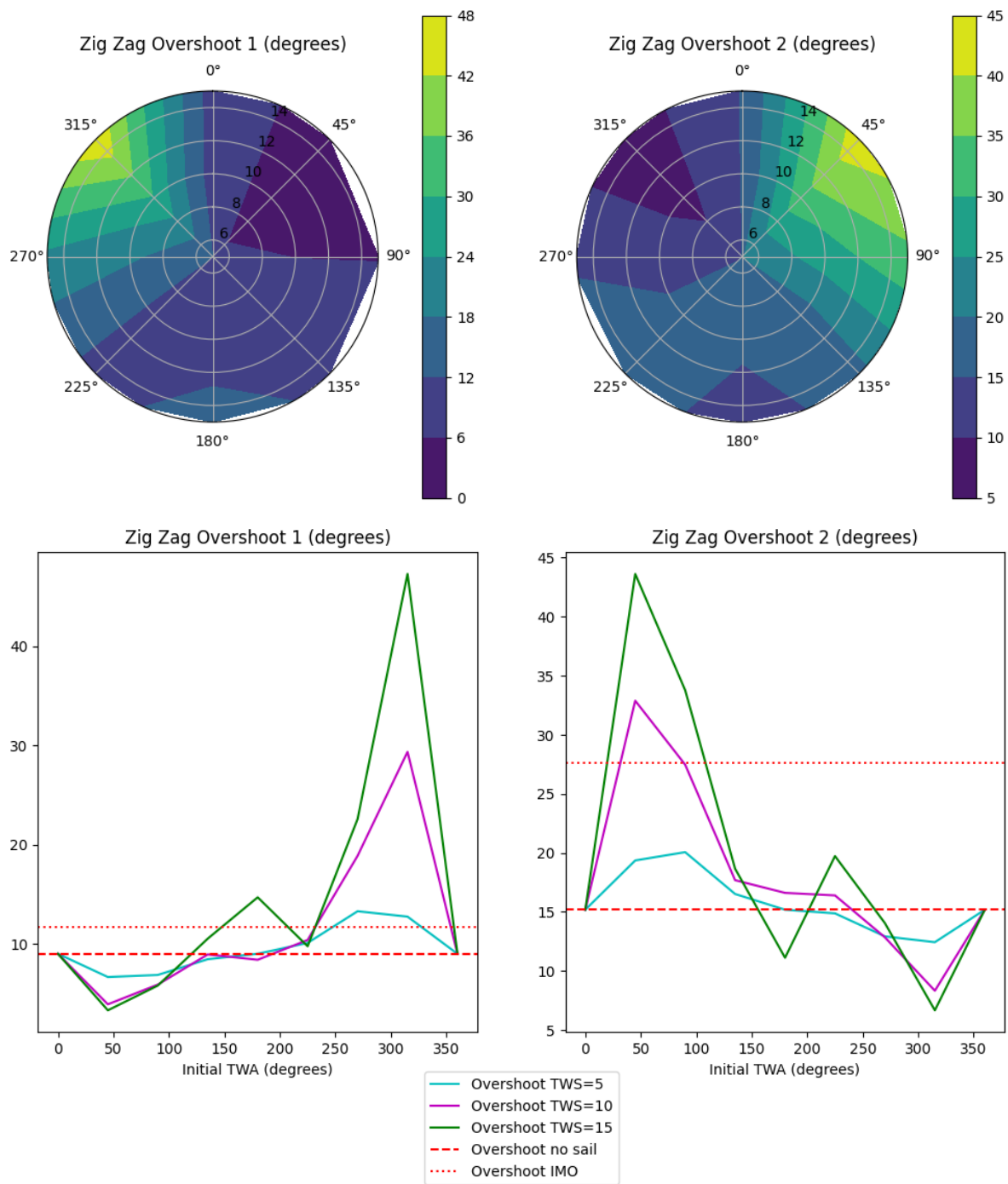


Figure B.17: Rotor Zig-Zag 10/10, Trim Setting: S-1 (radial axis: TWS in m/s , polar axis: TWA in $^\circ$)

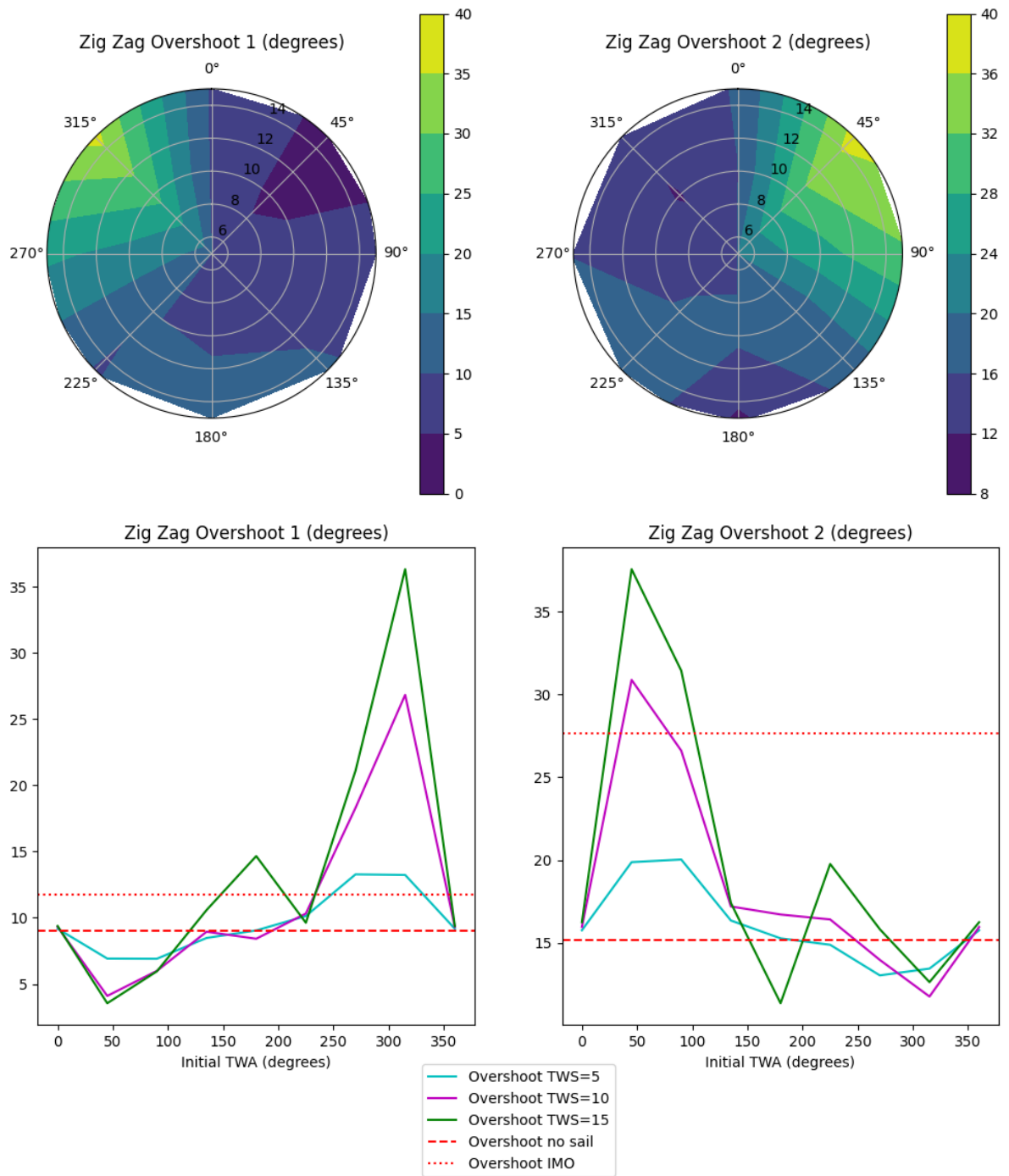


Figure B.18: Rotor Zig-Zag 10/10, Trim Setting: A-S1 (radial axis: TWS in m/s , polar axis: TWA in $^\circ$)

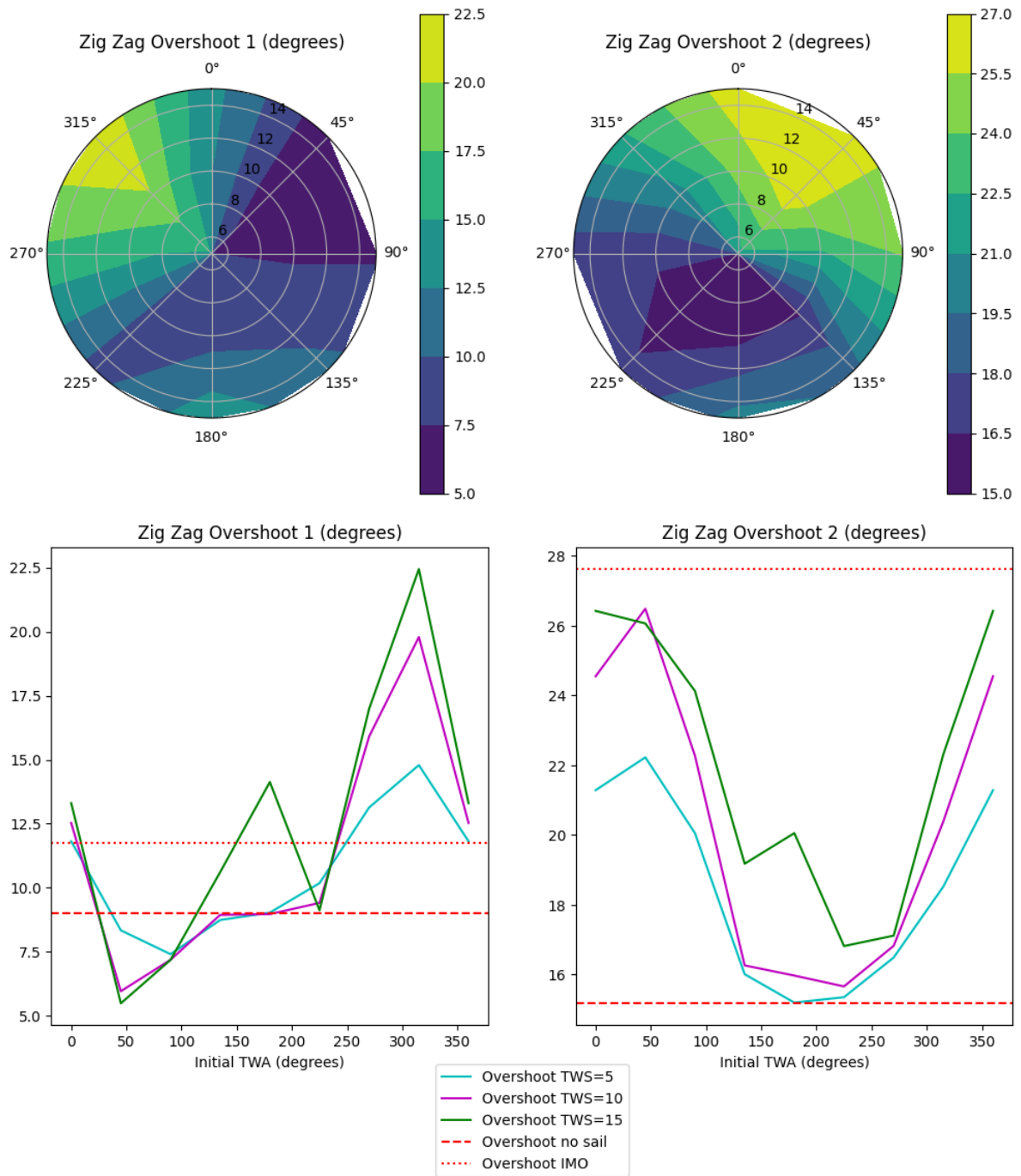


Figure B.19: Rotor Zig-Zag 10/10, Trim Setting: A-F1 (radial axis: TWS in m/s , polar axis: TWA in $^\circ$)

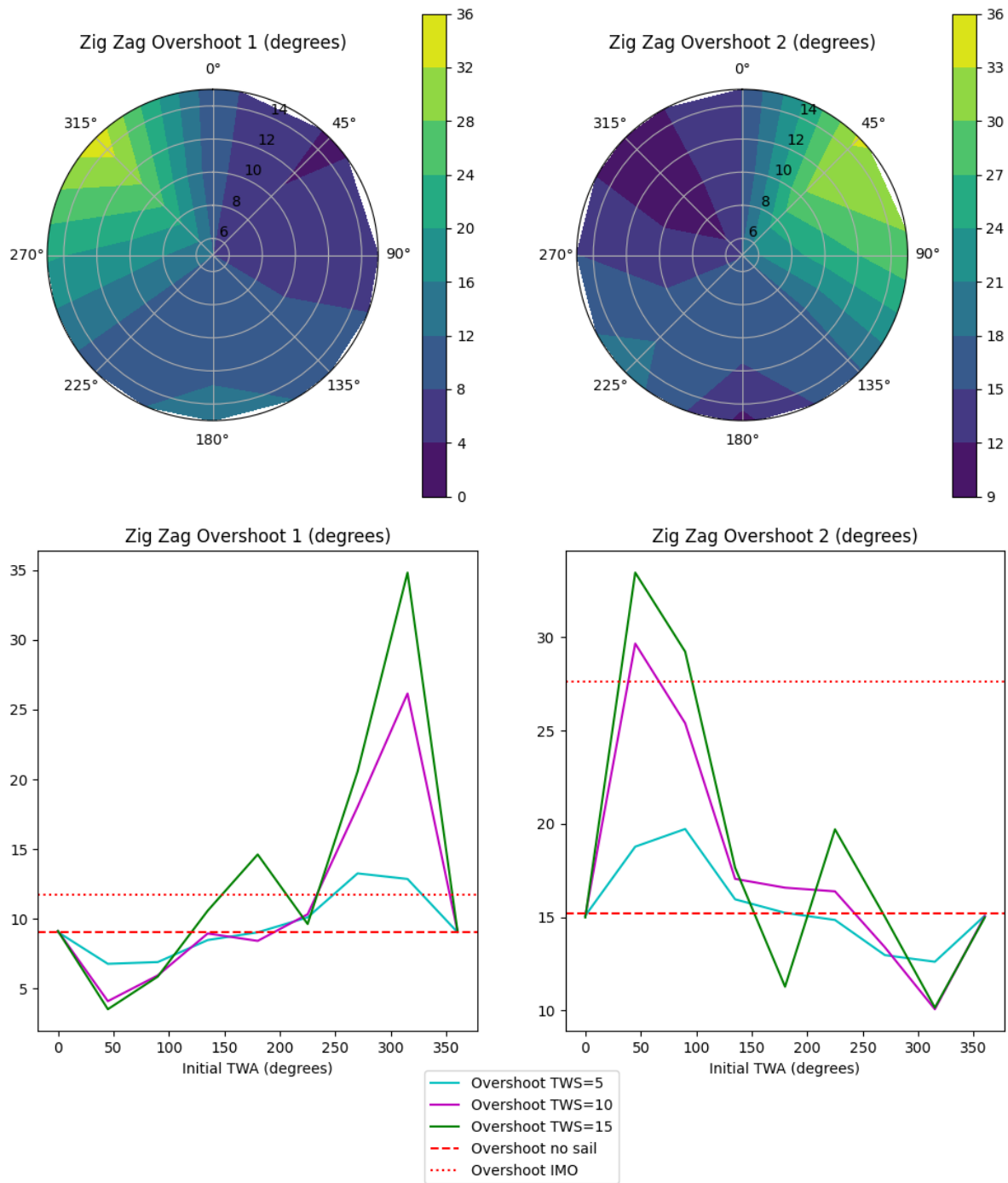


Figure B.20: Rotor Zig-Zag 10/10, Trim Setting: A-S2 (radial axis: TWS in m/s , polar axis: TWA in $^\circ$)

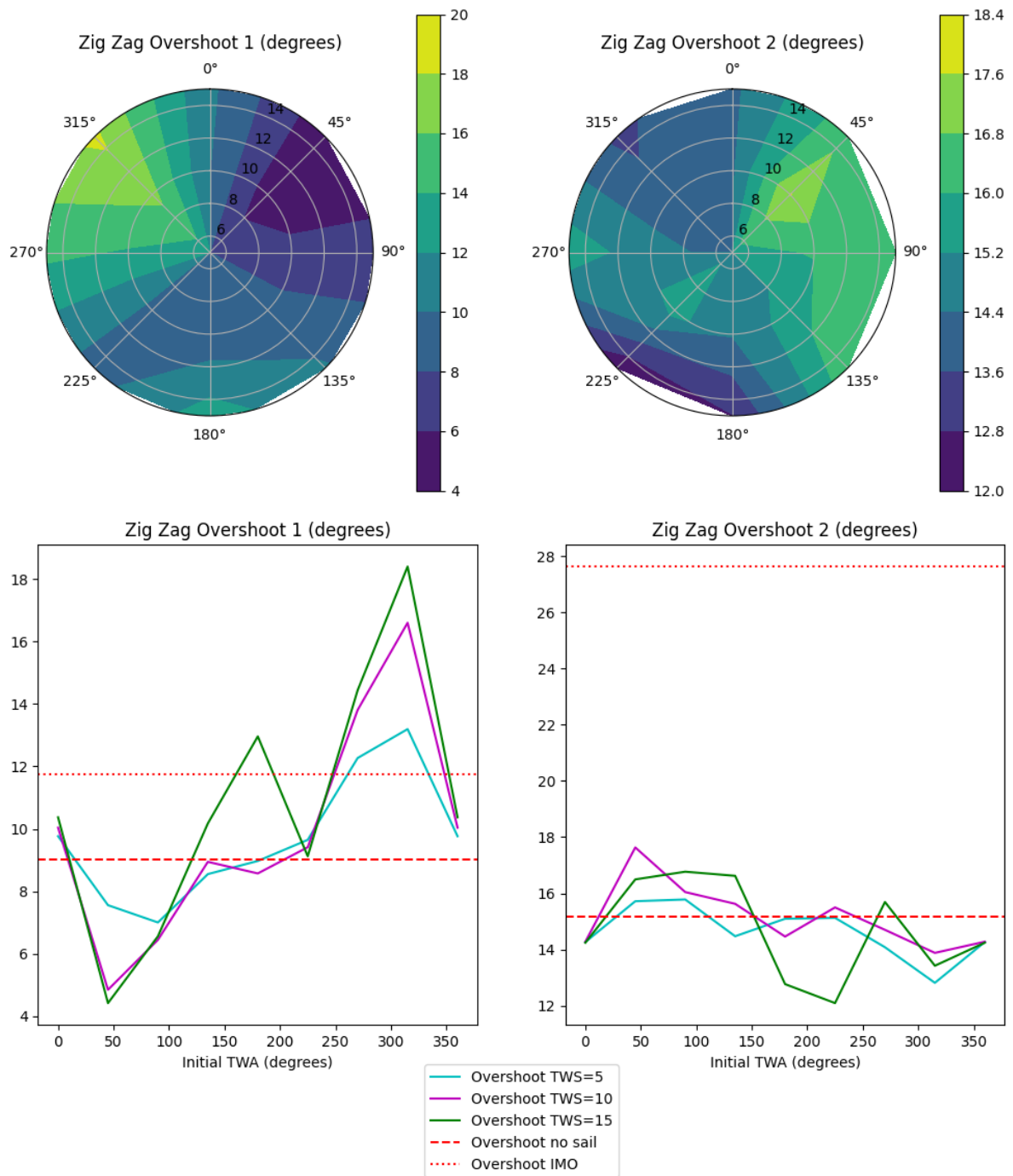


Figure B.21: Rotor Zig-Zag 10/10, Trim Setting: A-F2 (radial axis: TWS in m/s , polar axis: TWA in $^\circ$)

B.2.3. KVLCC2 1/3.7 Flettner Rotor Zig-Zag 20/20 Tests

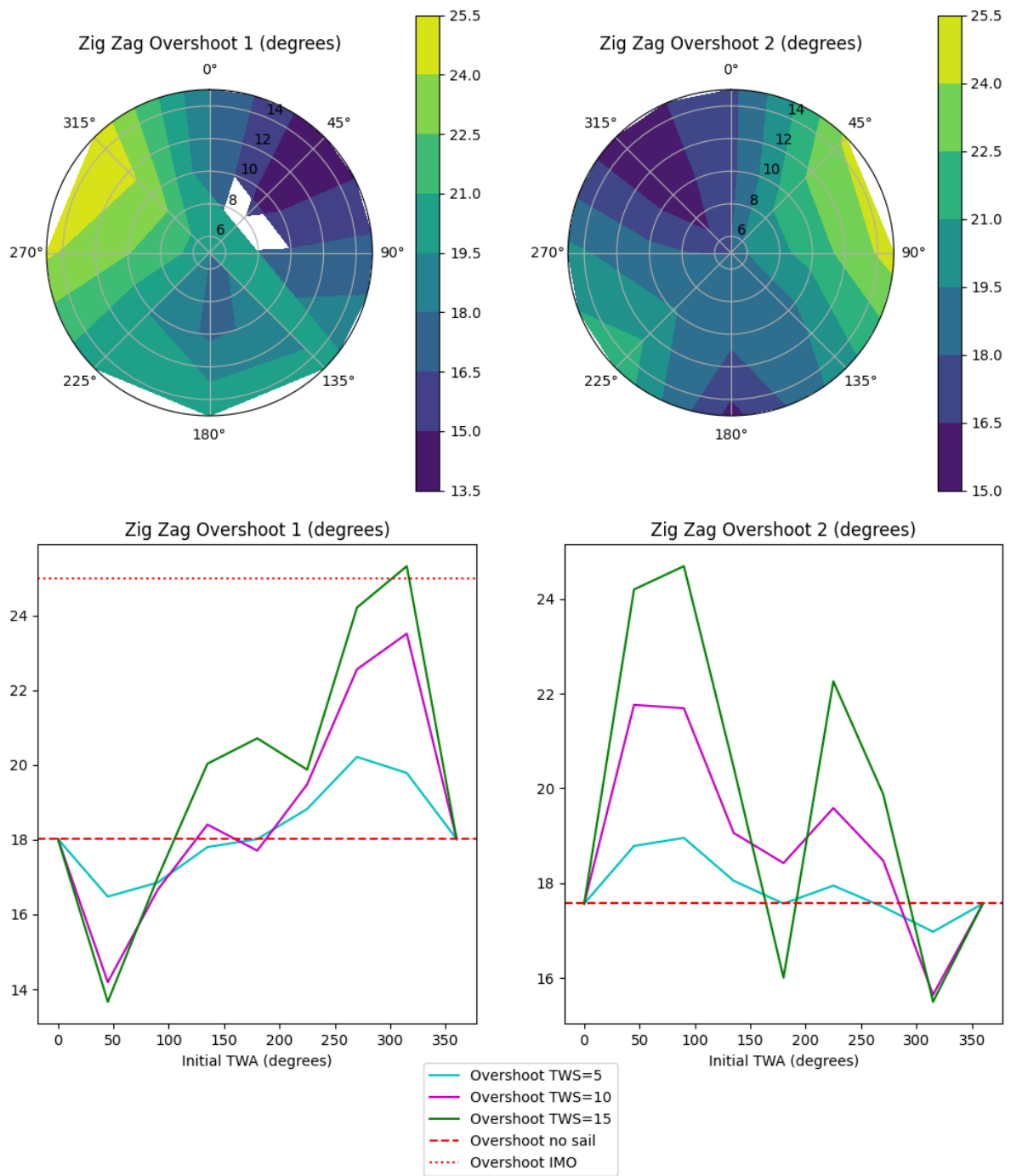


Figure B.22: Rotor Zig-Zag 20/20, Trim Setting: S-1 (radial axis: TWS in m/s , polar axis: TWA in $^\circ$)

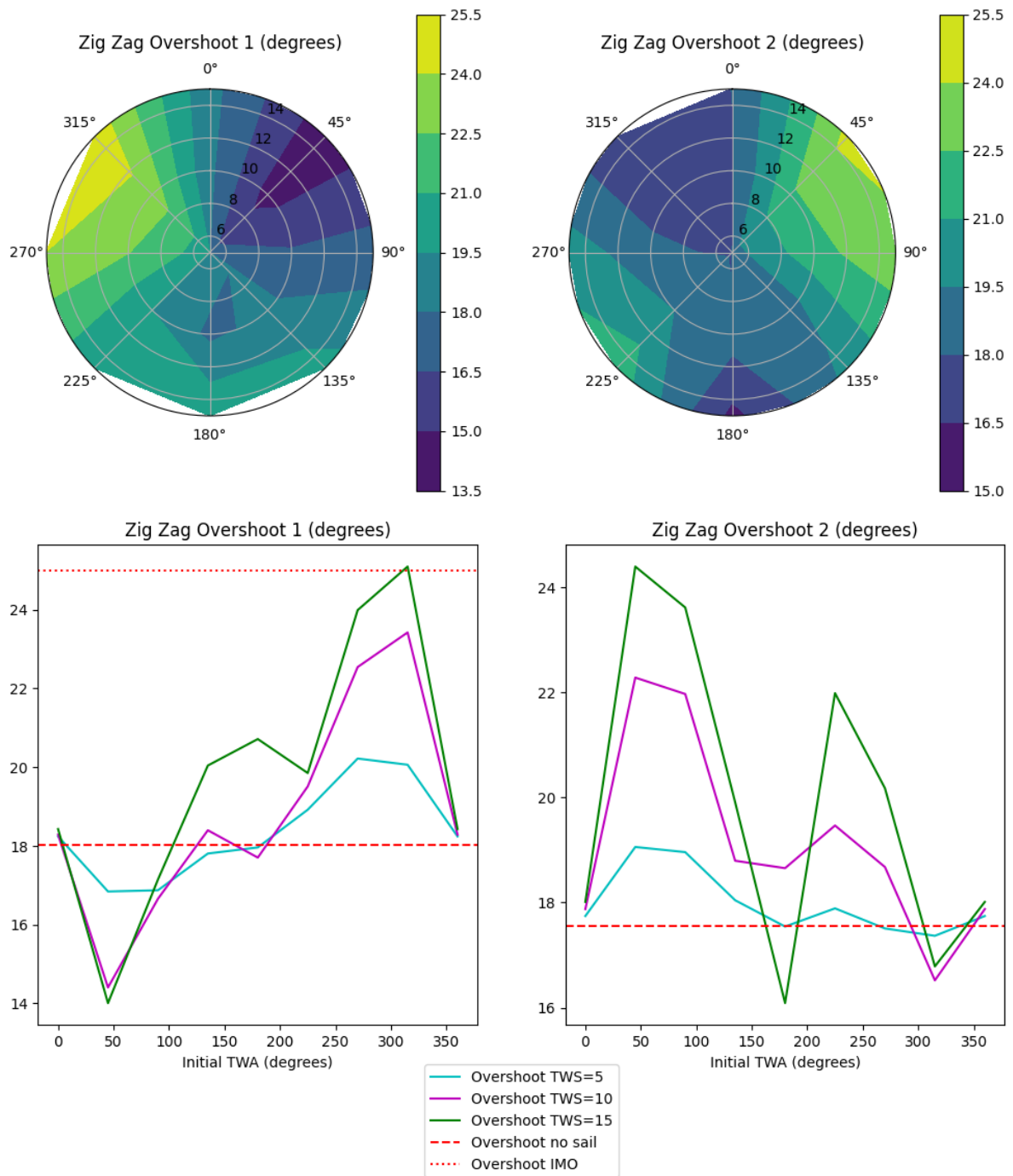


Figure B.23: Rotor Zig-Zag 20/20, Trim Setting: A-S1 (radial axis: TWS in m/s , polar axis: TWA in $^\circ$)

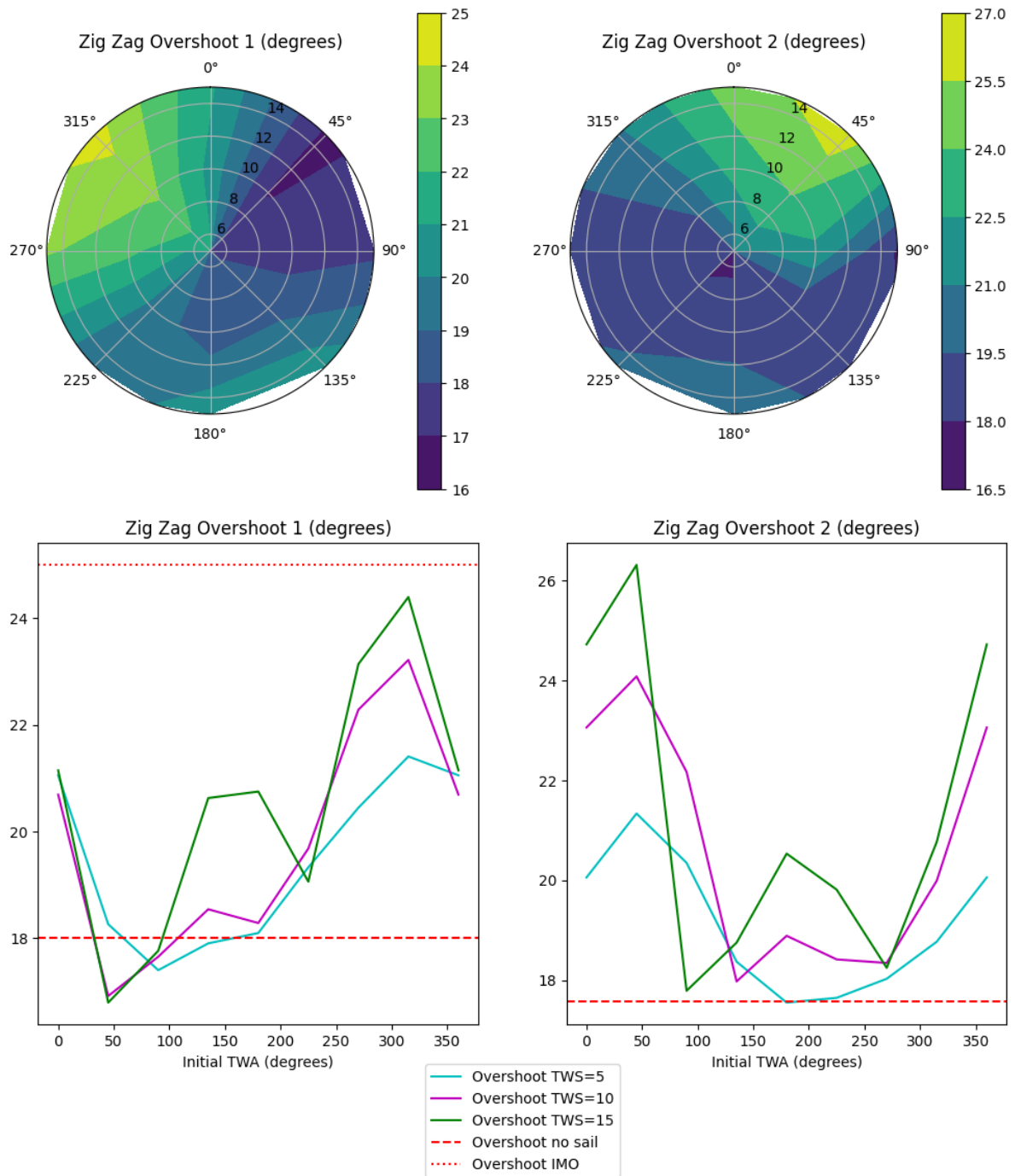


Figure B.24: Rotor Zig-Zag 20/20, Trim Setting: A-F1 (radial axis: TWS in m/s , polar axis: TWA in $^\circ$)

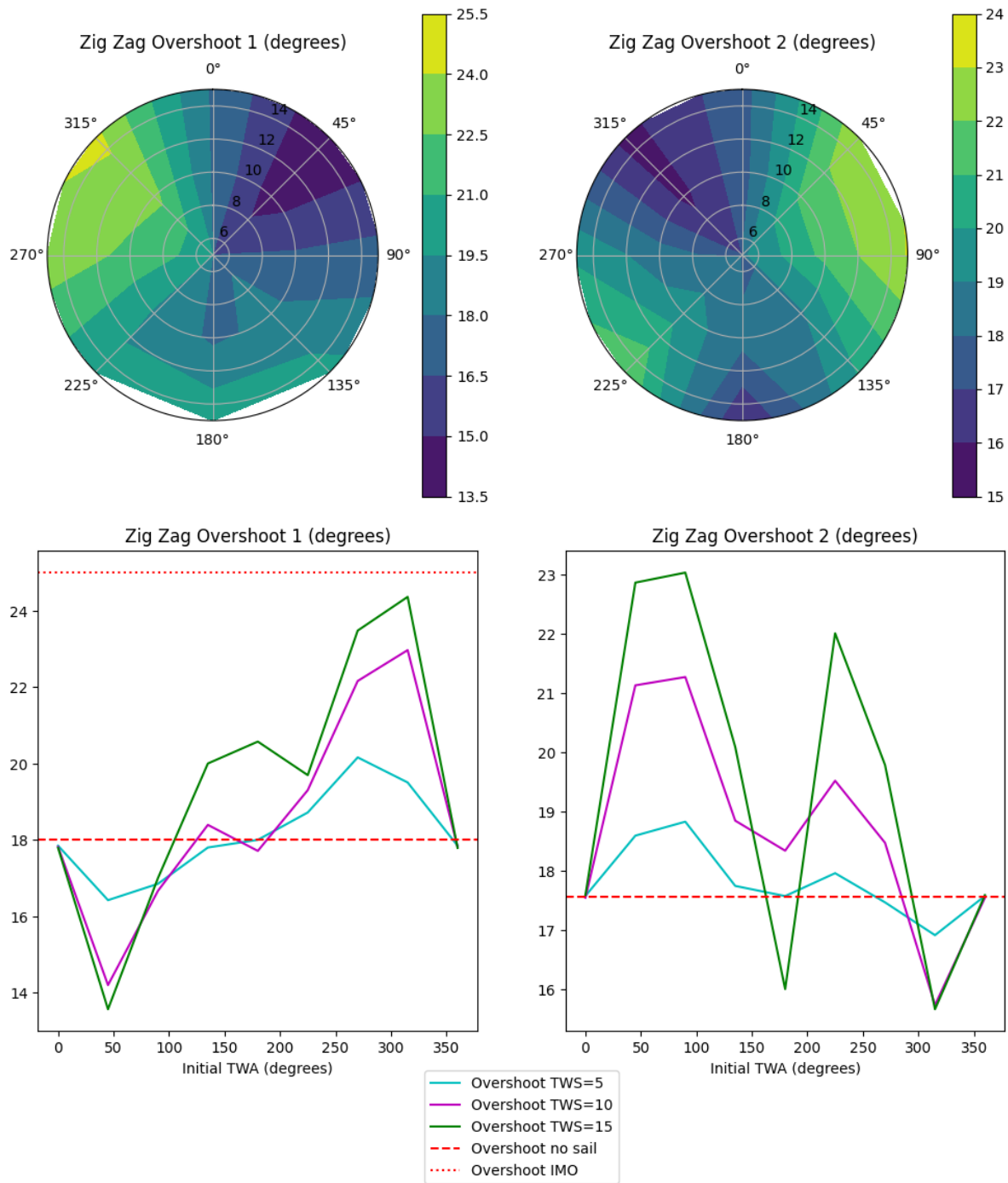


Figure B.25: Rotor Zig-Zag 20/20, Trim Setting: A-S2 (radial axis: TWS in m/s , polar axis: TWA in $^\circ$)

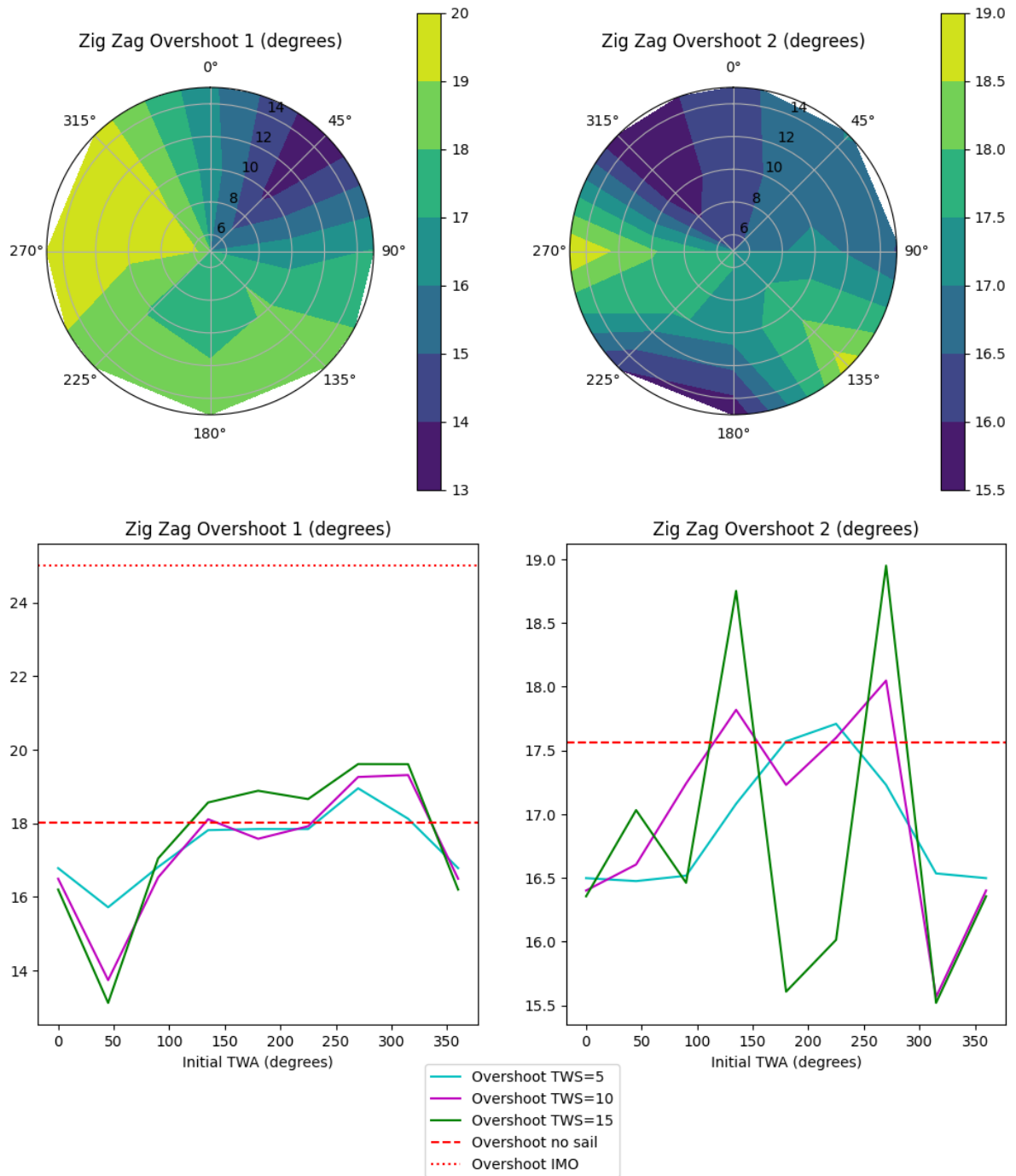


Figure B.26: Rotor Zig-Zag 20/20, Trim Setting: A-F2 (radial axis: TWS in m/s , polar axis: TWA in $^\circ$)

C

Plots - Non-Wind-Assist Validation

C.1. KVLCC2 1/45.7 Turning Circle Test

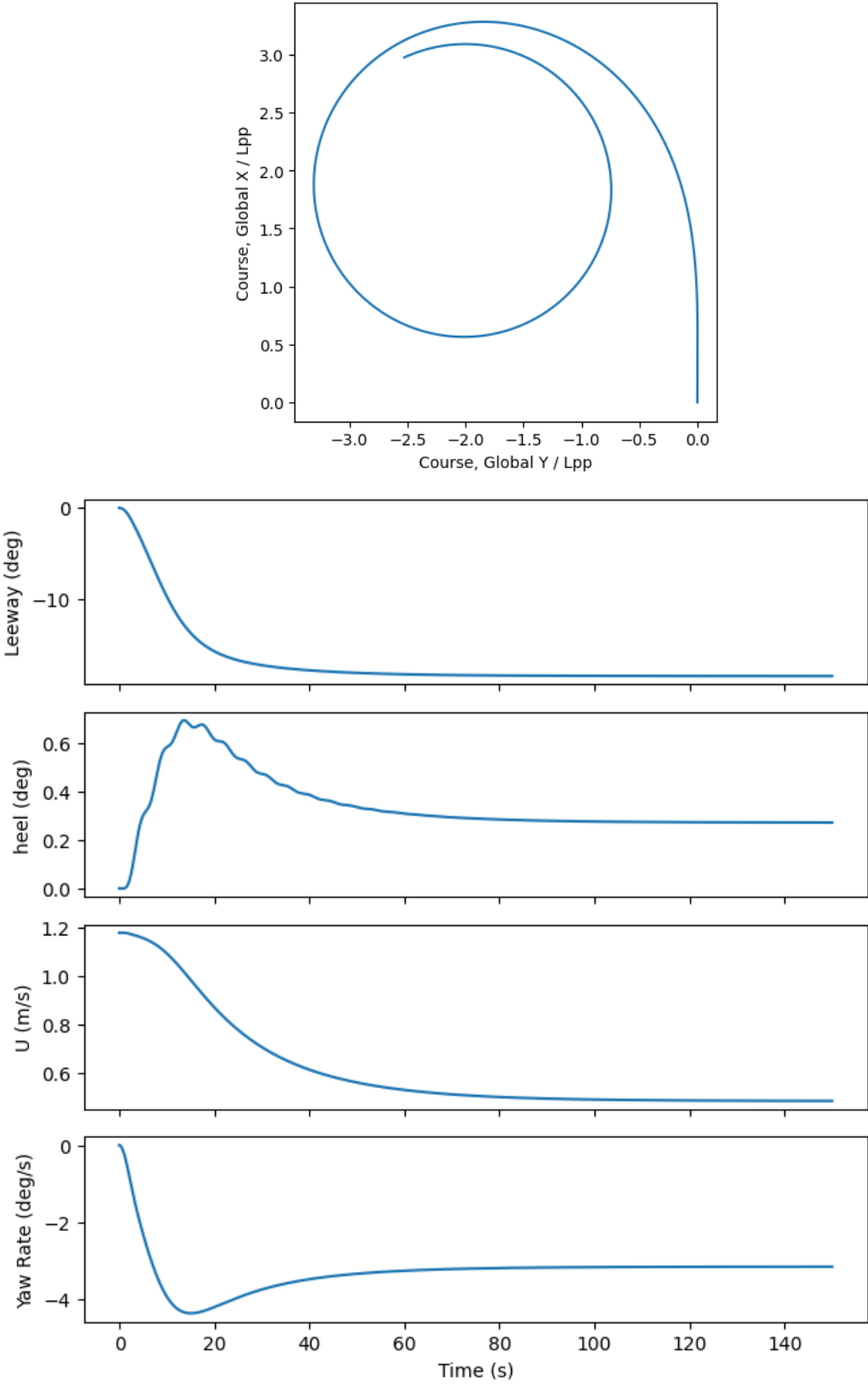


Figure C.1: KVLCC2 Model Scale Turning Circle Maneuver

C.2. KVLCC2 1/45.7 Zig-Zag 10/10 Test

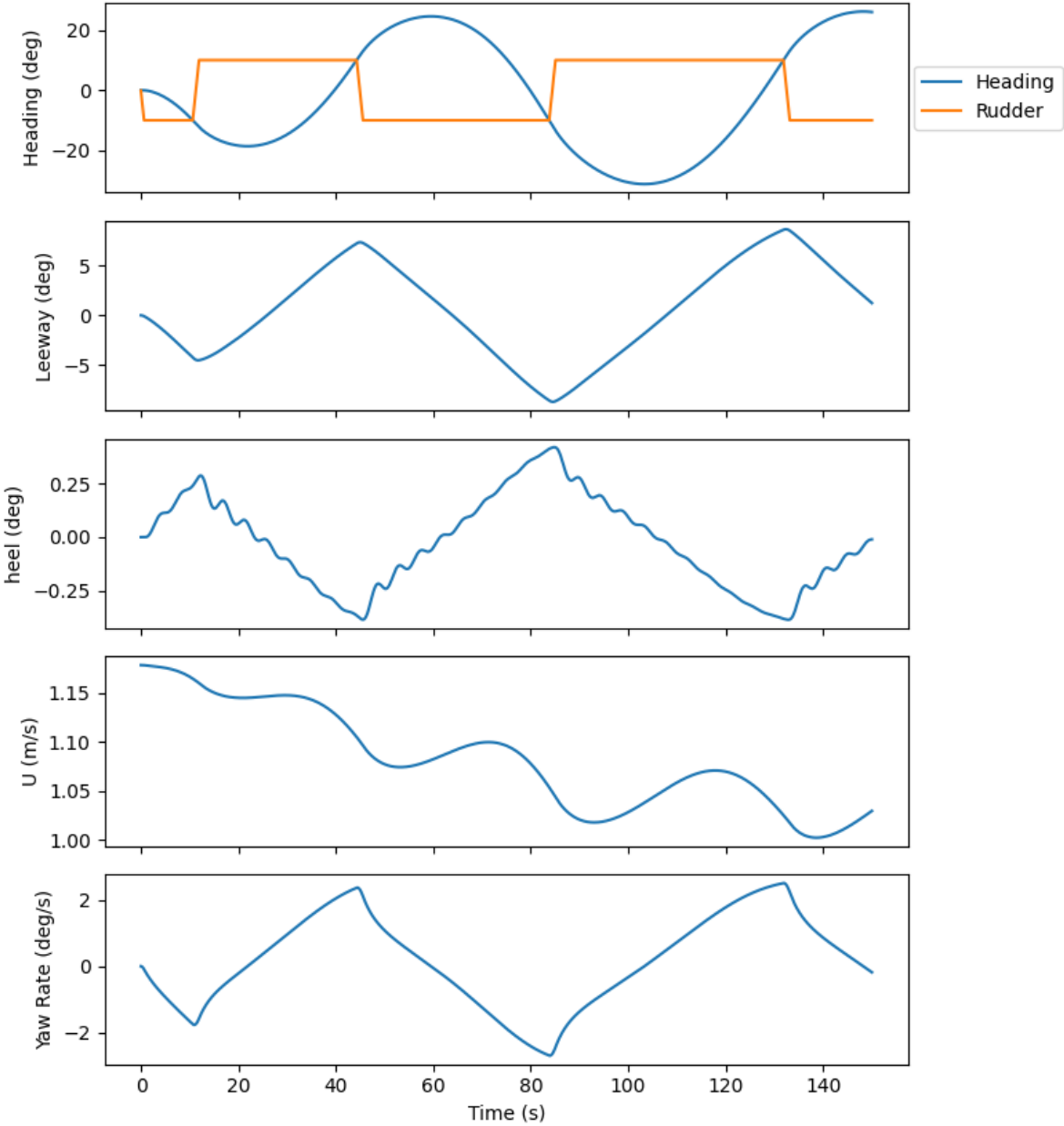


Figure C.2: KVLCC2 Model Scale Zig-Zag Maneuvers Zig-Zag 10/10

C.3. KVLCC2 1/45.7 Zig-Zag 20/20 Test

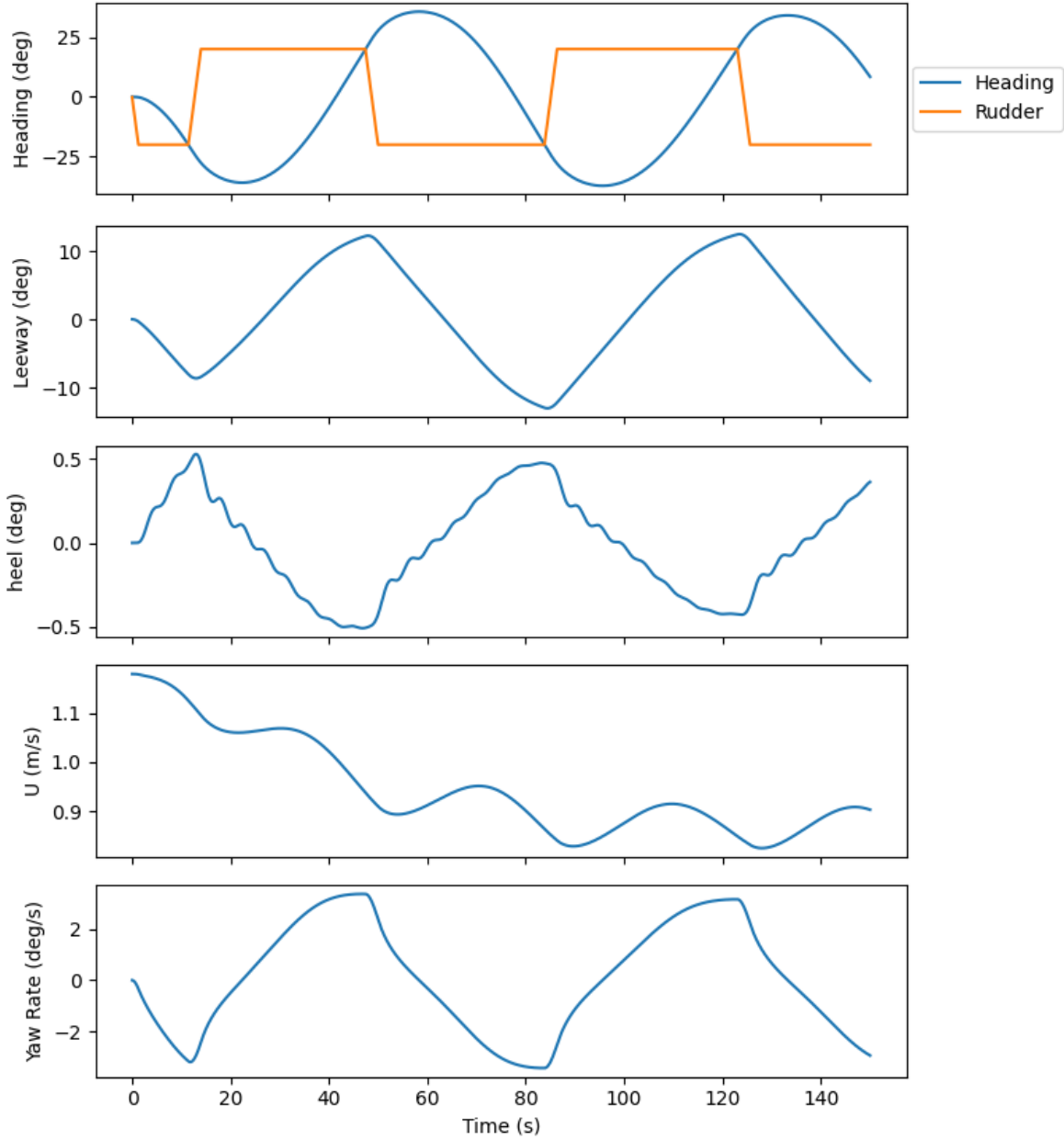


Figure C.3: KVLCC2 Model Scale Zig-Zag Maneuvers Zig-Zag 20/20